NTNU
Norwegian University of
Science and Technology

MYOCARDIAL STRAIN MEASUREMENTS WITH MRI USING FEATURE TRACKING

Mercy Kataike Victoria

MSc in Physics
Submission date: May 2016
Supervisor: Pål Erik Goa, IFY

Norwegian University of Science and Technology
Department of Physics

NTNU

Norwegian University of
Science and Technology

MYOCARDIAL STRAIN MEASUREMENTS WITH MRI USING FEATURE TRACKING

KATAIKE VICTORIA MERCY

MASTER OF SCIENCE IN PHYSICS (MSPHYS)

Submission Date: May 2016

Supervisor: Pål Erik Goa

Acknowledgement

This project has been a collaboration among three different bodies. These are; Department of Physics, Department of Circulation and Medical Imaging at NTNU and Clinic of Radiology and Clinic of Cardiology at St. Olav's hospital.

This project and the thesis was not a one-man show. Its successful completion is because of the input of a number of parties.

First and foremost, I would like to thank God Almighty for the wisdom, guidance, provision through my academic journey.

I would like to appreciate my supervisor Pål Erik Goa for his indispensable guidance and assistance right from the start of this journey up to its completion.

I am grateful to Tommy Arild Hammer, and his supervisor Knut Haakon Stensæth, both doctors at St. Olav's Hospital and partners in this project. The existence of this thesis is because of your cooperation and allowing me to be part of this project.

Many thanks go to Brage Amundsen, a cardiologist at St. Olav's hospital for helping with the Ultrasound part of the project and his helpful advice during the writing process.

I am very appreciative to the Norwegian Government and to Norwegian University of Science and Technology (NTNU) for the Quota scholarship scheme of which I was a beneficiary.

My mother and father, Mr. and Mrs. Taligoola and my siblings have played a wonderful role in my life. Every good seed they sowed into my life has helped me come this far. I dedicate this thesis to you.

Last but not the least, I am grateful to my friends who have helped me with the editing process, getting familiar with some of the concepts used in the thesis and for the advice. Selase Dewu, John Darkwah, Precious Kwadzo and Rebecca Nalwanga, I am forever grateful for your contribution to the successful completion of this thesis.

Abstract

Myocardial strain is increasingly used in determination of myocardial function in the medical field due to its ability to detect cardiac diseases in the early stages, its ability to quantify regional myocardial function and its prognostic power.

A number of methods have been developed to measure myocardial strain in Ultrasound, MRI and Computed Tomography. In the area of Ultrasound, Doppler imaging and Speckle Tracking Echocardiography are used to determine myocardial strain. Of the two, Speckle Tracking Echocardiography is preferred because it is angle independent and can be carried out in 2D and nowadays in 3D.

The standard for strain measurement in Cardiac MRI and in deformation imaging in general is myocardial tagging. Recently, a semi-automatic software-based method has been developed in Cardiac MRI and is known as Feature Tracking. Currently there are three software algorithms available for use; TomTec 2D Cardiac Performance Analysis MR (TomTec 2D CPA MR), Multimodality Tissue Tracking and CMR^{42} Tissue Tracking (CMR^{42} TT).

In this project, the Feature Tracking method was evaluated with Speckle Tracking Echocardiography, a software-based method in the Ultrasound field that is already established. 10 healthy volunteers underwent one Ultrasound scan and two MRI scans 6 months apart. Strain analysis in both Ultrasound and MRI was done offline.

Differences between strain values from TomTec 2D CPA MR and CMR^{42} TT software algorithms and Speckle Tracking Echocardiography were assessed using One-way ANOVA. With TomTec 2D CPA MR and STE, circumferential strain values were not statistically different ($P = 0.913$) while longitudinal strain values were statistically different ($P = 0.006$). For CMR^{42} TT and STE, circumferential strain values and longitudinal strain values were not statistically different ($P > 0.05$). In the comparison of both Feature Tracking software methods, TomTec 2D CPA MR and CMR^{42} TT, the strain values from all the three strain views were statistically different ($P < 0.05$).

Interobserver reproducibility of TomTec 2D CPA MR was good with CV=7.00% for circumferential strain, CV=15.54% for longitudinal strain, and CV=19.13% for radial strain.

Intraobserver reproducibility of CMR^{42} TT was high. It gave CV of 6.81%, (ICC=0.84) for circumferential strain, CV of 10.54%, (ICC=0.54) for longitudinal strain, and CV of 9.33%, (ICC=0.83) for radial strain.

Interstudy reproducibility for baseline and control measurements was high and it gave the following results for TomTec 2D CPA MR: CV=7.88% for circumferential strain, CV=14.44% for longitudinal strain and CV=6.24% for radial strain. The results from CMR[42] TT were: CV=9.45% for circumferential strain, CV=9.22% for longitudinal strain and CV=14.63% for radial strain.

The interstudy reproducibility of both TomTec 2D CPA MR and STE, as well as CMR[42] TT and STE was high with CV=9.26% and CV=11.09% respectively for circumferential strain, CV=14.83% and CV=8.64% respectively for longitudinal strain. Interstudy reproducibility of the FT software methods was good with CV=14.49% for circumferential strain, CV=13.62% for longitudinal strain, and CV=23.21% for radial strain.

The greatest contributor to the variance of the strain results was the variance due to the FT software methods.

Abbreviations

MRI: Magnetic Resonance Imaging

CMR: Cardiac Magnetic Resonance

EF: Ejection Fraction

FT: Feature Tracking

FT CMR: Feature Tracking Cardiac Magnetic Resonance

STE: Speckle Tracking Echocardiography

SSFP: Steady State Free Precession

LV: Left Ventricle / Left Ventricular

SE MRI: Spin Echo Magnetic Resonance Imaging

ECG: Electrocardiogram

CMR^{42} TT: CMR^{42} Tissue Tracking

TomTec 2D CPA MR: TomTec 2D Cardiac Performance Analysis MR

MTT: Multimodality Tissue Tracking

CV: Coefficient of Variation

ICC: Intraclass Correlation Coefficient

LOA: Limits of Agreement

CI: Confidence Interval

CR: Coefficient of Repeatability

Table of Contents

List of Figures

List of Tables

1 Introduction

Cardiac diseases remain the leading cause of mortality in the world according to statistics released by the World Health Organization for the past decade [1]. Therefore, determining Cardiac function efficiently is important in order to diagnose and treat cardiac diseases before they get into advanced stages where the damage they cause may be irreversible.

The human heart is divided into four chambers of which the Left Ventricle (LV) is the most important because it is responsible for pumping blood to all the parts of the body. Left Ventricular (LV) function can be determined using a number of indicators. These include; Ejection Fraction (EF), Wall motion score index (WMSI), Cardiac Output (CO), Left Ventricular Percentage Fractional shortening (% FS), Strain, and Strain Rate [2, 3].

Presently, major clinical and treatment decisions are based on Ejection Fraction [4, 5]. Ejection Fraction is the percentage of blood that is ejected from the heart during systole. Mathematically, it is defined as [6]:

$$EF = \frac{End\ diastolic\ volume - End\ systolic\ volume}{End\ diastolic\ volume} \times 100 \qquad (1.1)$$

Where End Systolic Volume is the amount of blood in the Left Ventricle (LV) at the end of systole and the End Diastolic Volume is the amount of blood in the LV at the end of diastole.

However, EF has some important limitations. Ejection Fraction is dependent on the loading condition of the heart, thus preload (the stretching of the cardiac muscle just before contraction begins) and afterload (force that opposes ejection of blood from the heart) have to be considered while measuring Ejection Fraction. This is a limitation because a suitable determinant of cardiac function should be load independent. Ejection Fraction does not consider regional function of the Left Ventricle, and it has a low reproducibility.

In addition to the above limitations, Ejection Fraction has been found not to detect cardiac diseases in their early stages. This was observed in patients with Hypertrophy Cardiomyopathy where the Ejection Fraction was preserved despite a significant reduction in the cardiac strain [7]. Ejection fraction was also found to be a low prognosticator of cardiac events. This was seen in one study where a number of indicators that predicted patients at increased risk of sudden death were studied [8]. One of the indicators under study was Ejection Fraction. From

this study, it was discovered that there was a low mortality for patients who had EF < 30% and no other risk factor, and that there was increased mortality for patients who had EF >30% along with other risk factors. Therefore, a more efficient marker of cardiac function is needed.

Cardiac strain or myocardial strain has been discovered to be a superior parameter of Cardiac function compared to EF. First and foremost, it is load independent and can quantify regional function of the heart. It can detect cardiac diseases in their early stages when EF is normal, or near normal [9]. A number of studies have also shown myocardial strain to be a superior parameter in the determining of cardiac events as compared to EF [10] [11]. In [12] for example, longitudinal strain emerged as the strongest predictor of mortality compared to EF and WMSI.

The use of strain in cardiology was first put forward by MIRSKY and PARMLEY [13]. It is a measure of the contractile function of the heart. LV Myocardial strain is measured along three axes of the heart. These are the radial axis which is across the thickness of the LV muscle, longitudinal axis which is along the direction of the intraventricular septum, and the circumferential axis which is the circumference of the LV cavity.

LV strain is measured invasively by Sonomicrometry and non-invasively by Magnetic Resonance Imaging (MRI), Ultrasound and Computed Tomography (CT) from which a number of methods have been developed. Of these imaging modalities, Ultrasound is used most widely compared to the others due to its availability. However, MRI is now receiving more interest because of the high quality images it produces compared to Ultrasound and CT.

The strain measurement methods that have been developed in the area of ultrasound also known as echocardiography are Doppler imaging and Speckle Tracking Echocardiography (STE), a software-based method.

A meta-analysis of papers published on LV strain looked at 24 studies and 2597 people. In this meta-analysis, strain was determined using Speckle Tracking Echocardiography and gave the following ranges of Global strain values [14];

- Global longitudinal strain = −15.9% to −22.1%
- Global circumferential strain = −20.9% to −27.8%
- Global radial strain = 35.1% to 59.1%

In the field of Cardiac MRI, the standard for strain measurement is myocardial tagging [15]. However, it has found difficulty being implemented into clinical use because it requires additional sequences and is time consuming [16]. Recently, a semi-automated, software-based method for determining myocardial strain has been developed in the field of MRI known as Feature Tracking [17]. It is the MRI equivalent of Speckle Tracking Echocardiography.

Since its introduction, it has found widespread clinical use, for example in the quantification of Left Ventricular Torsion and Diastolic Recoil [18], and in quantification of dyssynchrony [19, 20]. This method has been validated against myocardial tagging and it was found that there is agreement between both methods [21].

A range of normal LV strain values has also been published using Feature Tracking Cardiac Magnetic Resonance as a method of LV strain determination [22];

- Global longitudinal strain = -21.3 ± 4.8%
- Global circumferential strain = - 26.1 ± 3.8%
- Global radial strain = 39.8 ± 8.3%

Three software algorithms have so far been developed for use in Feature Tracking, namely, TomTec 2D Cardiac Performance Analysis MR (TomTec 2D CPA MR), Multimodality Tissue Tracking (MTT), and the newest being CMR^{42} Tissue Tracking (CMR^{42} TT) [23].

Feature Tracking Cardiac Magnetic Resonance (FT CMR) is picking interest as a method of determining myocardial strain due to the fact that it is faster and easier to use. Also, the cine MR images obtained from Steady State Free Precession sequences are known to have a high spatial resolution and tissue contrast therefore, the case of images being rejected in a study due to suboptimal quality is less likely to occur [24].

The development of Feature Tracking as a method of myocardial strain determination is a step forward towards standardization and reproducibility in strain imaging across imaging modalities. This has been a matter of concern in implementing cardiac strain imaging in routine clinical practice [25,26]. However, there is currently little information available comparing Feature Tracking and STE thereby validating Feature Tracking method as an equivalent to STE. Consequently, more research needs to be done to determine whether STE produces similar results as the Feature Tracking software algorithms.

More to that, there is no comparison between CMR^{42} TT, the newest Feature Tracking software algorithm with any other established method of LV strain measurement. Previously, TomTec

2D CPA MR and CMR[42] TT algorithms were compared in a study involving hypertensive patients, and the results showed a significant difference between the circumferential strain values from both methods, but no clear trend with the radial and longitudinal strain values. The authors recommended comparing the two methods with a gold standard [27].

This thesis therefore evaluates Feature Tracking Cardiac Magnetic Resonance (FT CMR) or Feature Tracking software method by comparing it with Speckle Tracking Echocardiography, which is an already established as method of determining myocardial strain.

The specific questions to be answered in this thesis are;

1. Are MRI strain based measurements by Feature Tracking Cardiac Magnetic Resonance the same as Ultrasound strain based measurements by STE?
2. Does Feature Tracking Cardiac Magnetic Resonance have a high reproducibility?
3. Is there agreement between CMR[42] Tissue Tracking and TomTec 2D Cardiac Performance Analysis MR strain values such that they are interchangeable?

2 Theory

2.1 Cardiac (Heart) Anatomy and Position

The heart is a muscular organ that pumps blood to all parts of the body. More specifically, it receives blood deficient of oxygen (deoxygenated blood) from the rest of the body and sends it to the lungs where it is oxygenated [28]. Once that blood is oxygenated, it returns to the heart, and it is pumped to the rest of the body. Approximately 7,571 liters of blood are pumped by the heart every day.

The heart is about the size of a closed human fist, and weighs between 200-450g. It has the shape of a cone and is hollow [29].

According to Jan Bogaert [30], the heart has a central location in the thorax with about 60% of it lying to the left side of the median plane of the body. It is bordered by the lungs on its left and right, the sternum to the front, and the diaphragm below it. The frontal view of the heart is shown below in Figure 2.1.

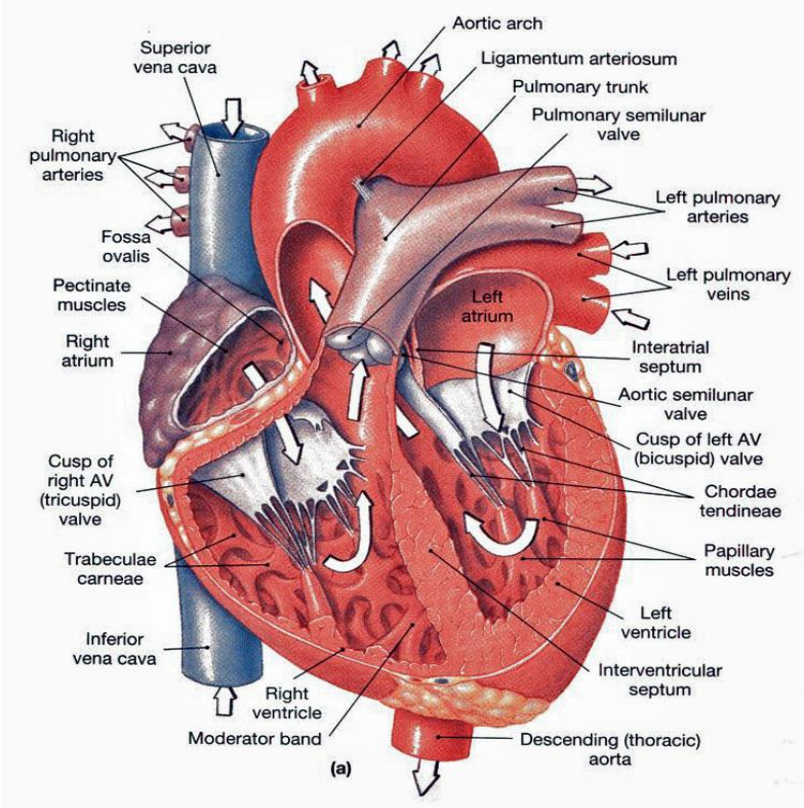

Figure 2.1: Frontal View of the human heart. Reproduced with permission [31]

The heart is protected by a membrane known as the Pericardium. The pericardium is composed of two layers between which is a narrow cavity filled with fluid which is a lubricant and thus prevents friction on the heart as it pumps blood.

The heart is divided into four chambers, Left Atrium, Right Atrium, Left Ventricle, and the Right Ventricle. The left and right side of the heart are divided by the Septum. The right side of the heart receives blood from the body and pumps it to the lungs, while the left side of the heart receives blood from the lungs and pumps it to the rest of the body [32].

2.2 Cardiac Cycle

The cardiac cycle is the continuous contraction and relaxation of the heart muscle as it pumps blood to the body. This is brought about by electrical activity of the heart. The normal heart rate is approximately 75 beats/minute. Each heartbeat consists of a contraction phase also known as systole and a relaxation phase also known as diastole [33]. Systole serves to increase pressure in one chamber of the heart so that blood moves from a region of higher pressure to a region of lower pressure. In diastole, the heart muscles relax so that the chambers fill with blood. The cycle is as follows:

- Atrial systole: The atria contract and send blood to the ventricles. This occurs in late Ventricular diastole.
- Isovolumetric contraction: The Atrioventricular valves and Semilunar valves close. The ventricles contract but with no change in volume. This occurs in early Ventricular systole.
- Ventricular Ejection: The ventricles contract. The high pressure created opens the atrioventricular and the semilunar valves. Blood is pushed to the atria.
- Isovolumetric relaxation: The ventricles are starting to relax. However, the pressure in the ventricles is still higher than that in the atria so the valves are still closed.
- Ventricular filling: Pressure in the ventricles decreases below that of the atria. The atrioventricular and semilunar valves are open and blood flows into the ventricles from the atria.

The above process of the cardiac cycle is illustrated in Figure 2.2.

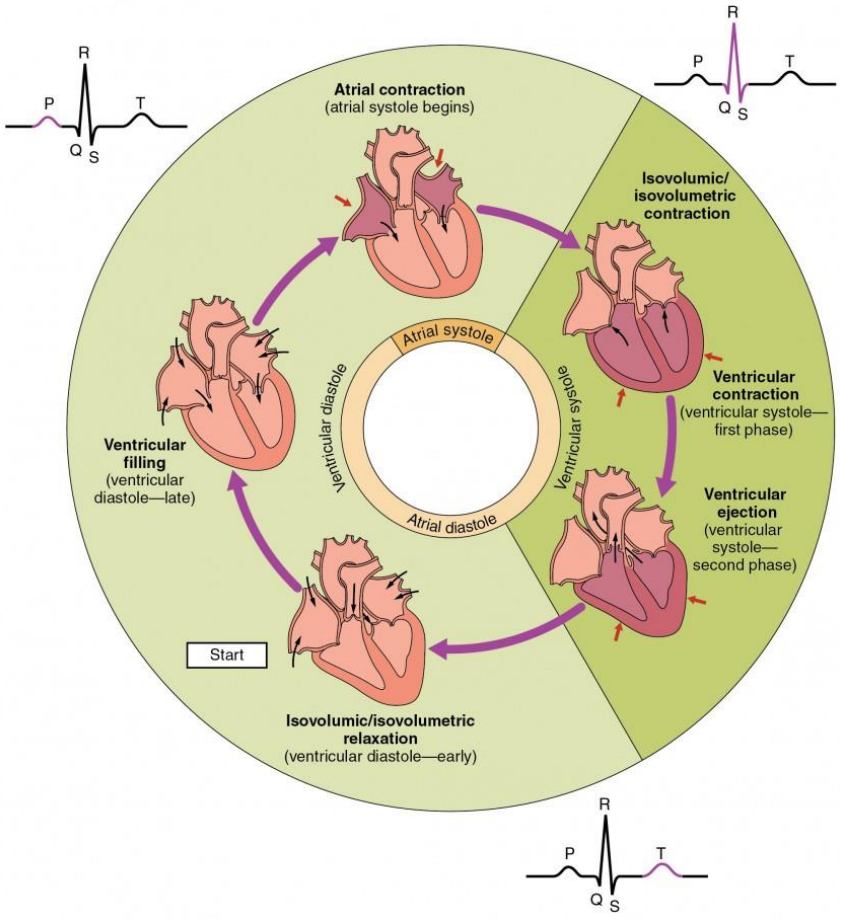

Figure 2.2: The phases of the cardiac cycle, the correlation with the ECG included [34].

2.3 Deformation of the heart during the Cardiac Cycle

A number of theories have been stated regarding how the heart contracts during the cardiac cycle. It was earlier believed that the heart pumps blood by radial squeezing. However, this has been disagreed upon because it then would mean that the heart contracts and relaxes homogeneously and that is not the case. This school of thought does not consider the complex arrangement of the fibers in the myocardium [35].

In principle, the motion of the heart, particularly the LV during its pumping action is multi-dimensional and is characterized by a decrease in the initial LV diameter, a thickening in the heart wall (radial direction), a longitudinal movement where the apex moves closer to the base, and a rotational movement [36]. The rotational movement occurs along the long axis of the heart. The apex rotates clockwise while the base rotates anti clockwise during systole, thus producing a wringing action or a twist. This aids in pumping as much blood out of the heart as

possible. The heart then untwists during diastole. The rotational movement of the heart is illustrated in Figure 2.3.

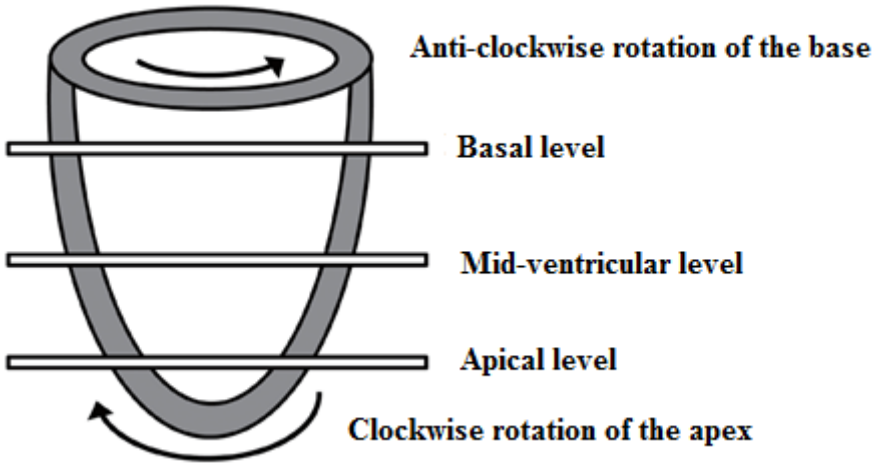

Figure 2.3: Rotational movement of the heart, adapted and modified from [37]. Reproduced with permission.

This complex deformation of the heart is due to the complex arrangement of the fibers in the myocardium. A number of explanations regarding the structure of the myocardium have been put forward in the past [38]. No single explanation has been fully accepted.

However, in 1957, Torrent- Guasp discovered that the fibers in the ventricular myocardium had a helical structure by a hand dissection [35]. He discovered that the fibers in the myocardium are arranged as a continuous band with 2 helices, an explanation that is now known as the Helical Ventricular Myocardial Band (HVMB) structure. Each of these helices or loops is divided into two segments. One loop is the basal loop divided into the left and right segments, and the other is the apical loop divided into the ascending and descending segments [38]. The basal loop is oriented transversely while the apical loop is oriented obliquely. The transversely or circumferentially oriented basal loop surrounds the oblique apical loop. This description has been proved by Diffusion Tensor Magnetic Resonance Imaging [39]. Torrent-Guasp's notion of the structure of the myocardium is one of the outstanding models. The helical nature of the heart is what creates the twisting motion of the heart. The HVBM is illustrated in Figure 2.4 below.

Currently, a more unified model is used when looking at the structure of the heart wall. Here, the heart wall is divided into the midmyocardium, the subepicardium and the subendocardium. The fibers in these three regions are oriented differently. The fibers in the midmyocardium are oriented circumferentially while the ones in the subendocardium and the subepicardium are longitudinally oriented [40-42].

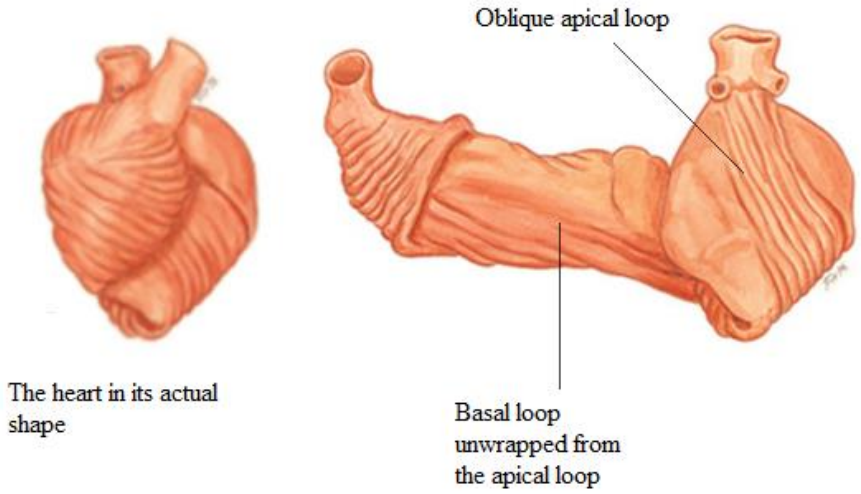

Figure 2.4: The Helical Ventricular Band Model of the heart. Image adapted from [43] and was modified.

2.4 Magnetic Resonance Imaging (MRI)

Magnetic Resonance Imaging (MRI) is an imaging modality that uses the magnetic field and radiofrequency pulses to obtain images of an organ or structure under study. MRI is based on the principle of Nuclear Magnetic Resonance (NMR). Nuclear Magnetic Resonance is grounded on the fact that nuclei have spins that create a magnetic field as they precess about their axes. Spin is a fundamental property of an atom [44] and it depends on the number of protons and nucleons in the nuclei of an atom. These spins act as transmitters and receivers [44]. The nuclei used in clinical MRI are the hydrogen nuclei found mostly in water and occasionally fat. Since the body is approximately 70% water, it is highly abundant in hydrogen nuclei.

Hydrogen nuclei are randomly oriented in the body. Once a person is placed in the bore of an MRI machine, some hydrogen nuclei or spins align themselves in the direction of the main magnetic field (parallel) and others are antiparallel to the direction of the main magnetic field. In quantum mechanical terms, the spins that align with the magnetic field are in a low energy state while those that are antiparallel are in a high energy state. The ones parallel to the main magnetic field are slightly more than those that are antiparallel thus leaving an excess in the direction of the magnetic field that is also known as the magnetization vector M [45], shown in Figure 2.5. The spins precess about the main magnetic field at a frequency known as the Larmor frequency.

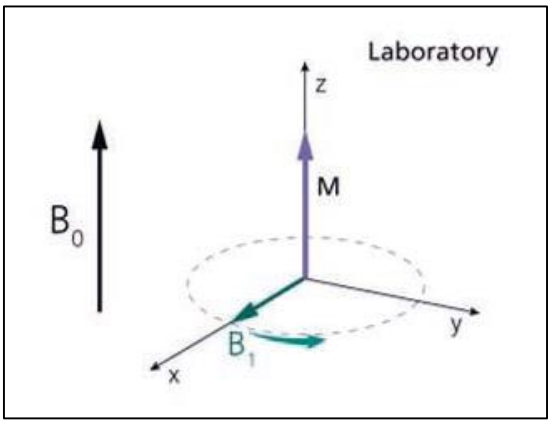

Figure 2.5: The Magnetization vector M in the direction of the main magnetic field B_0. This is in the laboratory frame of reference [45].

When a radiofrequency pulse at the same frequency as the Larmor frequency is applied to the spins, they obtain energy and are flipped away from the direction of the main magnetic field [46] (Figure 2.6a). A signal is then obtained using receiver coils. On removal of the pulse, the spins relax and return to precessing around the main magnetic field (Figure 2.6b).

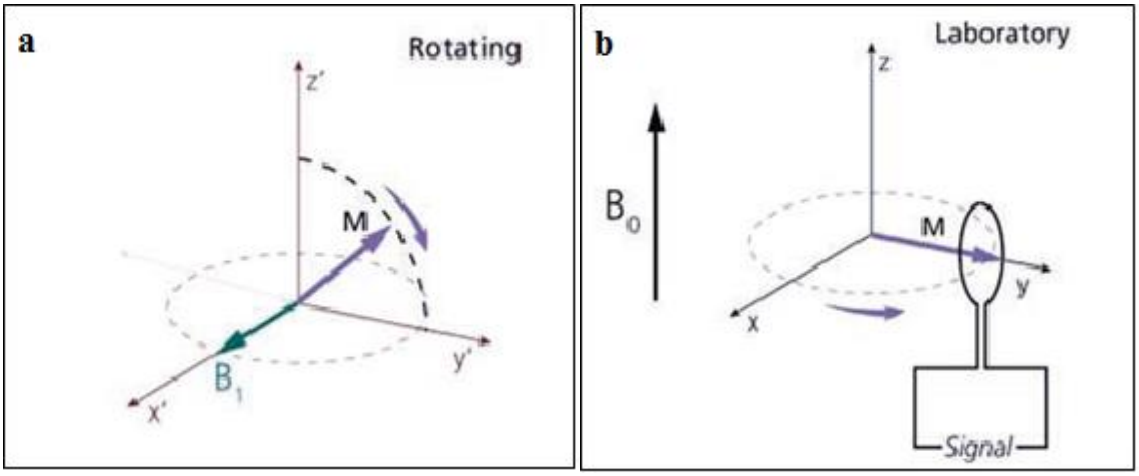

Figure 2.6a and b: The Magnetization vector flips away from the direction of the main magnetic field and a signal is obtained [45].

The signal received from the receiver coils is digitized and can be represented on a mathematical area known as k-space. K-space is a two dimensional representation of raw MRI data with the horizontal axis containing frequency information and the vertical axis containing phase information [47]. When an inverse Fourier Transform is applied to the k-space, an MRI image is obtained. Each pixel in the MRI image is the weighted sum of all the points in the k-space [48]. The filling of the k-space depends on the gradients in the MRI machine, particularly the phase encoding and the frequency encoding gradients [49].

The center of the k-space contains low spatial information responsible for image contrast of the MRI image while the edges contain high spatial information and are responsible for the sharp edges and resolution of the MRI image [30].

The flow of obtaining an MRI image is shown below in Figure 2.7.

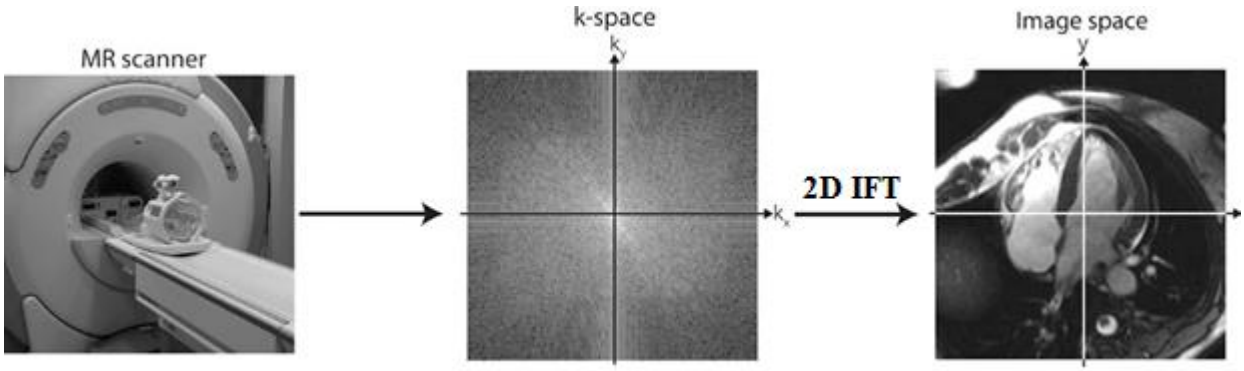

Figure 2.7: The flow of acquiring an MRI image [50].

2.5 Cardiac MRI

Cardiac MRI or Cardiovascular Magnetic Resonance imaging (CMR) is a form of Magnetic Resonance Imaging performed to non-invasively determine the structure and function of the cardiovascular system. With CMR, one can look at cardiac and vascular anatomy, myocardial function, and perfusion in a single examination.

There are a variety of pulse sequences that are used to image the heart. These are broadly divided into Bright blood and Black blood imaging techniques [51].

Black blood techniques suppress the signal from blood thus producing a low signal intensity appearance of blood. They are Spin echo sequences. They are normally used to visualize cardiac anatomy [51]. Spin Echo MRI was used previously. This has since been replaced by faster spin echo sequences and turbo spin echo sequences.

Bright blood techniques enhance the signal from blood thus producing a high signal intensity appearance of blood. They are Gradient echo sequences. These techniques are used to evaluate cardiac function [52]. These are currently more commonly used in cardiovascular MRI due to their speed and flexibility.

Two main coordinate systems are used in cardiac MRI; Body planes and Cardiac planes. Body planes are oriented perpendicular to the long axis of the body. They consist of coronal, sagittal, and axial planes as illustrated in Figure 2.8 a, b, and c respectively. These are used to derive the scout images and provide an overview of the morphology of the heart. The coronal plane divides the body into posterior and anterior sections. The sagittal plane divides the body into left and right halves. The axial plane divides the body into cranial and caudal parts. However,

these planes can only be used to observe the morphology of the heart and not obtain functional data as they are not perpendicular to the heart wall [52].

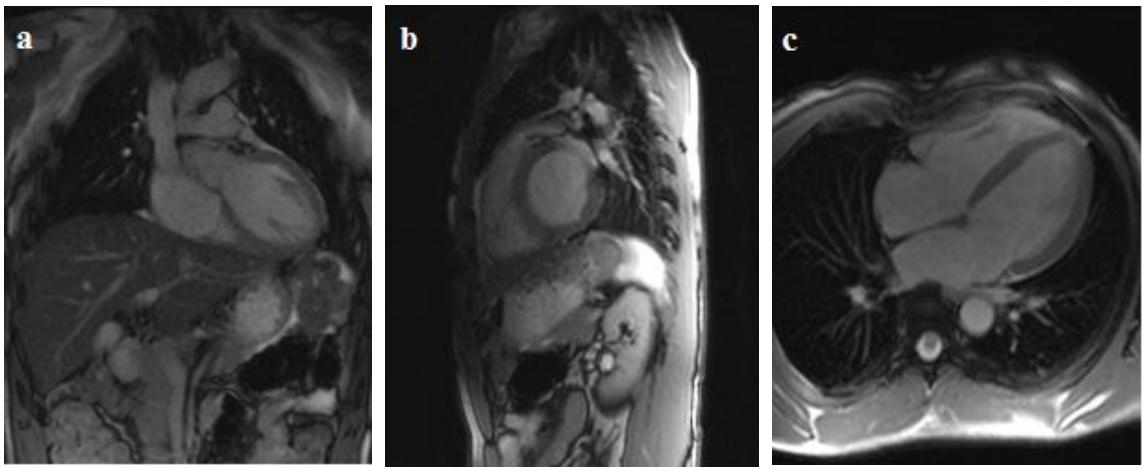

Figure 2.8: Body Planes: Coronal (a), Sagittal (b), and Axial (c)

Cardiac planes are created using the scout images. Scout images are images produced in order to establish the short axis and long axis views of the heart. These include the short axis, horizontal axis, and the vertical axis and their reference is the line from the apex of the heart to the mitral valve [52]. The cardiac planes are shown in Figure 2.9 a, b and c. Nonstandard imaging planes can be obtained in addition to the above in order to study a particular pathology [30].

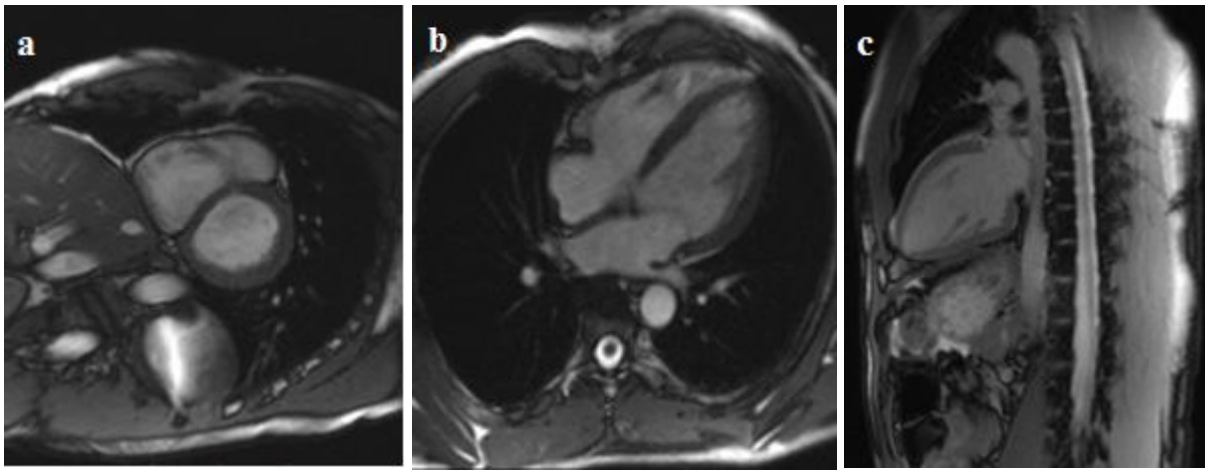

Figure 2.9: Cardiac Planes: Short Axis (a), Horizontal Long Axis (b), and Vertical Long Axis (c)

Cardiac MRI suffers from motion artefacts. This is due to the rapid and complex motion of the heart and vessels as well as respiratory motion. Therefore, adjustments have to be made to overcome this. These adjustments include cardiac gating, multi-phase acquisitions, and respiratory gating.

Cardiac gating is considered the most effective means of correcting the motion artifacts in cardiac MRI. Here, an Electrocardiogram (ECG) is used to synchronize the acquisition of data with cardiac motion. Data can then be obtained from a specific phase of the cardiac cycle. This data is acquired over a number of cycles. Two electrodes connected to the ECG are pre-coated with jelly and are placed on the chest of the patient who is then moved into the scanner. The R wave is taken to be the reference for data acquisition [53]

ECG gating can be done prospectively or retrospectively. In prospective gating, the acquisition of data occurs after a predetermined delay and this occurs at the same point in the cardiac cycle. In retrospective gating, MRI acquisition is done continuously with simultaneous ECG recording. The MR data is then reordered with the phase with the cardiorespiratory cycle [54]. The difference between the two types of ECG gating is clearly demonstrated in Figure 2.10.

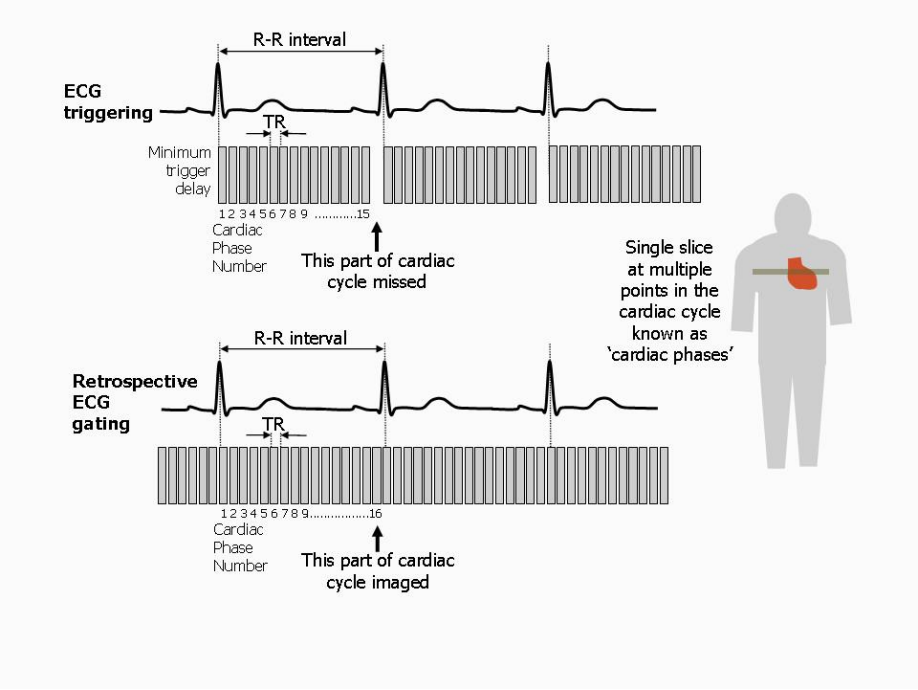

Figure 2.10: Prospective and Retrospective gating [55]

A standard Cardiac MRI examination consists of screening the patient and setting up the cardiac gating. An overview of the heart is then obtained as scout images. Localization of the axes is done on the scout images. After the location of the axes of the ventricles has been determined, then cine images can be obtained in both longitudinal and short axis orientations, as well as optional images depending on what needs to be found out about the specific patient [45]. A comprehensive MRI scan can take up to 1 hour.

2.6 Cine Imaging

The ability to synchronize image acquisition with the cardiac cycle allows the reconstruction of high quality movies [45]. These images of the heart are obtained over several cardiac cycles. This is known as cine imaging. Multiple static images are obtained from this kind of imaging which can be rapidly displayed as a loop or a short movie also known as a cine. Gradient echo sequences are used for this technique and they provide bright blood images of the heart. TE (Echo time) is made as short as possible for fast acquisition.

Only a small proportion of data needed to fill a given k-space is obtained from one cardiac cycle. So in order to fill the whole k- space, the data has to be collected over a number of cardiac cycles [56].

Steady State Free Precession (SSFP) is the backbone of Cine cardiac MRI imaging. Here, a steady state of residual transverse magnetization and the longitudinal magnetization is maintained between successive cycles. This is made possible by using a low flip angle which is usually less than 90 degrees and a short repetition time (TR). TR should be less than the T2 relaxation times of the tissue [57].

An advantage of cine imaging is it generates images with high Signal to Noise Ratio (SNR) and a contrast between blood and the myocardium. It also has the advantage of short acquisition times [58].

2.7 Segmentation of the Left Ventricle

The left ventricle (LV) can be divided into a number of segments depending on the imaging modality used. This is done to assess both global and regional LV function. The segments can vary from as low as 9 to as high as 400. However, recommendations have been made regarding the number of segments the LV can be divided into in order to create uniformity across imaging

modalities. The current recommended number of segments is 17 [59]. Nevertheless, 16, 18, and 20 segments can also be used to divide the LV. For functional imaging, the 17 segment model is not used as the apex does not contract in this particular model.

Regardless of the number of segments used, the LV is first sectioned into three thirds perpendicular to the longitudinal axis; the basal, mid ventricular and apical levels. These levels have been demarcated in the image of the Left Ventricle in Figure 2.3. Starting from the anterior insertion point of the right ventricle and going counterclockwise, the LV wall and cavity are divided into six segments on each short axis level [60]. The 6 segments are;

- Anterior
- Inferior
- Lateral
- Posterior
- Septal
- Anteroseptal

The variation in the number of segments used in a particular situation is due to the different ways in which the segments of the apex are divided. This is shown in Figure 2.11a, b and c.

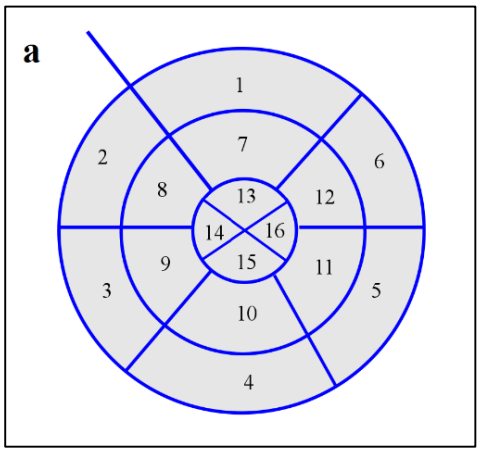

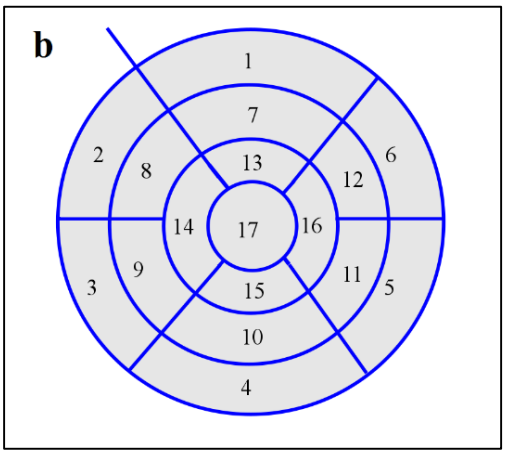

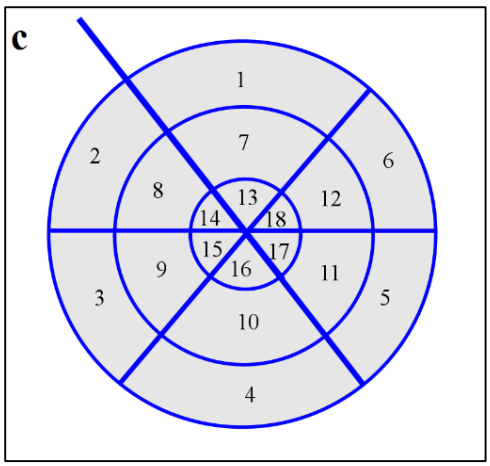

Figure 2.11:16 segment (a), 17 segment (b) and 18 segment (c) models. The protruding line marks the anterior insertion of the right ventricle where counting of the segments begins on the basal, mid-ventricular and apical levels.

2.8 Myocardial Strain

Strain is the fractional or percentage change from the original or unstressed dimensions when a stress is applied [13]. Myocardial strain therefore is the shortening or lengthening of a segment of the myocardium in relation to its original length. Mathematically, it is defined as

$$\varepsilon = \frac{L_0 - L}{L_0} \tag{2.1}$$

Where L_0 represents the unstressed dimension and L represents the stressed dimension. Positive strain implies lengthening or expansion while Negative strain implies shortening or compression.

Strain measurements are of two types; Strain can be measured with relation to the initial length. This is known as Lagrangian strain and its formula is the same as the formula of strain shown above (equation 2.1). Strain can also be measured with relation to the length at a previous time, and this is known as natural strain. It is given by the formula;

$$\varepsilon = \frac{L(t_0) - L(t)}{L(t_0)} \tag{2.2}$$

Where $L(t_0)$ is the length at a previous time t_0, and $L(t)$ is the length at a time instant t [61]. The type of strain to be determined depends on the imaging modality used. Speckle Tracking Echocardiography in ultrasound for example analyses the Lagrangian strain where the myocardium in diastolic state is the initial length [62].

Strain is one of the parameters that describe myocardial function. It provides us with a way of measuring the extent of myocardial contraction. It has been discovered to provide more accurate information on myocardial function compared to Ejection Fraction in that it enables the diagnosis of cardiovascular diseases in their early stages [9]. The comparison is made with Ejection Fraction because it is the parameter used to make clinical decisions, as already explained in the introduction chapter.

In addition to early determination of cardiac diseases, myocardial strain can also be used in a number of areas. It can be used to quantify between active and passive movement of the myocardial segments which is not the case for Ejection Fraction (EF). This enables the quantification of regional myocardial function [63]. It also quantifies areas of myocardial function that cannot be visually assessed [61].

Myocardial strain provides prognostic information for a number of cardiac diseases thereby aiding clinicians to make accurate decisions for patients [63]. One example is in the case of a myocardial infarction [64].

Myocardial Strain is used in the follow up of the outcomes and effectiveness of different treatment therapies for example in Cardiac Resynchronization Therapy and Cancer Therapy [65]. In the area of cancer therapy, myocardial strain has been used to quantify myocardial toxicity during the course of chemotherapy treatment [65].

Strain imaging can also help to differentiate between the normal thickening of the heart walls in athletes and the abnormal thickening also known as Hypertrophy Cardiomyopathy [66, 67]. Here it was discovered that patients with hypertrophy cardiomyopathy had severely reduced myocardial strain which is not the case for the athletes.

2.9 Measurement of myocardial strain

The myocardium has three normal strains and six shear strains [61] thus deformation is three dimensional in nature as already explained in section 2.3. Myocardial strain can be measured globally and regionally.

Myocardial strain measurements can be taken in three different orientations; Longitudinal strain, Circumferential Strain, and Radial Strain as portrayed in Figure 2.12. With reference to the Left Ventricle, the longitudinal strain signifies the shortening of the LV along its long axis, the circumferential strain denotes the reduction of the circumference of the LV cavity during

the cardiac cycle while the radial strain portrays the thickening of the LV wall [68]. Images from two chamber, three chamber and four chamber views are required to measure longitudinal strain, while for radial and circumferential strains, short axis images are used.

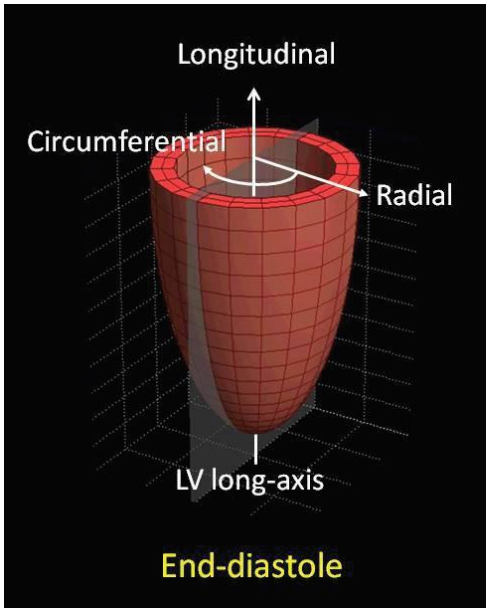

Figure 2.12: Orientations of strain in the LV. Reproduced with permission [69]

The radial and circumferential strain is measured on the three short axis levels along the long axis of the LV, that is; Basal, Mid Ventricular and Apical levels (Figure 2.3) [70].

A number of imaging modalities are used to measure myocardial strain. These include Ultrasound (Echocardiography), Magnetic Resonance Imaging and Computed Tomography (CT) [71]. The focus of this thesis is on strain imaging in Magnetic Resonance Imaging and Ultrasound and these are explained in the following sections 2.10 – 2.14.

2.10 Ultrasound (Echocardiography) Strain Imaging

Ultrasound is an imaging modality that makes use of high frequency sound waves to make images. These sound waves are emitted from a probe or a transducer to the organ or area of interest. The returning wave that has been reflected off the area of interest is then detected and is used to form an image.

Ultrasound as an imaging modality is advantageous and thus has a widespread clinical use because it is portable, and has a comparatively high temporal resolution [72]. Strain imaging in Echocardiography is commonly referred to as Deformation imaging. In the field of

Echocardiography, myocardial strain is quantified by Tissue Doppler Imaging and Speckle Tracking methods.

Strain imaging actually began with **Tissue Doppler Imaging (TDI).** It is based on the Doppler Effect. Information on velocity is obtained from the shifts of the ultrasound frequency as detected by the transducer. Strain rate is then obtained from velocity information, which when integrated results in strain [72]. TDI can be performed in both pulsed wave modes and color modes.

However, TDI derived strain values are not highly reproducible. This is because the strain values are obtained from only 1 dimensional values of velocity yet the heart deforms in 3 dimensions all at once. There are also limits to spatial resolution in that it is not high at high temporal resolution [61]. It also has the disadvantage of angle dependency. The strain values depend greatly on the insonation angle. The insonation angle is the angle between the ultrasound beam and the myocardial wall.

Speckle Tracking Echocardiography (STE) on the other hand is a post- processing software-based technique. In this method, gray scale digital images are used. It makes use of the fact that gray scale images contain natural acoustic markers known as speckles throughout the myocardium. The speckle patterns are formed by scattering of the ultrasound beam by tissue and are relatively stable from one image to another. The STE software detects these speckles and then tracks them in the subsequent images using 'sum of the absolute differences' algorithm [68] thereby providing information on displacement, strain, strain rate and velocity of that segment.

The method works as follows; a cine loop of ultrasound images is obtained and exported to a workstation. They are then loaded onto the software. The endocardium is manually traced on the frame at the end of systole. The epicardial trace is automatically generated by the software thus creating a user defined region of interest. This can be seen in Figure 2.13a and b. The region of interest is then adjusted manually to ensure that the myocardium is well traced. The tracking quality is then graded, and those images with suboptimal quality are excluded from the analysis. Once the area of interest is optimized, the software divides the region of interest into six segments and then generates strain curves for each segment as shown in Figure 2.14 [73].

This process is done for the three chamber view, four chamber view, two chamber view and the short axis images separately.

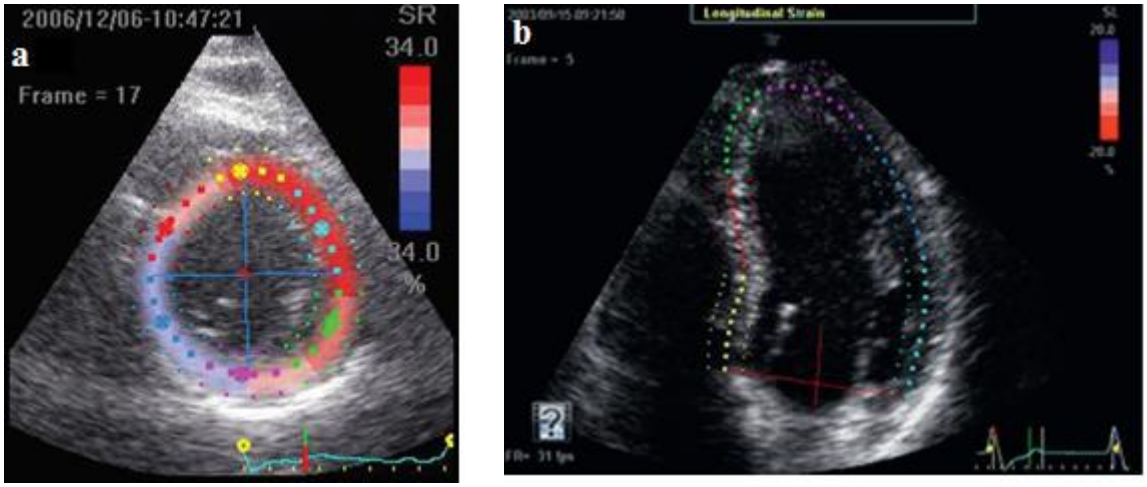

Figure 2.13: Example of tracking of the short axis (a) and longitudinal axis (b) using STE [74, 75]

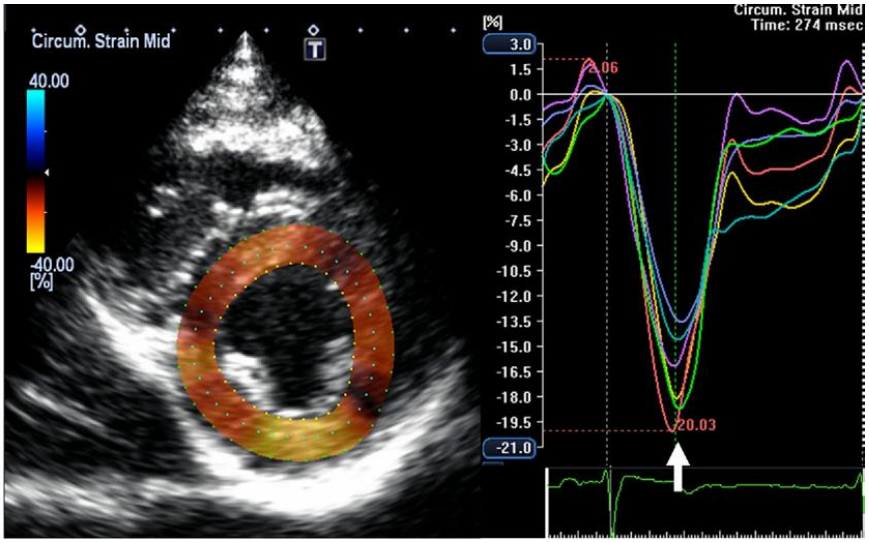

Figure 2.14: Example of Circumferential strain measurement using STE. The strain- time plot of circumferential strain is shown on the right [72].

Speckle Tracking Echocardiography is an established method of determining myocardial strain. It has been validated with Sonomicrometry and myocardial tagging and it has been found to correlate well with both methods [76]. It has also been used in a variety of patient situations for example in the prediction of Sudden Cardiovascular events [12, 77]. Thus it was used as the standard for this project.

Currently, there is 3D Speckle Tracking Echocardiography. This method tracks the motion of speckles in a volume. Therefore in addition to longitudinal strain, circumferential strain, and radial strain, 3D STE also provides information on rotation and twist of the LV [24].

STE is done offline, that is, the images are stored in digital format and analysed offline. However, analysis can also be done online though this has now been restricted to determining longitudinal strain as it is difficult [68].

The advantage of 2D STE over TDI is that it tracks motion in two dimensions and is not limited to the direction of the ultrasound beam, thereby making it angle independent [61]. The weakness with STE however is its high dependency on high image quality. Suboptimal image quality can lead to suboptimal tracking which results in inaccurate strain values. More to that, any artifacts that resemble speckles can affect the speckle tracking quality. TDI becomes advantageous in this regard. Likewise, STE values are also different from vendor to vendor due to the different ways the vendors determine the region of interest and the way the tracking is done [78]. This affects standardization of determination of myocardial function in Echocardiography and Cardiology as a whole.

2.11 MRI Strain Imaging

MRI is superior to Echocardiography due to its high spatial resolution and independence from anatomical windows [79]. Echocardiography is also limited by operator dependency, poor acoustic windows and relatively low sensitivity in the case of subtle abnormalities [80].

A number of techniques have been developed in the area of Cardiac Magnetic Resonance Imaging to measure myocardial strain. Myocardial Tagging is one of them. It is the gold standard for quantification of myocardial deformation [81]. Here, the myocardium being imaged is marked with demagnetization lines or grid patterns using special pulse sequences at the start of the cardiac cycle. The deformation of these lines is then followed throughout the cardiac cycle from which myocardial strain is calculated [82].

There are a number of tagging techniques available. The most used are Harmonic Phase imaging (HARP), Displacement encoding with stimulated echoes (DENSE), Strain encoding (SENC) and Spatial Modulation of Magnetization (SPAMM). However, myocardial tagging is difficult to implement into clinical practice. This is because it is time consuming due to the laborious post processing, complex and require additional sequences. In addition to that, the tagged images have a low spatial and temporal resolution and the tag overlay fades during the cardiac cycle due to T1 relaxation [83].

However, a more practical and a semi-automated technique which does not require additional sequences and is angle independent has been introduced. This method is known as Feature Tracking. It will be covered in detail in the following sections 2.13 and 2.14.

2.12 Feature Tracking

Feature tracking is a 2D post processing software-based technique for determining myocardial deformation (strain, velocity, displacement) from SSFP Cine CMR images. It is the MR equivalent of Speckle Tracking used in Echocardiography.

It works as follows; Cine MR Images are loaded onto the software. The endocardial border or the endocardial and the epicardial borders of the Left Ventricle for example are manually traced in both the long axis and short axis views at the end diastolic phase. The software algorithm then searches for the same features in the subsequent image or frame. Thus the points that make up the trace in the first frame are followed in time through all the frames. This means that motion of the tracked features of the Left Ventricle is followed throughout the cardiac cycle. Myocardial deformation is then quantified [21], [17]. The software uses the method of maximum likelihood to obtain the features on the subsequent frames.

Features tracked by the FT software include the boundary between the cavity and tissue, as well as anatomical structures that are different along the tissue [17].

A modified 16 segment model is applied to the LV during Feature Tracking, which omits the apical cap [84].

The parameters that can be obtained from the software are global, regional and segmental strain, strain rate, velocity, displacement as well as torsion. For reasons of this project, the parameter of interest is strain.

Global parameters are those obtained over the whole LV myocardium. Regional parameters are those measured on the Basal, Mid Ventricular and Apical levels. Segmental Parameters are those values on each of the 16 segments of the LV.

Three software algorithms have so far been developed for Feature Tracking. These are TomTec 2D Cardiac Performance Analysis (TomTec CPA MR) released by TomTec Imaging Systems, Munich, Germany [85], Multimodality Tissue Tracking (MTT) developed by Toshiba, Tokyo, Japan and CMR^{42} Tissue Tracking (CMR^{42} TT) released by Circle Cardiovascular Imaging

Inc. Calgary, Canada. CMR[42] TT was introduced only last year as a Plugin to CMR[42] an already established software for evaluating Cardiovascular MR images. Thus CMR[42] TT is currently being used for research purposes only [86].

2.13 The basis of the Feature Tracking Method

Feature Tracking software method, along with Speckle Tracking in Echocardiography fall under a technique known as Optical Image analysis in advanced image analysis. Feature Tracking in particular is a combination of a border tracking algorithm and a pattern tracking algorithm [87]. The local displacement of a point is the basis of Feature Tracking.

The trace that is made on either the epicardial border or the endocardial border of an MRI image of the heart is a sequence of N points. The tracking of each point is based on a hierarchical algorithm and a combination of 1D and 2D tracking techniques [17]. Lines are drawn across the myocardial border, through each of the points that make up the trace. These lines are called transmural cuts (see Figure 2.15a). Other lines are also marked along the border through the points making up the trace (see Figure 2.15b). Tracking is done in the direction perpendicular to the border being tracked in order to get its displacement.

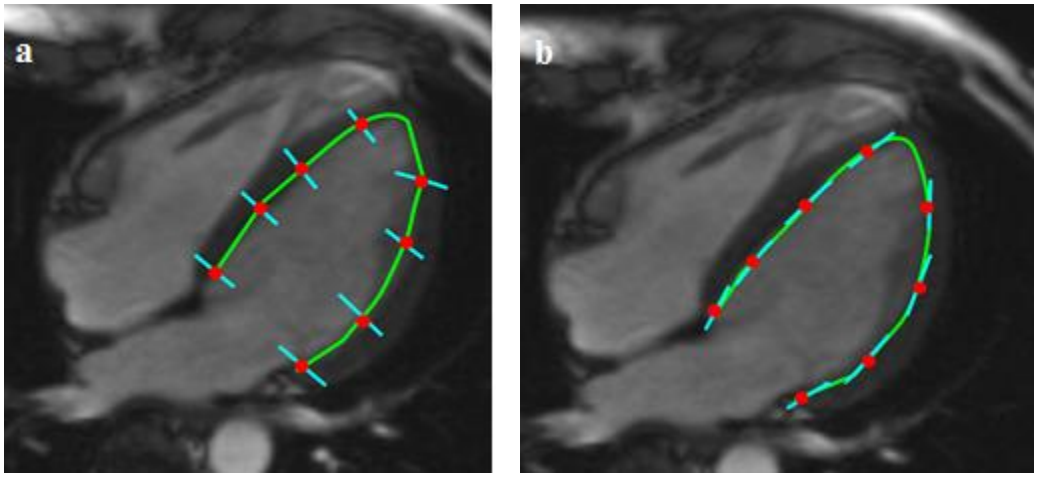

Figure 2.15: Transmural cuts (blue lines) across the myocardial border through points (red dots) in the trace (a) and lines parallel to the trace.

The pixels in the transmural cuts are placed in columns, with each column for one frame of a sequence of images. This can be represented in a space time representation. The thickness of

the transmural cuts is increased in cases of images with low signal to noise ratio. Border tracking is then performed in the space time representation.

2D displacement is then analysed using a standard 2D tracking technique performed for each point on a moving window [17] which contains the point being tracked.

2.14 Statistical Analysis

When a new method is to be measured against an already existing method, their reproducibility is considered. Reproducibility is defined as the degree to which measurements on the same subjects give similar results [88].

Reproducibility consists of Agreement and Reliability. According to Bartlett and Frost [89], Agreement refers to how close two measurements on the same subject are to each other. Reliability on the other hand measures the extent to which subjects are distinguished from one another, despite measurement errors. Reliability relates measurement error to the variation between subjects. If measurement error is small relative to the variation between subjects, then the reliability is high. The reverse is also true [88].

There are three types of reproducibility studies that can be done when comparing a method.

- Repeatability or intraobserver reproducibility; this is done on repeated measurements made by the same observer using the same method on the same subjects after a short period of time.
- Interstudy reproducibility; this is done on measurements made by two different methods by the same observer on the same subject.
- Interobserver reproducibility; this is done on measurements done by two different observers using the same method on the same subject.

3 Materials and Methods

3.1 Volunteer Recruitment

Volunteers participating in an ongoing study of the effectiveness of a Renal Denervation Treatment were chosen for the study. 10 healthy volunteers (1 female and 9 male) were recruited for this study. Volunteers underwent Cardiac Magnetic Resonance scans and thereafter immediately had Echocardiography scans. 6 months later, 8 of the volunteers, all males returned for retests and they underwent Cardiac Magnetic Resonance scans.

Permission to perform the study was granted by the Regional Committees for Medical and Health Research Ethics for the Northern region (REC north) in Norway. The volunteers signed informed consent forms before being recruited for the study.

3.2 Magnetic Resonance Imaging

End-diastolic chamber volume (EDV) and ejection fraction (EF) were measured. MRI studies were performed on a 1.5T Siemens scanner by an experienced radiographer.

Imaging of the entire heart was done using ECG gated breath-hold multishot echo-planar imaging to obtain a stack of short axis cine loops covering the Left Ventricle, and also to obtain images in the long axis. The imaging parameters used are as follows; Echo Time = 1.48 ms, Repetition Time = 74.36 ms, Flip Angle = 80 degrees, Field of View = 340 mm, matrix size = 192 x 134, slice thickness = 8 mm, and temporal resolution = 2.48 ms per cardiac phase, depending on the heart rate.

3.3 Echocardiography (Ultrasound)

Echocardiographic studies were performed by a Vivid E95 scanner using a 2.5 MHz cardiac probe (GE – Vingmed, Horten, Norway) by an experienced cardiologist.

Short axis and apical four chamber, two chamber and three chamber view recordings of the heart were obtained as 2D cine Grayscale loops from 3 consecutive cardiac cycles. The frame rate was between 60-110 frames per second, and second harmonic imaging was used. Care was taken to avoid foreshortening of the myocardium and to optimize endocardial definition [73], [90].

3.4 Speckle Tracking Echocardiography

The strain analysis was performed by the cardiologist who obtained the ultrasound images. B-mode digital gray scale images were analysed using Echopac 2D strain BT12 (GE Vingmed).

Images from the short axis view were used to determine the apical, mid ventricular and basal strain in the radial and circumferential views. Four-chamber view images were used to determine the LV longitudinal strain.

The apical long-axis view was analysed first in order to view the movement of the aortic valve. The timing of the Aortic Valve closure found here was used for timing in the four chamber view. Aortic Valve Closure is considered as the reference point for analysis in STE [68].

The endocardial border was manually traced at end diastole. The software automatically generated the epicardial border, which was then manually adjusted to avoid inclusion of the pericardium. Both borders defined the Region of Interest (ROI) [26]. The software tracked the speckles in all the frames thus forming a cine with traces. These could be viewed to check if the tracking was well done by the software. In case, this wasn't done well, the ROI was edited or in other cases, a new ROI was set. The tracking quality was done for the images and some were excluded from the study due to suboptimal quality. Once the tracking was satisfactory, the strain analysis was done. The software displayed values of segmental and global longitudinal strain which were represented as strain time plots. Analysis of the four chamber view took 2-5 minutes depending on the image quality.

The short axis images were also treated in the same way in order to obtain segmental and global radial and circumferential strain.

3.5 Feature Tracking

Two dedicated software were used, TomTec 2D Cardiac Performance Analysis MR (Image Arena Version 4.6) and CMR^{42} Tissue Tracking plugin (Version 5.2.1).

3.5.1 TomTec 2D Cardiac Performance Analysis MR

Cine MR Images were loaded onto the software. Cine short axis images were selected to determine the radial and circumferential strain at the basal, mid ventricular, and apical levels. The suitable slice that represented the basal level was selected. The endocardial and the epicardial borders were manually delineated in the end diastolic phase as shown in Figure 3.1a. The software algorithm then searched for the same features in the subsequent frames. A 16

segment model which is a modification of the standard 17 segment model with the apical cap removed was applied [70] to the MRI images by the software.

Myocardial strain was calculated and the results were displayed in terms of average values, segmental values and global values of both radial and circumferential strain. A Strain- Time plot was also displayed showing the segmental values and average value of the strain in both the radial and circumferential views. A cine showing the frames with the tracing was viewed in order to check that the tracking was correctly done. If the tracking was unsatisfactory, the endocardial and epicardial borders were edited on the original phase and the strain analysis re-done. Information about the strain was exported as a text file.

A suitable slice was then selected to represent the mid ventricular level and another slice representing the apical levels. The strain values in both levels were obtained the same way as in the basal slice.

Next, the cine longitudinal axis images were loaded onto the software to determine the longitudinal strain. Four chamber view images were used. The endocardial border was delineated as shown in Figure 3.1b. Thereafter, strain analysis was done. The display of results was the same as that in the short axis images. Correction of the trace was also done where necessary and then the strain analysis redone.

Separate strain time plots were obtained for the endocardial and epicardial borders in the circumferential and longitudinal strain views. A combined value of the endocardial and epicardial strain was obtained in the radial view, hence only one strain time plot was displayed.

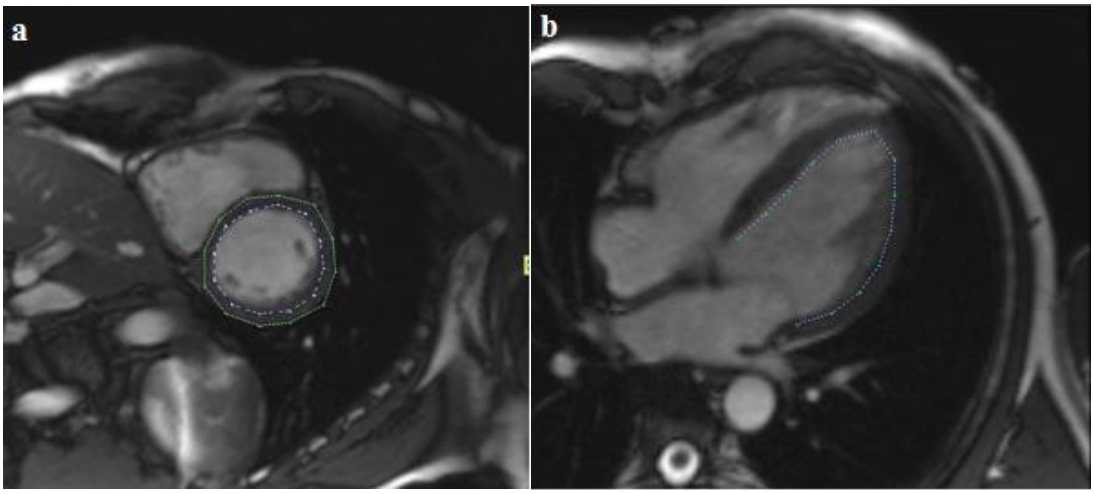

Figure 3.1: Delineation of the endocardial and epicardial border in the short axis view (a) and the endocardial border in the longitudinal axis (b) using TomTec 2D CPA MR

3.5.2 CMR[42] Tissue Tracking

It works in the same way as TomTec 2D CPA MR, however, there are additional steps in the treatment of the short axis and long axis images before obtaining the strain results.

The short axis slices for the basal, mid ventricular and apical levels were selected and then they were demarcated at end diastole and end systole. An example of the demarcation is shown in Figure 3.2a. Short Axis (SAX) reference points were then placed at the superior and inferior insertion points of the right ventricle. These are the blue and pink points in the myocardium wall in Figure 3.2a.

For the long axis images, cine 4 chamber view images were chosen. The LV extent contour was included before demarcating the endocardial and epicardial borders to identify the basal slice. It stretched to the level of the mitral valves. This is the blue structure in Figure 3.2b. Figure 3.2b shows what the longitudinal axis looks like after placing the different traces on the MRI image.

The software also divided the LV into 16 segments as in TomTec 2D CPA MR. The strain analysis was then done. Like TomTec 2D CPA MR, segmental values were displayed on a 16 segment model and a strain – time plot was obtained displaying both segmental and global strain.

In CMR[42] TT, separate values of the endocardial and epicardial traces are obtained for the circumferential, longitudinal and radial views.

A report containing the segmental strain values, as well as global, endocardial, and epicardial strain values of the radial, circumferential, and longitudinal orientations was created in single document. This report was exported in text file or XML format. A selection of results could also be copied and pasted to an Excel spreadsheet.

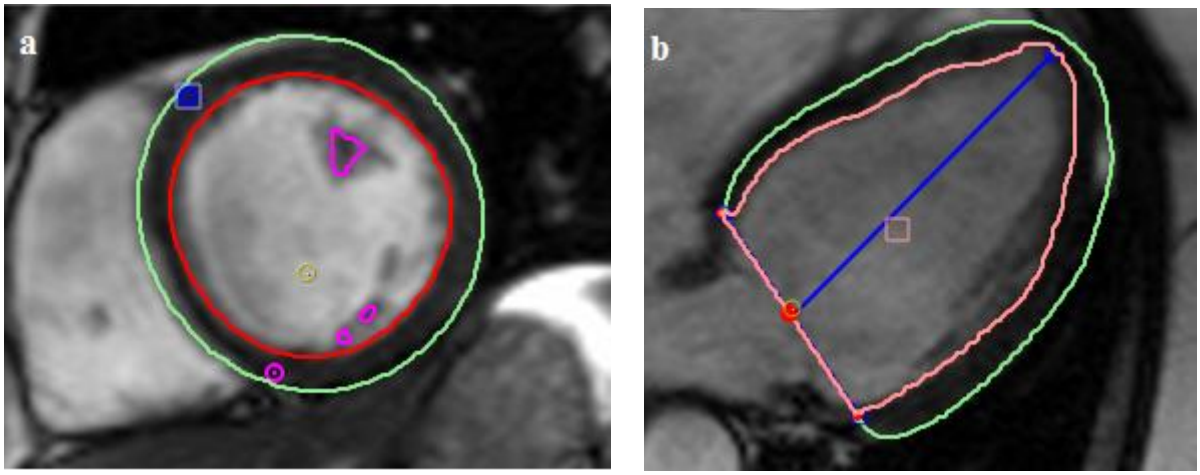

Figure 3.2: Tracing of the endocardial and epicardial borders in the short axis (a) and the long axis (b) views using CMR^{42} TT.

3.6 Statistical Analyses

Statistical analyses were performed using IBM SPSS Statistics version 22, Microsoft Excel and MedCalc software version 16.4.

The strain values are presented in terms of mean ± standard deviation. The criteria for significance was $p < 0.05$. Normality was tested for using Shapiro Wilk test.

The different software algorithms were denoted as follows.

- Echopac 2D strain BT12 - STE
- TomTec 2D Cardiac Performance Analysis MR – TomTec 2D CPA MR
- CMR^{42} Tissue Tracking – CMR^{42} TT

Comparison was done along the following axes in order to answer the questions set at the start of the project:

- **Comparison between methods**

A One-way ANOVA was conducted to compare the effect of strain measurement method on the strain values obtained thereby testing the null hypothesis which is 'MRI based strain gives the same results as ultrasound based strain'. The effect size of the differences between the strain values as portrayed by the results from the ANOVA test was then calculated for using eta squared. It is given by the formula [91]:

$$Eta\ squared = \frac{Sum\ of\ squares\ between\ groups}{Total\ sum\ of\ squares} \quad (3.1)$$

- **Comparison between observers**

Two observers who will be identified as Mercy, the author of the thesis, and Tommy, a radiologist as St. Olav's hospital each took strain measurements using TomTec 2D CPA MR at different times. They were blind to one another's analysis. Interobserver reproducibility of TomTec 2D CPA MR was then determined using Coefficient of Variation (CV) and graphically using Bland Altman plots [92].

- **Comparison of two measurements obtained using the same method by the same observer (test-re-tests)**

Two sets of strain measurements were obtained using CMR[42] TT by Mercy. These measurements were taken four weeks apart and intraobserver reproducibility was assessed using the Coefficient of Repeatability (CR), the Intraclass Correlation Coefficient (ICC) and graphically using Bland Altman plots [92].

- **Comparison between MRI measurements**

As earlier mentioned, MRI scans were run twice on 8 of the volunteers. The period between the two measurements was 6 months. The second round of MRI measurements will be referred to as Control measurements while those from the first round of MRI measurements will be referred to as Baseline measurements. A Kruskal Wallis test was run to analyse the difference between strain values from TomTec 2D CPA MR and CMR[42] TT for the Control measurements.

The Interstudy reproducibility was determined using the Coefficient of Variation (CV) and graphically using Bland Altman plots [92].

- **Comparison between modalities**

This was done by taking the average of the results obtained from the FT software methods and comparing them with those from ultrasound to assess the bias.

- **Contribution of factors to the variance**

In each comparison, there are different factors that led to the variance in the strain values. In order to determine which of the factors contributed the greatest to the variance in the strain values, the Coefficient of Variation (CV) values corresponding to the different factors were compared.

Association between the differences and means in the Bland Altman plots was checked for by testing whether the correlation coefficient between the differences and the means were significantly different from zero [89]. This has to be checked for because one of the assumptions of Bland Altman analysis is that there should be no correlation or association between the differences and mean of the two methods. In case that correlation exists, then the data has to be transformed and thereafter the means and differences recalculated from the transformed data.

The scatter diagrams showing the nature of results obtained from the above comparisons are presented in the Appendix section.

The parameters obtained from the statistical analysis are defined as follows;

- **Bias:** The bias is the mean of the difference of the two measurements being compared.
- **Limits of agreement (LOA):** The Limits of Agreement give the range where 95% of differences will be found in case future measurements are made on the two methods. They are calculated as $mean \pm (1.96 * SD)$ [93].
- **Coefficient of Repeatability (CR):** The Coefficient of Repeatability (CR) is a measure of agreement in repeatability studies. It gives the maximum value of the difference that will exist between two methods that will be observed in case of future measurements [89]. The coefficient of repeatability was determined to quantify the agreement between the test-retest measurements using CMR[42] TT and it is given as twice the standard deviation of the differences, calculated by the formula [92];

$$CR = 2 \times \sqrt{\frac{\sum (Differences)^2}{n}} \tag{3.2}$$

- **Coefficient of Variation (CV):** This is given by the standard deviation of the differences divided by the mean [94]. This was the measure of reproducibility in this project.

- **Intraclass Correlation Coefficient (ICC):** It is a measure of reliability. For ICC > 0.74, reliability is excellent, for ICC = 0.60 – 0.74, it is good, for ICC = 0.40 – 0.59, it is fair, and lastly for ICC < 0.4, reliability is poor [95]

4 Results

4.1 Display of Results

A color coded plot of strain versus time is displayed in Figures 4.1 and 4.2 for TomTec 2D CPA MR, each color representing one segment of the short axis level being measured (basal, mid-ventricular or apical). The white curve which is marked with the black arrows for all the three strain views represents the average value of the segmental strain. The Figure 4.1 below shows the apical strain in the radial (top half) and circumferential (bottom half) views for volunteer PWV 207. On the left, the peak systolic segmental strain and time to peak segmental strain for each segment is displayed.

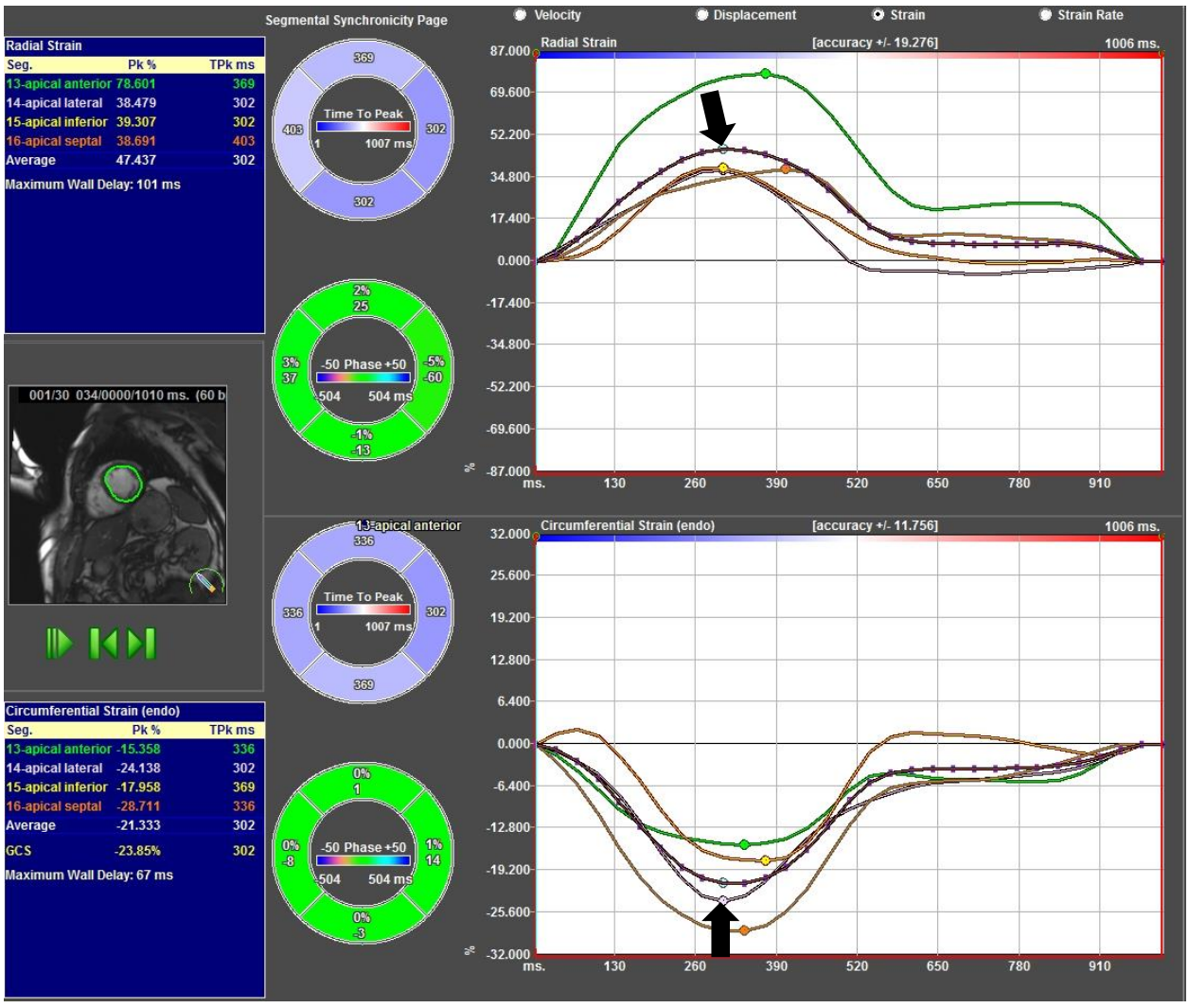

Figure 4.1: Radial strain and Circumferential strain in TomTec 2D CPA MR.

Figure 4.2 shows the display of the results obtained in the longitudinal view of the Left Ventricle.

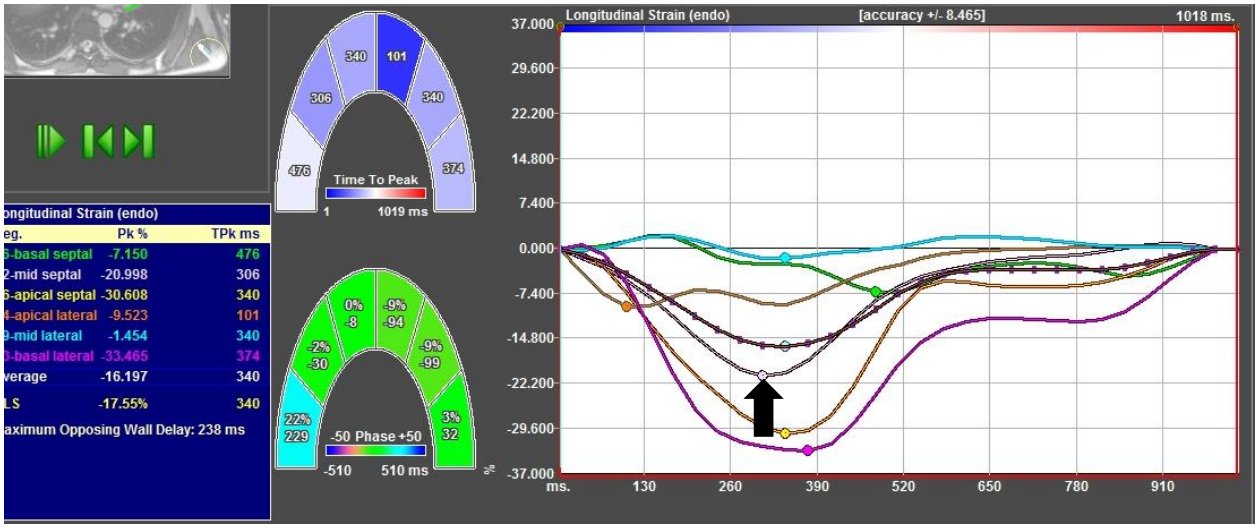

Figure 4.2: Longitudinal strain in TomTec 2D CPA MR

In CMR[42] TT, a single plot of strain versus time is displayed. There is also a display of the 16 segments, each of the segments marked with the respective segmental strain. The resulting display of the results from both the Short axis (radial and circumferential) and longitudinal axis strain views is shown in the Figures 4.3 and 4.4.

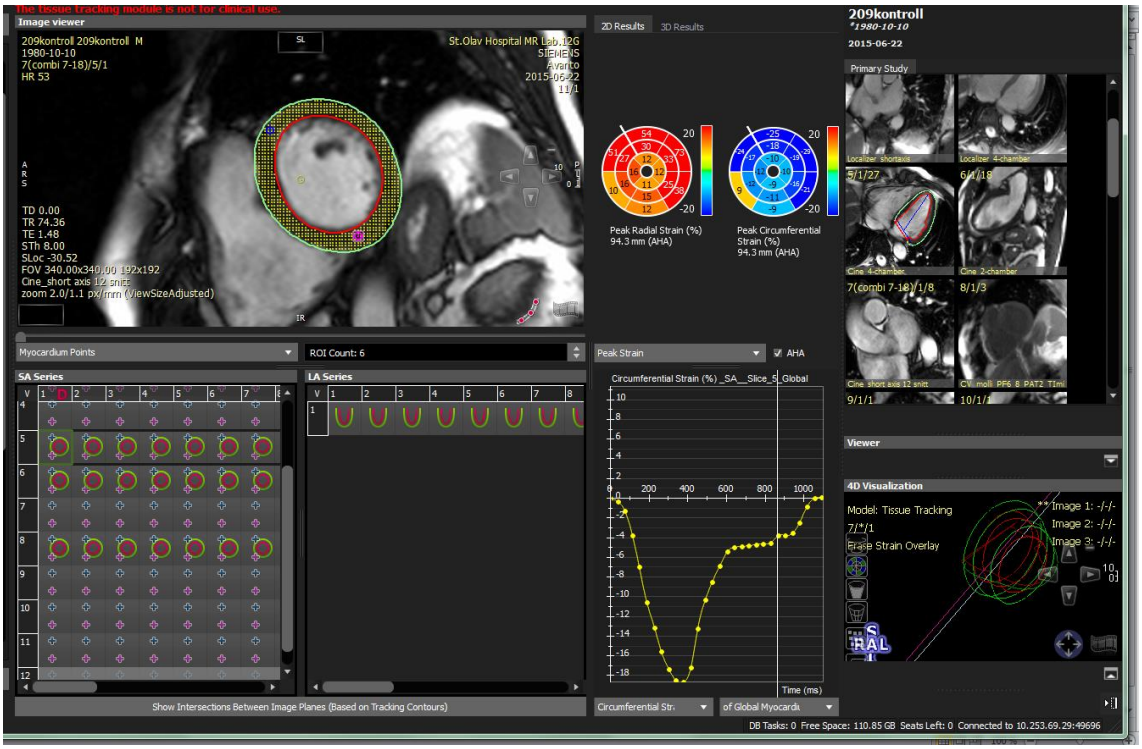

Figure 4.3: Radial and circumferential strain in CMR[42] TT

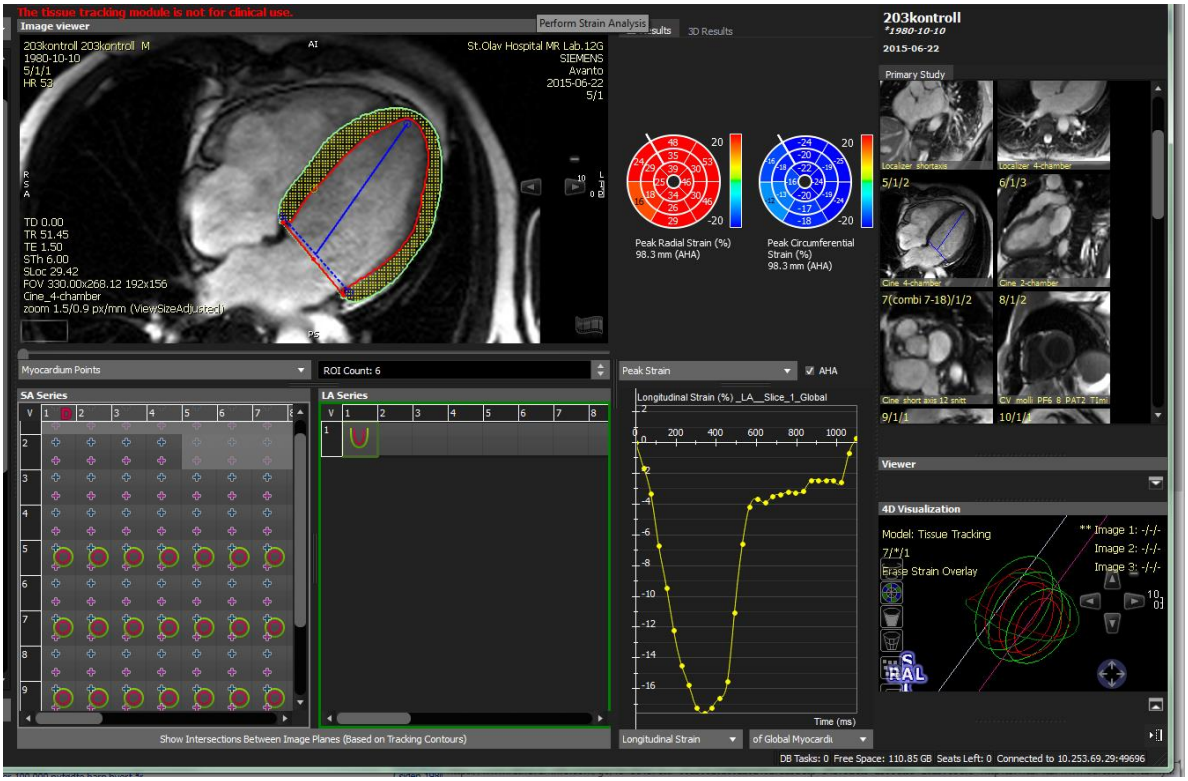

Figure 4.4: Longitudinal strain in CMR[42] TT

4.2 Volunteer Characteristics

Table 4.1 below shows the characteristics of the volunteers. They are presented as mean ± standard deviation. These measurements were done using MRI.

Table 4.1: Table showing the volunteer characteristics.

Parameter	**Result**
Number of volunteers	10
Body Mass Index (BMI)	24.98 ± 1.75
Heart rate (s^{-1})	58 ± 8.69
LV end diastolic volume(ml)	194.8 ± 53.93
LV end systolic volume(ml)	75.7 ± 30.21
Ejection fraction (%)	61.9 ± 8.319

4.3 Overall Results

The results from the different software and the different axes of comparison done in this project as stated in the materials and methods chapter were all combined into three graphs of global strain versus volunteers. These graphs are shown below where Figure 4.5 contains global radial strain values, Figure 4.6 contains global circumferential strain values, and Figure 4.7 contains global longitudinal strain values.

For each of the graphs, the bigger symbols stand for the first MRI measurements in the case of TomTec 2D CPA MR and CMR^{42} TT, and the smaller symbols stand for the strain values from the second MRI measurements, which were done six months later as explained in the Materials and Methods Chapter. It should also be noted that only 8 out of the 10 had second measurements.

Otherwise, the meaning of the symbols is as follows;

○ - Global strain values obtained by Mercy using TomTec 2D CPA MR

○ - Global strain values obtained by Tommy using TomTec 2D CPA MR

○ - Global strain values obtained by Mercy using TomTec 2D CPA MR (Second MRI measurement)

○ - Global strain values of obtained by Tommy using TomTec 2D CPA MR (Second MRI measurement)

△ - Global strain values obtained by Mercy using CMR^{42} TT

△ - Global strain values obtained by Mercy using CMR^{42} TT (Second MRI measurement)

✳ - Global strain values obtained by Mercy using CMR^{42} TT on the second round of the same MRI measurements.

□ - Global strain values obtained using STE

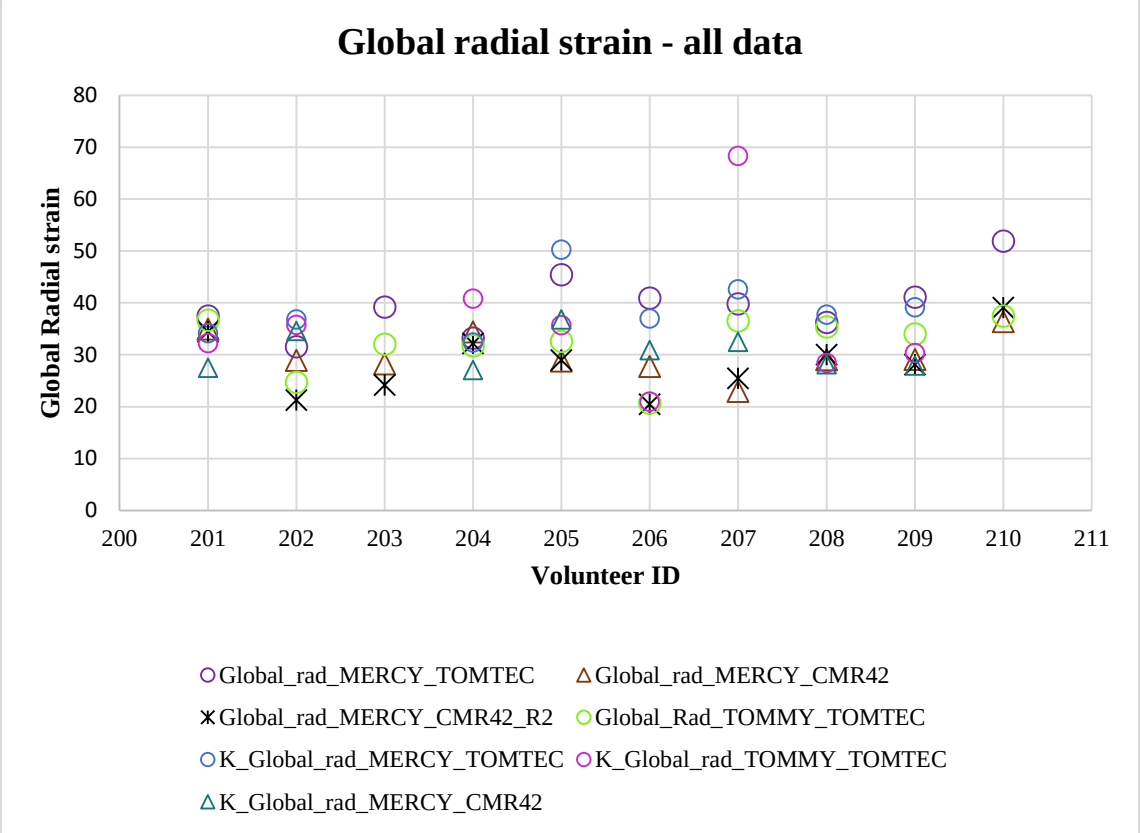

Figure 4.5: Graph showing the global radial strain results from all software, operator and retest measurements.

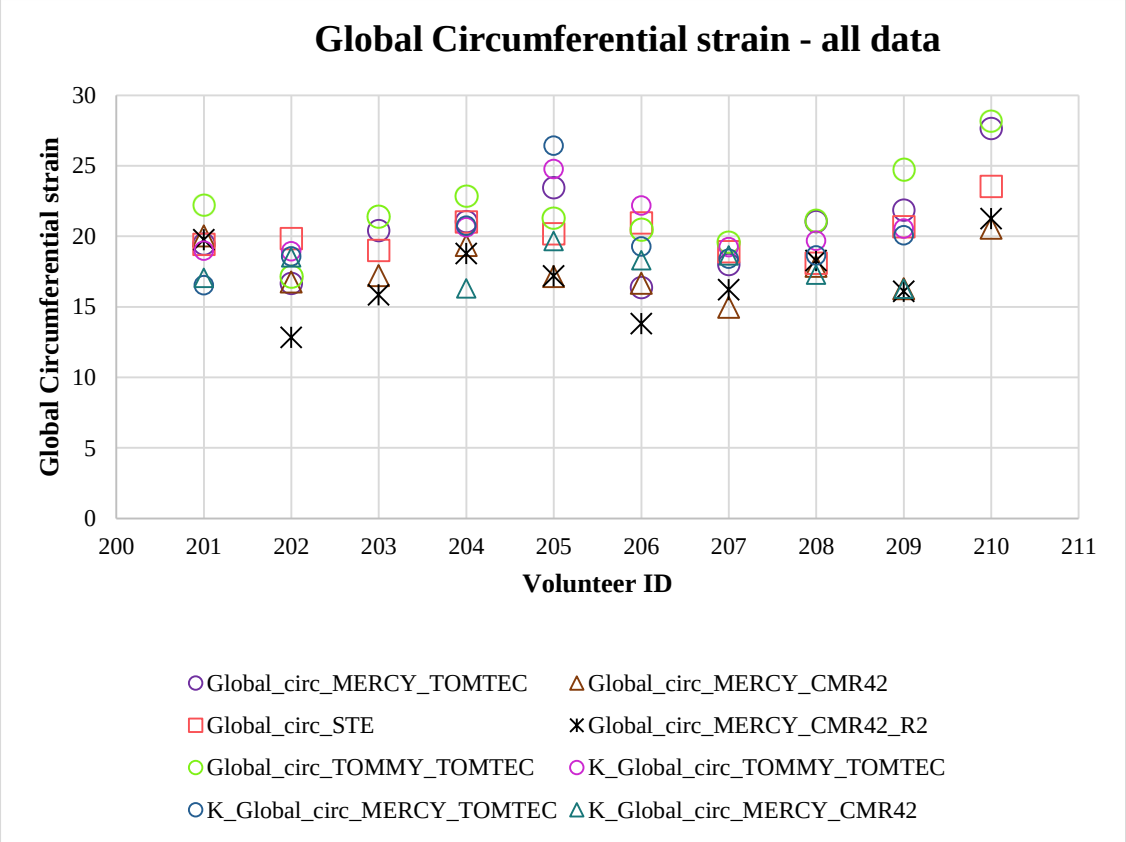

Figure 4.6: Graph showing the global circumferential strain results from all software, operator and retest measurements.

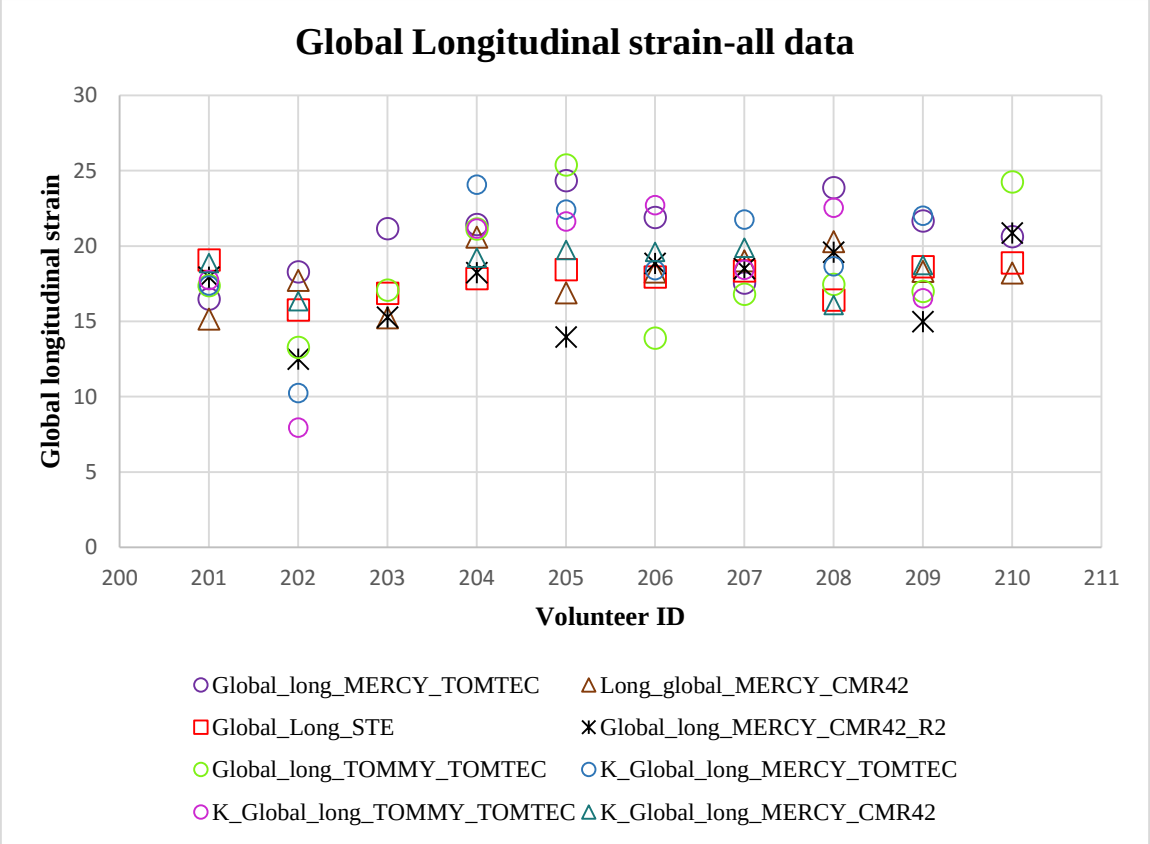

Figure 4.7: Graph showing the global longitudinal strain results from all software, operator and retest measurements.

The ranges of strain values from all the comparisons as shown in Figures 4.5, 4.6 and 4.7 in the radial, longitudinal and circumferential views are;

- Radial strain = 20.45% to 68.35%
- Circumferential strain = - 12.85% to - 28.19%
- Longitudinal strain = - 7.94% to - 25.38 %

Thus, the values of the radial strain have the greatest variation while the values of the circumferential strain have the smallest variation. In addition to that, there is an outlier on one control radial strain measurement of volunteer PWV 207.

Volunteers PWV 205 and PWV 206 have the largest variation in their strain values. Volunteer PWV 201 has the smallest variation in the strain values from all the different comparisons.

Across the volunteers, there is a similar trend in the strain values for each volunteer in all the three strain axes. For example, PWV 201 has higher strain values than PWV202, then the values increase in volunteers PWV 203, PWV 204, and peak at PWV 205. There is a decrease

after that till 207. Lastly, there is a rise in the strain values all the way up to volunteer PWV 210.

4.4 Comparison of strain measurement method

The mean and standard deviation of the strain values obtained from all the methods of strain measurement are shown in Table 4.2 below;

Table 4.2: Table showing the strain values obtained from the three different methods

Global strain in %	**TomTec 2D CPA MR**	**CMR^{42} TT**	**STE**
Circumferential strain	20.61 ± 3.35	17.69 ± 1.77	20.18 ± 1.52
Longitudinal strain	20.74 ± 2.58	17.97 ± 1.83	17.82 ± 1.11
Radial strain	39.7 ± 5.88	30.05 ± 4.05	Not robust

The data was checked for normality and homogeneity of variances and it was found that the data was normally distributed and that the variances were homogeneous.

Results from the One-way ANOVA were significant for circumferential [$F_{(2, 27)} = 4.465$, $p = 0.021$], longitudinal [$F_{(2, 27)} = 7.181$, $p = 0.003$] and radial strain [$F_{(1, 18)} = 18.820$, $p = 0.000$] for all the three strain measurement methods.

Post hoc comparison was done using Tukey Honestly Significant Difference (HSD) to see which of the pairs of the strain measurements was significantly different from another. The results from that are shown in Table 4.3 below.

Table 4.3: Table showing the comparison between the different strain measurement methods as determined using Tukey HSD.

	***P*-value**	
Comparison between groups	**Circumferential Strain**	**Longitudinal strain**
TomTec Vs CMR^{42} TT	0.026*	0.010*
TomTec Vs STE	0.913	0.006*
CMR^{42} TT Vs STE	0.064	0.985

*= *P*-value is significant at 0.05 level

Post hoc comparisons could not be done for radial strain values by SPSS because there were no values from STE.

The results in Table 4.3 indicate that the longitudinal strain values are statistically different in STE and TomTec 2D CPA MR, while the circumferential strain values are not statistically different. In the comparison between STE and CMR^{42} TT, both circumferential strain values and longitudinal strain values are not statistically different. Comparison of both FT software methods (TomTec 2D CPA MR and CMR^{42} TT) shows a statistically significant difference in the values of both the longitudinal and circumferential strain.

The effect size for all the three strain views is 0.2 for circumferential strain, 0.3 for longitudinal strain, and 0.5 for radial strain.

A second One-way ANOVA test was run excluding the STE values to see the effect of strain measurement method on the radial strain. The results, as tabulated in Table 4.4 show that both TomTec 2D CPA MR and CMR^{42} TT give significantly different values of the radial strain with $F_{(1,18)} = 5.929$, $F_{(1,18)} = 7.649$ and $F_{(1,18)} = 18.280$.

Table 4.4: Table showing the *P*-values from the comparison of TomTec 2D CPA MR and CMR^{42} TT.

	***P*-value**		
Comparison between groups	**Circumferential strain**	**Longitudinal Strain**	**Radial Strain**
TomTec Vs CMR^{42} TT	0.026*	0.013*	0.000*

*=*P*-value is significant at the 0.05 level

4.5 Comparison of strain values from different observers

The mean strain values from the two observers are tabulated below (see Table 4.5).

Table 4.5: Table showing the mean strain values in all views from two observers (Mercy and Tommy) that used TomTec 2D CPA MR.

Global strain in %	**Observer 1 (Mercy)**	**Observer 2 (Tommy)**
Radial strain	39.70±5.88	32.19±5.47
Circumferential strain	20.61±3.35	21.90±2.98

Longitudinal strain	20.74±2.58	18.37±4.02

Tabulated in Table 4.6 is the information obtained from the interobserver reproducibility test of TomTec 2D CPA MR. In this table, it can be noted that the circumferential strain has the narrowest LOA (±3.43%), followed by longitudinal strain (±7.41%), and the radial strain has the widest LOA (±12.78%).

Circumferential strain has the smallest bias, followed by the longitudinal strain, and then the radial strain. The bias is not systematic, that is to say, for circumferential strain, the values of the second observer (Tommy) were higher than those of the first observer (Mercy), while for the longitudinal and radial strains, the values of the Mercy were higher than those of Tommy. This bias is statistically significant in both the radial and circumferential strain while in the case of longitudinal strain, it is not statistically significant.

Table 4.6: Table showing the values of various parameters obtained from the interobserver reproducibility of TomTec 2D CPA MR.

Strain View	Bias (%)	LOA (%)	CV (%)	*P*-value
Radial Strain	7.51	-5.27 to 20.29	19.13	0.0054*
Circumferential Strain	-1.3	-4.72 to 2.13	7.00	0.0437*
Longitudinal Strain	2.37	-5.04 to 9.78	15.54	0.0789

* = *P*-value is significant at 0.05 level, LOA= Limits of Agreement, CV=Coefficient of Variation

Figure 4.8 contains the Bland Altman plots illustrating the interobserver reproducibility of TomTec 2D CPA MR in the radial (a), circumferential (b), and longitudinal (c) views. No correlation is observed between the differences and the means of the strain values.

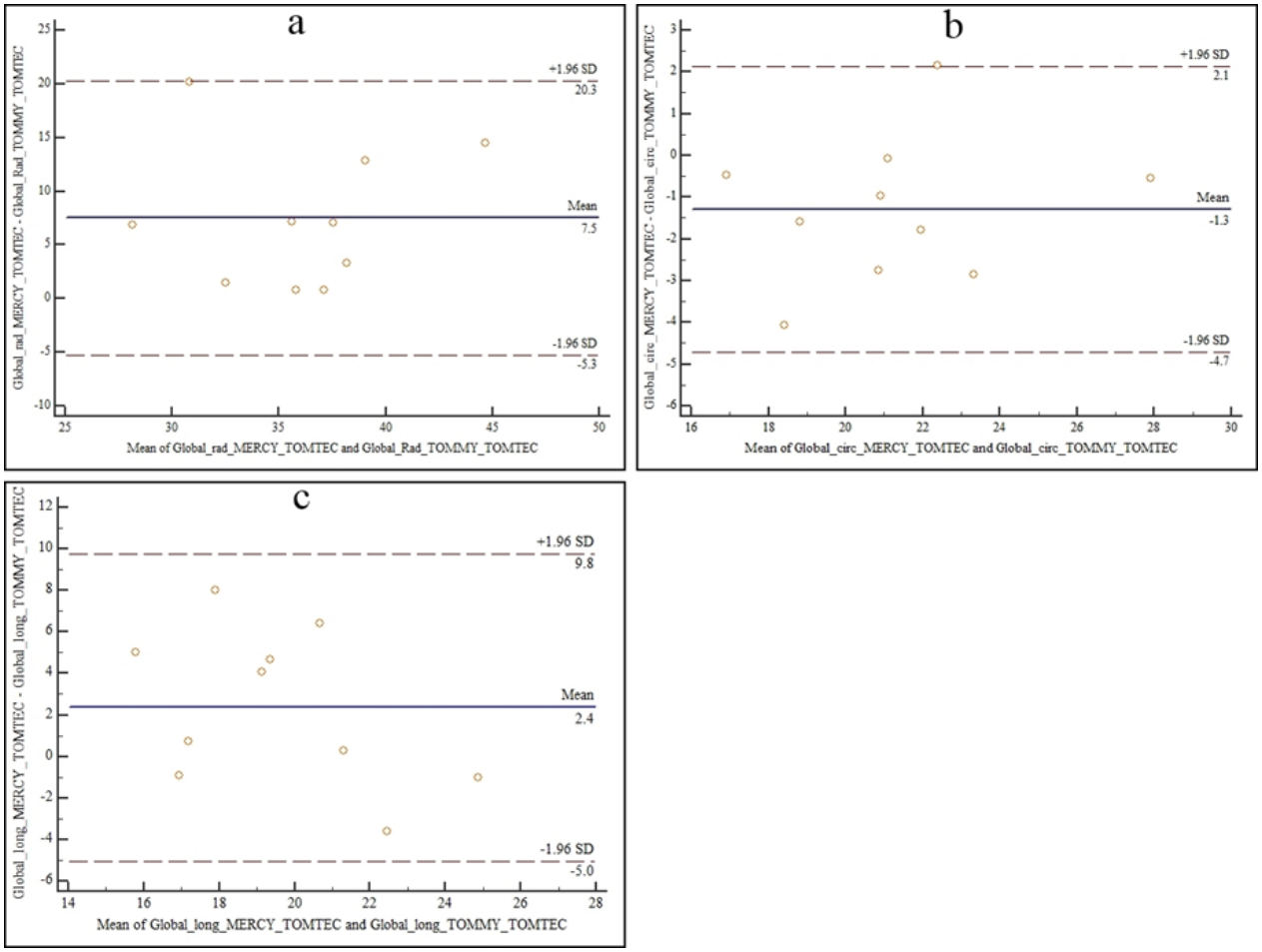

Figure 4.8: Bland Altman plots showing comparisons of radial (a), circumferential (b) and longitudinal (c) strain values from the two observers.

4.6 Comparison of two measurements using the same method by the same observer (test-re-tests)

Table 4.7 below contains the mean strain values obtained from two rounds of strain measurement using CMR[42] TT by the same observer (Mercy).

Table 4.7: Table displaying the mean strain values obtained from two rounds of measurement using CMR[42] TT by the same observer (Mercy)

Global strain in %	**Test 1**	**Test 2 (Re-test)**
Radial Strain	30.05±4.05	28.42±5.86
Circumferential Strain	17.69±1.77	17.02±2.60
Longitudinal Strain	17.96±1.83	17.07±2.71

The intraobserver reproducibility test results are presented below in Table 4.8. It can be seen that circumferential strain has the lowest CR, followed by the longitudinal strain and then the radial strain. Intraobserver agreement is therefore highest in circumferential strain since it has the lowest CR and lowest in radial strain with the largest CR.

Reliability was quantified by the Intraclass Correlation Coefficient (ICC). According to the classification used in [95], intraobserver reliability is excellent in radial strain and circumferential strain, while in longitudinal strain, intraobserver reliability is fair.

Table 4.8: Table showing the parameters from the Bland Altman plots assessing the intraobserver reproducibility of strain values obtained from CMR[42] TT.

Strain View	**CV (%)**	**ICC (95% CI)**	**CR**
Radial Strain	9.33	0.83 (0.38 to 0.96)	7.56
Circumferential Strain	6.81	0.84 (0.41 to 0.96)	3.27
Longitudinal Strain	10.54	0.54 (-0.70 to 0.88)	5.12

CI= Confidence Interval, CV= Coefficient of Variability, ICC= Intraclass Correlation Coefficient

The Bland Altman plots showing the intraobserver reproducibility of CMR[42] TT are shown below in Figure 4.9 a (radial strain), b (circumferential strain) and c (longitudinal strain). No correlation between the differences and mean was obtained.

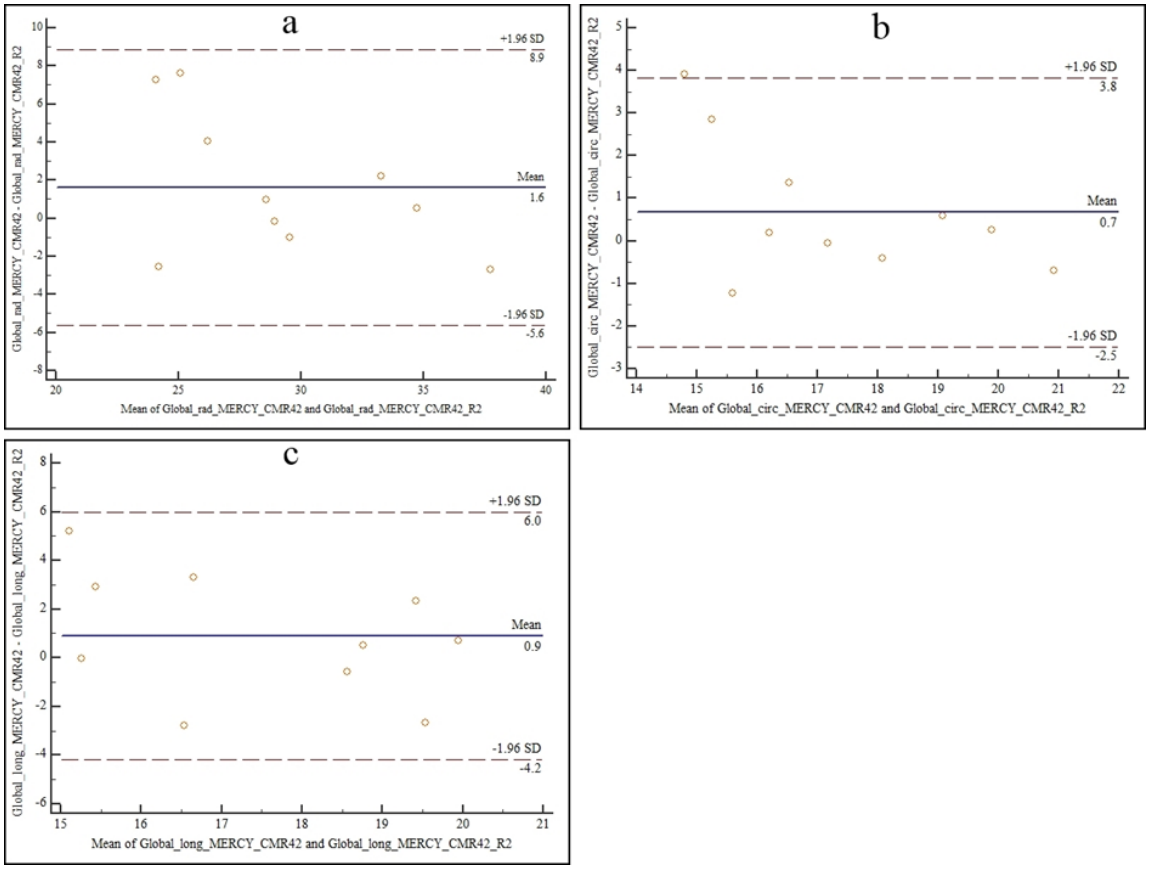

Figure 4.9: Bland Altman plots showing comparisons of two radial (a), two circumferential (b) and two longitudinal (c) strain values obtained using CMR^{42} TT

4.7 Comparison of two MRI measurements

The mean strain values of the Baseline and Control measurements obtained using TomTec 2D CPA MR are shown below in Table 4.9;

Table 4.9: Table showing the strain values of Control measurements obtained using TomTec 2D CPA MR and CMR^{42} TT

Global strain in %	**TomTec 2D CPA MR**	**CMR^{42} TT**
Radial Strain	38.76±5.58	30.68±3.65
Circumferential strain	19.84±2.94	17.77±1.21
Longitudinal strain	19.37±4.36	18.56±1.50

Normality tests carried out on the control measurements showed that they are not normal.

A Kruskal-Wallis test carried out to see if the results obtained from comparing the TomTec 2D CPA MR and CMR[42] TT were the same as those obtained from the Baseline measurements showed that the strain values of TomTec 2D CPA MR are greater than those of CMR[42] TT in all cases. The circumferential strain [H (1) = 3.574] has a mean rank of 10.75 for TomTec 2D CPA MR, and 6.25 for CMR[42] TT. Longitudinal strain [H (1) =0.397] has a mean rank of 9.25 for TomTec 2D CPA MR and 7.75 for CMR[42] TT, and the radial strain [H (1) =8.040] has a mean rank of 11.88 for TomTec 2D CPA MR and 5.13 for CMR[42] TT. The significance levels of the above observations are tabulated below in Table 4.10.

Table 4.10: Table showing the *P*-values obtained from the Kruskal-Wallis test analysis of Control strain measurements

	***P*-value**		
Comparison between groups	**Circumferential strain**	**Longitudinal Strain**	**Radial Strain**
TomTec Vs CMR[42] TT	0.059	0.529	0.005*

*=*P*-value is significant at the 0.05 level.

From the Table 4.10 above, the circumferential strain values and longitudinal strain values are not statistically different while the radial strain values are statistically different.

Results from the Interstudy reproducibility tests done to compare the baseline and control measurements from TomTec 2D CPA MR and CMR[42] TT are shown in Figure 4.10 and Table 4.11, and Figure 4.11 and Table 4.12 respectively. In the Bland Altman plots, no correlation between the differences and the means is acquired.

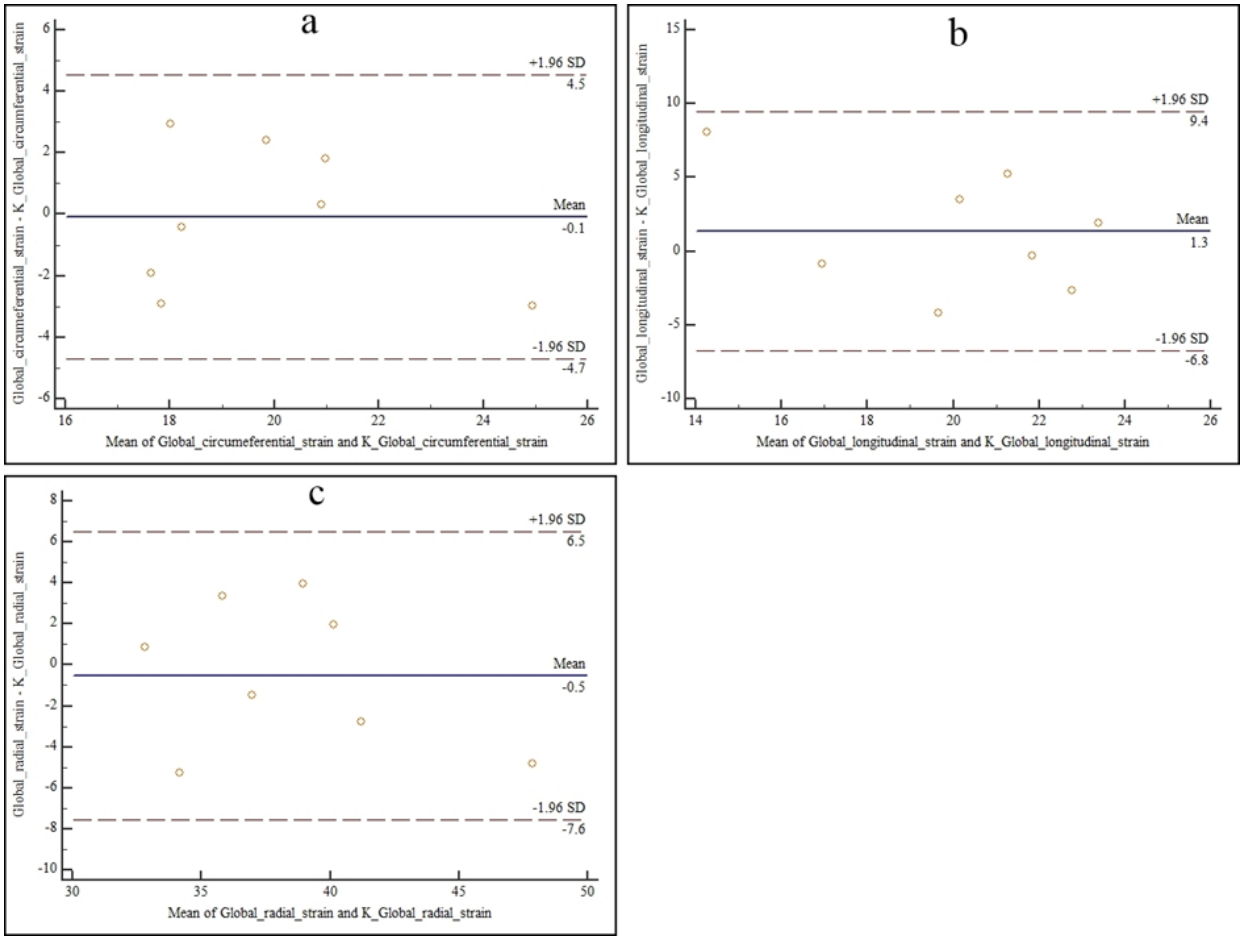

Figure 4.10: Bland Altman plots of Baseline and Control circumferential (a), longitudinal (b) and radial (c) strain measurements using TomTec 2D CPA MR

Table 4.11: Table showing the interstudy reproducibility of the MRI measurements using TomTec 2D CPA MR

Strain View	**Bias (%)**	**LOA (%)**	**CV (%)**	***P*-value**
Radial Strain	-0.52	-7.56 to 6.52	6.24	0.6943
Circumferential Strain	-0.09	-4.71 to 4.53	7.88	0.9148
Longitudinal Strain	1.33	-6.77 to 9.43	14.44	0.3917

LOA=Limits of Agreement, CV=Coefficient of Variation

From Table 4.11 and Figure 4.10, it can be noted that there is a bias observed in the comparison of the strain values from the MRI measurements using both TomTec 2D CPA MR, though it was not systematic. Circumferential strain has the smallest bias, followed by the radial strain and then the longitudinal strain.

In terms of the Limits of Agreement, the circumferential strain has the narrowest LOA (±4.62%), followed by the radial strain (±7.04%) and lastly the longitudinal strain (±8.10%). The radial strain has the lowest CV (6.24%). It is followed by the circumferential strain (CV=7.88%) and lastly, the longitudinal strain (CV=14.44%).

Below are the Bland Altman plots for the comparison of strain results from CMR[42] TT.

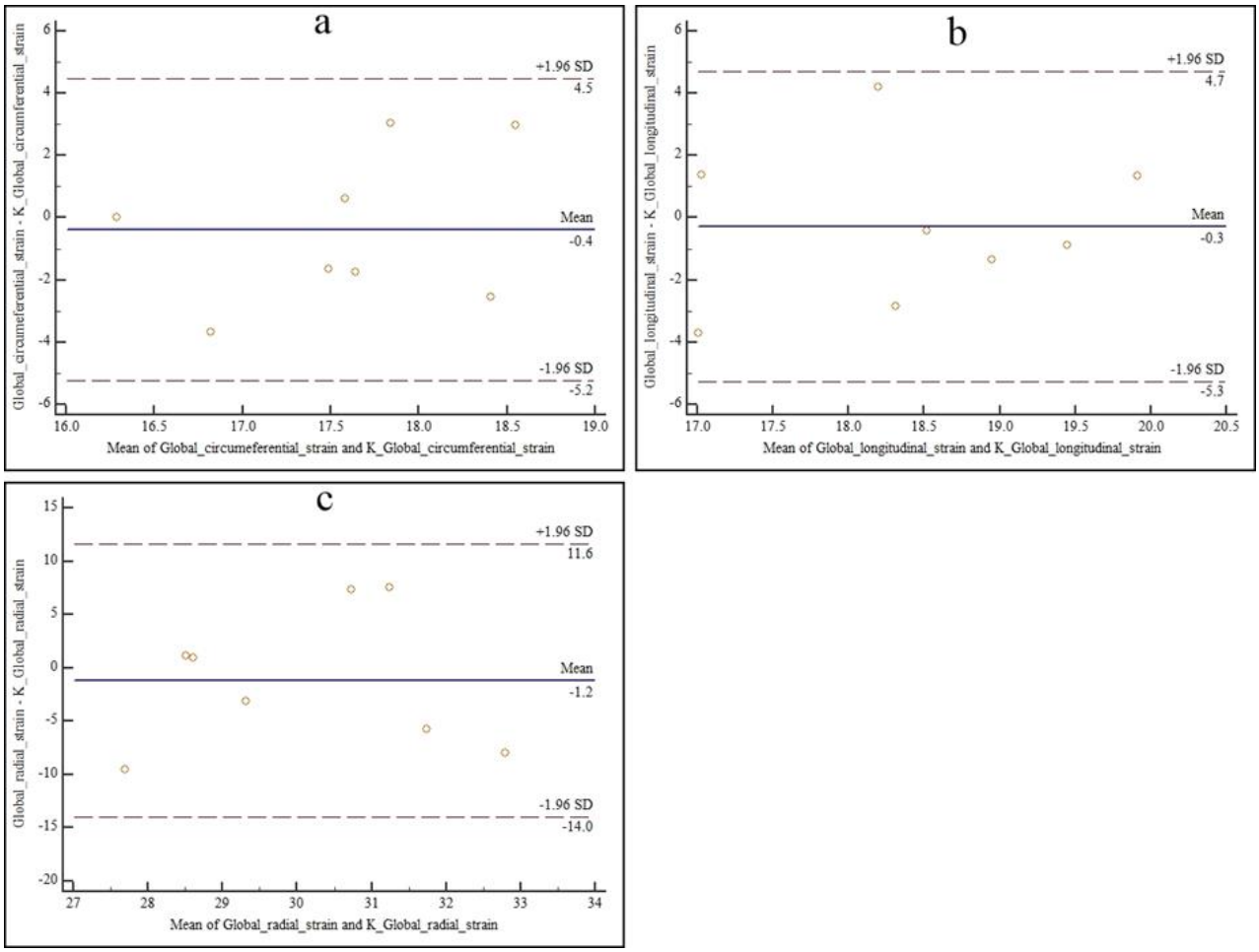

Figure 4.11: Bland Altman plots of Baseline and Control circumferential (a), longitudinal (b) and radial (c) strain measurements using CMR[42] TT

Table 4.12: Table showing the interstudy reproducibility of the MRI measurements using CMR[42] TT

Strain view	**Bias (%)**	**LOA (%)**	**CV (%)**	***P*-value**
Radial Strain	-1.19	-13.99 to 11.60	14.63	0.6210
Circumferential Strain	-0.38	-5.24 to 4.48	9.45	0.6796
Longitudinal Strain	-0.28	-5.27 to 4.71	9.22	0.7641

LOA=Limits of Agreement, CV=Coefficient of Variation

For CMR[42] TT, the bias is systematic, with circumferential strain having the lowest bias, which is followed by the longitudinal strain and lastly the radial strain. Circumferential strain has the narrowest LOA (±4.86%), followed closely by the longitudinal strain (±4.99%) and lastly the radial strain (±12.89%). In terms of CV, the longitudinal strain has the lowest value (CV=9.22%), followed by the circumferential strain (CV=9.45%), and lastly the radial strain (CV=14.65%).

The mean strain values of the Baseline measurements and Control measurements from TomTec 2D CPA MR and CMR[42] TT are displayed below in Table 4.13 and 4.14.

Table 4.13: Table showing the mean strain values of baseline and control measurements from TomTec 2D CPA MR.

Global strain in %	**Baseline**	**Controls**
Radial strain	38.24±4.54	38.76±5.58
Circumferential strain	19.75±2.55	19.84±2.94
Longitudinal strain	20.70±2.92	19.37±4.36

Table 4.14: Table showing the mean strain values of Baseline and Controls obtained using CMR[42] TT.

Global strain in %	**Baseline**	**Control**
Radial strain	29.48±3.81	30.68±3.65
Circumferential strain	17.39±1.65	17.77±1.21
Longitudinal strain	18.28±1.77	18.56±1.50

4.8 Comparison of modalities

The comparison between MRI and ultrasound is illustrated graphically below.

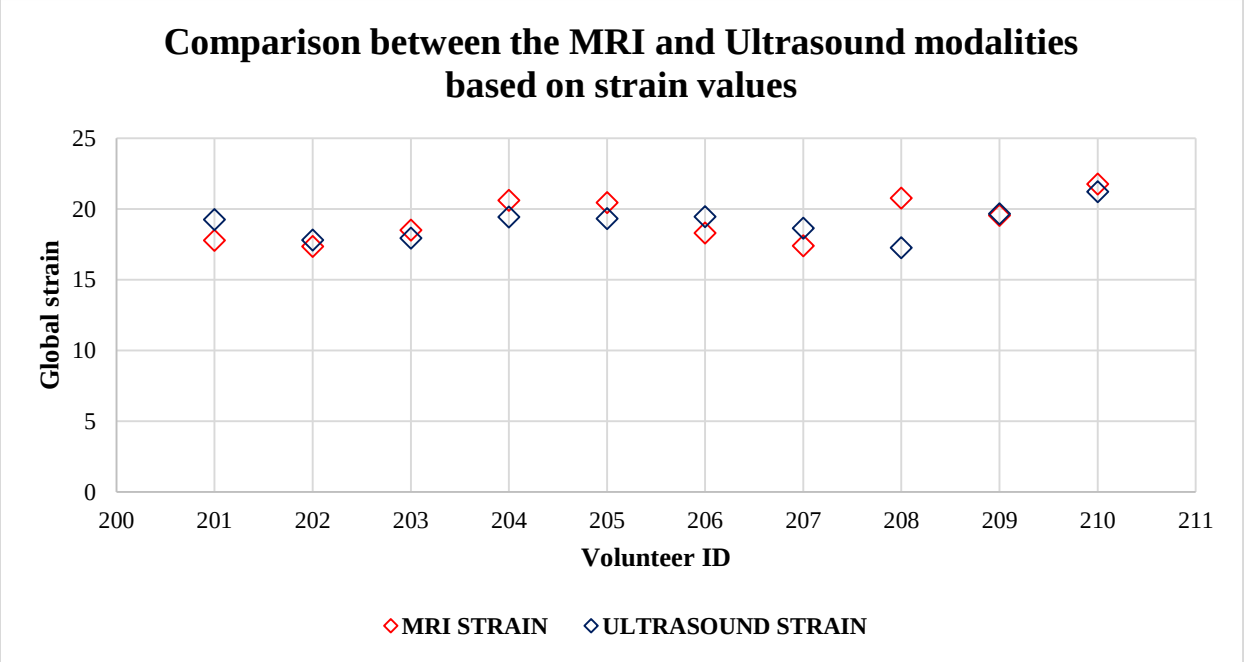

Figure 4.12: Graph comparing Ultrasound and MRI basing on strain values

From the Figure 4.12, it can be noted that there exists a bias between the two modalities. This bias is not systematic and it varies across the different volunteers with Volunteer PWV 209 having close to no bias at all. The bias is the largest in PWV 208.

4.9 Additional comparisons

4.9.1 Interstudy Reproducibility

A scientific paper released by Altman and Bland [96] states that comparison of means "give little information on the accuracy of the results." ANOVA only tests for significance and does not give information on the bias between the two methods. With this found information during the course of the project, an interstudy reproducibility was therefore carried out to determine the agreement between the FT software methods and STE, and also between the FT software methods.

Tabulated below in Tables 4.15, 4.16 and 4.17 are the results from the different comparisons.

4.9.1.1 Comparison of TomTec 2D CPA MR and STE

Table 4.15: Interstudy reproducibility of TomTec 2D CPA MR and STE

Strain View	Bias (%)	LOA (%)	CV (%)	*P*-value
Circumferential Strain	0.43	-5.02 to 5.87	9.26	0.6377

Longitudinal Strain	2.91	-2.88 to 8.71	14.83	0.0124*

* = *P*-value is significant at 0.05 level, LOA= Limits of Agreement, CV=Coefficient of Variation

Table 4.15 shows that the bias between TomTec 2D CPA MR and STE is smaller in circumferential strain, and large in longitudinal strain. In terms of LOA, circumferential strain had the smaller LOA (±5.44%), and the LOA in longitudinal strain are slightly higher (±5.81%). The CV values follow the same trend with circumferential strain having the lower CV and longitudinal strain having the higher CV.

It is also observed that the bias is significant in longitudinal strain but not in circumferential strain.

The above results in Table 4.15 are shown graphically below in Figure 4.13. The differences and mean have no association.

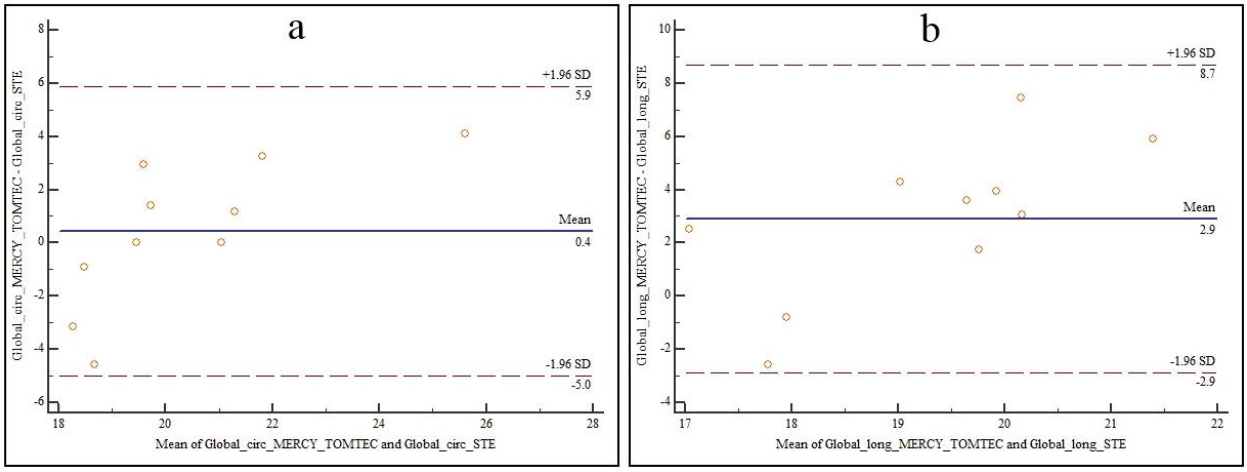

Figure 4.13: Bland Altman plots showing the interstudy reproducibility of TomTec 2D CPA MR and STE in circumferential (a) and longitudinal (b) views

4.9.1.2 Comparison of CMR[42] TT and STE

The Table 4.16 below portrays that the bias in the longitudinal strain is smaller than that of the circumferential strain, and it is not systematic. The bias is significant in the case of the circumferential strain. However, the LOA are smaller in circumferential strain (±3.31%) than

in longitudinal strain (±4.51%). Longitudinal strain has a lower value of CV than the circumferential strain.

Table 4.16: Interstudy reproducibility of CMR[42] TT and STE

Strain View	Bias (%)	LOA (%)	CV (%)	*P*-value
Circumferential Strain	-2.49	-5.80 to 0.82	11.06	0.0012*
Longitudinal Strain	0.14	-4.37 to 4.65	8.64	0.8475

* = *P*-value is significant at 0.05 level, LOA= Limits of Agreement, CV=Coefficient of Variation

The interstudy reproducibility of CMR[42] TT and STE is shown graphically below in Figure 4.14. The differences and means have no association.

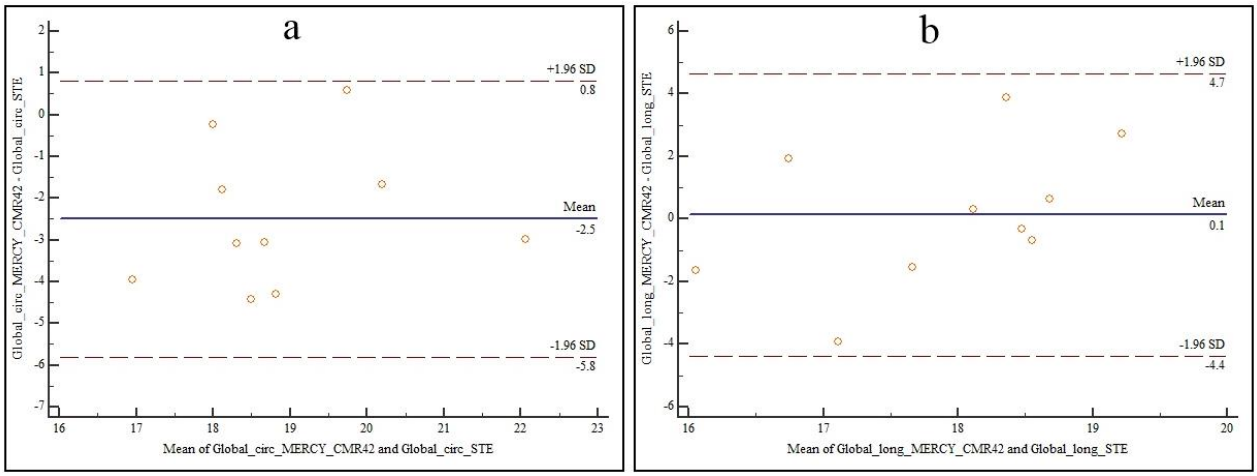

Figure 4.14: Bland Altman plots of interstudy reproducibility of CMR[42] TT and STE in circumferential (a) and longitudinal (b) views

4.9.1.3 Comparison of TomTec 2D CPA MR and CMR[42] TT

Table 4.17: Interstudy reproducibility of TomTec 2D CPA MR and CMR[42] TT.

Strain View	Bias (%)	LOA (%)	CV (%)	*P*-value
Radial Strain	9.65	-3.06 to 22.37	23.21	0.0011*
Circumferential Strain	2.92	-2.50 to 8.34	14.49	0.0087*
Longitudinal Strain	2.77	-2.38 to 7.92	13.62	0.0088*

*=*P*-value is significant at 0.05 level, LOA= Limits of Agreement, CV=Coefficient of Variation

In the comparison of the two Feature Tracking software algorithms, the bias is smallest in the longitudinal strain, which is followed closely by the circumferential strain and then the radial strain as displayed in Table 4.17. This bias is statistically significant in all the three strain views. The LOA are smallest in the longitudinal strain (±5.15%), followed by the circumferential strain (± 5.42%) and lastly the radial strain (± 12.72%). In terms of CV, longitudinal strain has the smallest value, followed by the circumferential strain and lastly the radial strain.

Below in Figure 4.15 are the Bland Altman plots for the interstudy reproducibility of TomTec 2D CPA MR and CMR[42] TT. In this case however, a correlation was observed between the differences and the means. Transformation of data did not improve results, therefore it was assumed that the within subject Standard Deviations are unequal as recommended by Bartlett and Frost [89]. In that way, there is no relationship between the bias and true value. One can then proceed with the analysis.

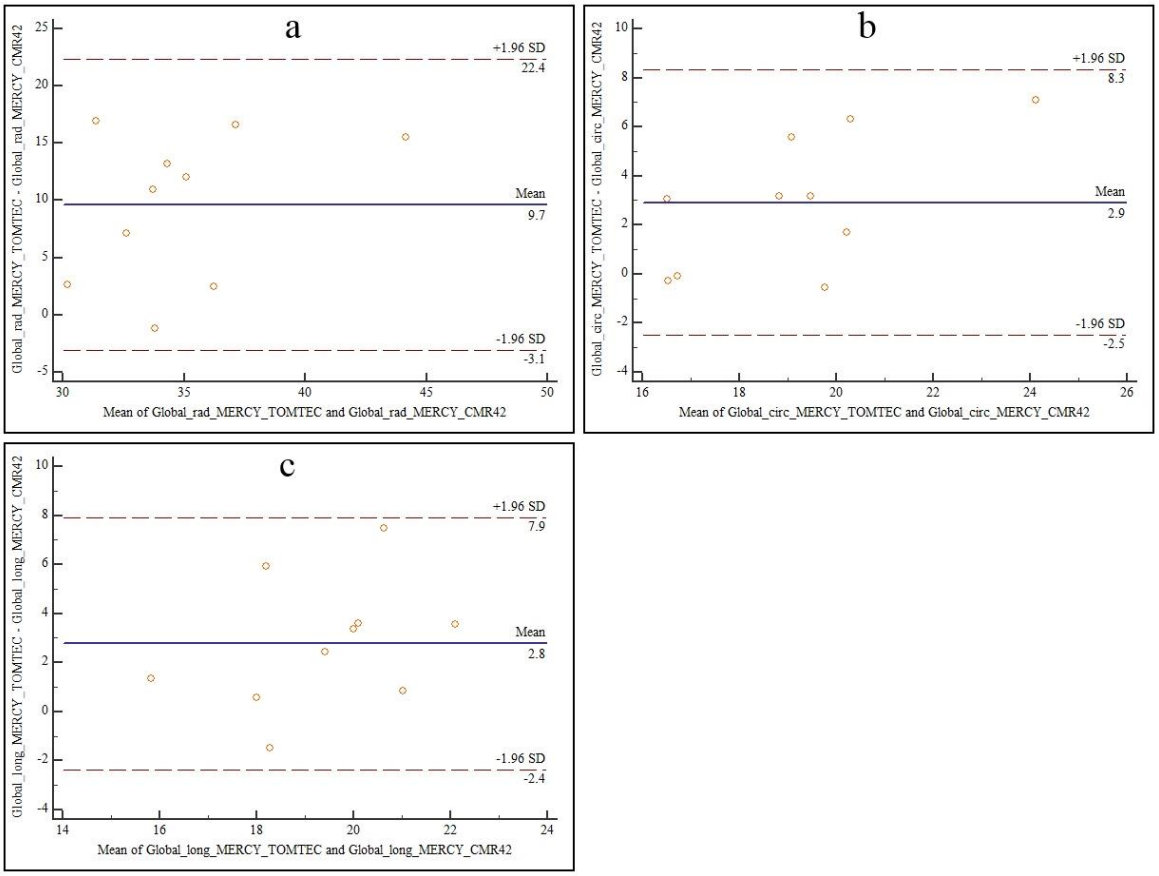

Figure 4.15: Bland Altman plots of Interstudy Reproducibility of TomTec 2D CPA MR and CMR[42] TT in the radial (a), circumferential (b), and longitudinal (c) views

4.9.2 Kruskal-Wallis test

The Kruskal-Wallis test was performed on the Baseline measurements to see if the statistical significance varied from the one obtained using One-way ANOVA. It was also done to have a leveled ground to compare the significance of Baseline and Control measurements.

The results from running this analysis are shown below in Table 4.18. The values of strain from TomTec 2D CPA MR and CMR[42] TT differ statistically in all the three strain views.

Table 4.18: Table showing the p-values obtained from the Kruskal-Wallis test analysis of Baseline strain measurements

	***P*-value**		
Comparison between groups	**Circumferential strain**	**Longitudinal Strain**	**Radial Strain**
TomTec Vs CMR[42] TT	0.028*	0.019*	0.001*

*=*P*-value is significant at the 0.05 level.

4.10 Contribution of factors to the variance

Five different comparisons were assessed to determine the greatest contributor to the variance. From these, five equations of variance were formed;

Five different comparisons were. The variance obtained in these different comparisons are;

a) $$Var\left(intraobserver\right) = Var\left(test - retest\right) \quad (4.1)$$

b) $$Var\left(interobserver\right) = Var\left(test - retest\right) + Var\left(observer\right) \quad (4.2)$$

c) $$Var\left(MRI\ measurements\right) = Var\left(test - retest\right) + Var\left(re - measurement\right) \quad (4.3)$$

d) $$Var\left(FT\ versus\ STE\right) = Var\left(test - retest\right) + Var\begin{pmatrix} paired\ measurement \\ of\ method \end{pmatrix} + Var\left(each\ software\right) \quad (4.4)$$

e) $$Var\left(FT\ software\right) = Var\left(test - retest\right) + Var\left(each\ FT\ software\right) \quad (4.5)$$

All the CV values from the several factors that led to variance in the different comparisons are presented below in Table 4.19.

Table 4.19: Table showing the CV values from the different comparisons

	STRAIN VIEW- CV VALUES IN %		
COMPARISON	**CIRCUMFERENTIAL**	**LONGITUDINAL**	**RADIAL**
Var(test-retest)	6.81	10.54	9.33
Var(observer)	7.00	15.54	19.13
Var [2 MRI (TomTec)]	7.88	14.44	6.24
Var[2 MRI (CMR^{42})]	9.45	9.22	14.63
Pairwise Method comparison			
Var(TomTec Vs STE)	9.26	14.83	
Var(CMR^{42} Vs STE)	11.06	8.64	
Var(TomTec Vs CMR^{42})	14.49	13.62	23.21

TomTec refers to TomTec 2D CPA MR, CMR^{42} refers to CMR^{42} TT, 2 MRI refers to MRI Re-measurement.

Table 4.19 is used in the Discussion chapter, Section 5.9.

5 Discussion

5.1 All Strain data graphs

The variation in the results in the different strain views as stated by the ranges of strain in section 4.3 and seen in the graphs (Figure 4.5, 4.6, and 4.7) can be attributed to the structure of the heart wall. As already explained in Section 2.3 of the theory chapter, the heart wall is made up of the midmyocardium which is circumferentially oriented, and the subendocardium along with the subepicardium which are longitudinally oriented. The midmyocardium is greater in mass than the subepicardium and the subendocardium. Conversely, none of the fibers in the myocardium wall is radially oriented. The radial strain measurement is taken across the thickness of the myocardium wall with the fibers running perpendicular to the measurement hence the high variation.

The outlier seen on the control radial strain measurement of volunteer PWV 207 in Figure 4.5 can be accounted for as an error made by the observer who took the strain measurement.

The variation of strain values observed in each volunteer could be the result of the variance of one or more factors. These factors include the observers who took the measurements, and the inherent variability of the methods used to determine the strain.

The difference in average strain values across the volunteers despite the fact that all are healthy is due to their differences in physical characteristics. For example, the values of strain are dependent on the age and gender of the volunteers [68]. A study done by Andre, Steen [84] showed that the men had a higher radial strain than women, while the circumferential and longitudinal strains were lower in men than in women. Cardiac factors such as the size of the Left Ventricle and the wall thickness can also affect the strain values [97].

5.2 Comparison of strain measurement method

The One-Way ANOVA test was run to assess the differences in strain values obtained from TomTec 2D CPA, CMR[42] TT and STE. The F-statistic or F-ratio in ANOVA is a measure of the variance of the group means, divided by the variance between groups. When the F-statistic is equal to 1, it signifies that there is no variance between the group means and the null hypothesis is true. Thus, the closer it is to 1 or the smaller it is, the smaller the variance between the group means, and the farther it is from 1 or the larger it is, the greater the variance between the group means [91]. The groups in this case are the three different strain determination

methods (TomTec 2D CPA MR, CMR[42] TT and STE). Therefore, from the results of the One-way ANOVA test in Section 4.4, the circumferential strain results from the three measurement methods vary the least while those from the radial strain vary the most even though only two methods were considered in this view. The reason is still due to the structure of the heart wall as explained in the previous Section 5.1 and Section 2.3.

Judging also from the effect size, the values were big for all strain groups in accordance with the classification from Cohen implying that the statistical difference in the different groups is real [98]. This arose due to the F ratio being statistically different between any two pairs of the strain measurement methods. Thus there was a need for pairwise comparisons to determine which of the pairs of measurements were statistically different (see Table 4.3).

The statistical difference of the strain values from TomTec 2D CPA MR and CMR[42] TT as shown in Tables 4.3 and 4.4 poses a challenge in the determination of strain in clinical practice because these methods do not give similar values and so cannot be interchangeably used. This result shows that the software algorithms need to be improved in order to produce similar strain values.

A study carried out by Almutairi, Zemrak [27] to compare the two methods in measuring strain of hypertensive patients, also showed a statistically significant difference in the circumferential strain but no trend in radial and circumferential strain. Comparing the FT software methods with a gold standard would shed some light on which is closer to the accepted values of strain, thus the comparison with Speckle Tracking Echocardiography, which in this thesis was considered as the gold standard. This also confirms the differences obtained in the current study as true.

As already stated in the Results Chapter, Table 4.3 shows a difference in the trend of statistical significance of the strain views when TomTec 2D CPA MR is compared with STE, and when CMR[42] TT is compared with STE. The similarity of all longitudinal and circumferential strain values between CMR[42] TT and STE, which is not the case in TomTec 2D CPA MR suggests that CMR[42] TT could be a more accurate FT strain measurement method than TomTec 2D CPA MR.

Unfortunately, due to the absence of the radial strain values in STE, the comparison of the FT methods cannot be made with STE in that particular strain view which would have provided a complete comparison of the strain methods. Post hoc comparisons could not be done for the radial strain view because the radial values in STE were not robust enough to be included in

this study. However, this is not something new. The inaccuracy of the radial strain values has been attributed to the fact that there are fewer speckles in the radial direction compared to other directions in the ultrasound image [24]. This also highlights the advantage of MRI over Ultrasound in terms of determining myocardial strain.

Similar preceding studies that compare Speckle Tracking Echocardiography and Feature Tracking in the determination of myocardial strain assess the agreement and reliability between the methods, and do not analyse the differences in means [25, 87]. The reason is that the difference in means does not give a complete picture on the comparison between two methods. Two methods may not have similar results but may agree. Also, the comparison of means tells very little about the accuracy of a measurement. The accuracy of a measurement is determined by its bias [99]. Thus, Altman and Bland [96] advise the usage of agreement rather than comparison of means. This was later done in this project. The results are tabulated in section 4.9.1 (see Tables 4.15- 4.17), and the discussion of results is presented later on in this chapter in Section 5.7.

5.3 Comparison of strain values from different observers

The results obtained in Table 4.6 indicate that the interobserver reproducibility of TomTec 2D CPA MR varies greatly in terms of the strain view with circumferential strain having the highest reproducibility while radial strain having the lowest reproducibility. The low values of bias and LOA in the longitudinal and circumferential views suggests that agreement is higher in those views than in the radial view.

A previous study using the same software-based method, TomTec 2D CPA MR also showed a similar variability in the reproducibility of the strain values [22]. According to that study, the fact that radial strain has the lowest reproducibility is attributed to the fact that the values of strain are obtained from a concurrent tracking of both the epicardial and endocardial regions of the radial view. This is not the case in longitudinal strain and circumferential strain where the endocardial and epicardial regions of the LV are tracked separately thus giving separate values of endocardial and epicardial strain which can be averaged to give one value of longitudinal strain and circumferential strain.

In CMR^{42} TT however, the radial strain is calculated at both the epicardial and the endocardial regions separately so in case there was an assessment of interobserver reproducibility, it is probable that it would be more reproducible than it is in TomTec 2D CPA MR.

The structure of the heart wall as already explained in Sections 2.3 and 5.1 also cannot be ruled out when looking at the reasons for variability in the interobserver reproducibility of TomTec 2D CPA MR.

A good reproducibility of circumferential and longitudinal strain has also been observed in the comparison of Feature Tracking and myocardial tagging [21]. This is worth noting because myocardial tagging is currently the standard for measuring myocardial strain in the field of MRI as earlier mentioned in this thesis. This shows the circumferential view as the most reproducible strain view in general.

The existence of the bias between the strain values from the different observers as shown in Table 4.6 could be because of the difference in training that the observers had on the software. The difference in training is due to the fact that both observers did not spend an equal time on the software. The existence of a bias is also attributed to the fact that the basal, mid ventricular and apical levels are determined by the observer and not the software method used, therefore the strain values are subject to differences depending on the observer's choice of image to analyse the strain and how the tracing of the endocardial and epicardial borders is done.

In comparison with STE, Cheng, Larson [100] carried out a study to test for reproducibility of STE with a sample of 20 subjects with varying cardiovascular burden. For interobserver reproducibility, none of the biases from the three strain views was statistically significant. The longitudinal and circumferential strains were highly reproducible both with CV < 4.00% while the radial strain was the least reproducible strain with CV <8.00%. However, all the three strains had ICC > 0.80 thereby implying a high reliability of STE. This study involved three observers though, but it does give a fair representation of the interobserver reproducibility of STE, as there is limited literature available on the reproducibility of STE.

Comparing the interobserver reproducibility of STE and that of FT software methods shows that it is similar in terms of the trend with circumferential and longitudinal strains being highly reproducible and radial strain being the least reproducible.

On the whole, looking at the Coefficient of Variation values, the interobserver reproducibility of TomTec 2D CPA MR is good.

Other sources of variance include the inherent variability of the software-based method in this case, TomTec 2D CPA MR.

5.4 Comparison of two measurements using the same method by the same observer (test-re-tests)

Assessing intraobserver reproducibility in terms of CV shows that circumferential strain is the most reproducible strain as indicated by its low CV which is demonstrated in Table 4.8. This finding is consistent with available literature from past studies done on healthy volunteers and patients [101, 102]. In all those studies, TomTec 2D CPA MR was used and not CMR^{42} TT as there is currently no intraobserver reproducibility test on CMR^{42} TT. This project is the first to do so. On the other hand, the consistency with past literature shows that CMR^{42} TT could be a credible FT software algorithm.

As shown in Table 4.8, the longitudinal strain is the least reproducible strain, having a CV that is slightly higher than that of radial strain. The past studies on the intraobserver reproducibility of Feature Tracking cited above however show that radial strain is the least reproducible strain. Despite the fact that in those studies, TomTec 2D CPA MR was used and not CMR^{42} TT, the trend of reproducibility is expected to be the same owing to the structure of the heart wall as already explained in Section 2.3. However, since two values of the radial strain, that is from the epicardial and the endocardial borders of the LV are obtained with CMR^{42} TT, and not in TomTec 2D CPA MR as noted by Taylor, Moody [22], this could have made its reproducibility better.

Ideally the CV should be zero. However, it is non-zero due to the fact that the initial stages of the strain analysis are manually done as already discussed. The manual tracing is therefore subject to differences. On top of that, both measurements are done in a sufficiently apart time for the observer not to recall how she traced the MRI images during the first analysis.

In comparison with STE, an intraobserver reproducibility study of STE on 20 healthy adults by Oxborough, George [103] showed that overall, myocardial strain had a high interobserver reproducibility except for radial strain which had a very high CV of 19.00%, unlike circumferential strain (CV=7.00%) and longitudinal strain (CV=6.00%). Though the intraobserver reproducibility was done on two acquisitions of the ultrasound images rather than two strain measurements on the same images, the trend of reproducibility is the same. In the area of STE, longitudinal strain is the most reproducible strain because it is measured along the direction of the ultrasound beam [78]

The CV values in STE and CMR^{42} TT are not very different from each other. However, in the case of radial strain, the difference in the CV values is 10%. This difference is very big and can

be attributed to the insufficient tracking of STE. Despite that, the trend of reproducibility is the same in STE and in CMR[42] TT.

The low values of CV indicate that intraobserver reproducibility in CMR[42] TT is high. This is attributed to the fact that the same observer will delineate the borders of the LV in almost the same way unlike in the interobserver reproducibility where each observer has their own way of delineating the endocardial and epicardial borders, depending on their level of experience with the software and the MRI images.

Other sources of variations include the inherent variability of the software-based method.

5.5 Comparison of two MRI measurements

The two MRI measurements were taken in order to determine whether the measurements had an effect on the turnout of the strain values using the FT software methods.

The control measurements were not normal when tested for normality unlike the baseline measurements whose results were not statistically significant according to the Shapiro Wilk test. However, it should be noted that the result of normality in the circumferential view in the baseline results was at the borderline of being statistically significant or not ($p = 0.057$, results are not shown). Additionally, only 8 out of the 10 volunteers had control measurements. This led to the change in the results for normality due to the decrease in statistical power.

The statistical significance results from the Kruskal-Wallis for the Control measurements as shown in Table 4.10 differ from the results obtained in the Baseline measurements whose strain values from all FT software methods in all the three strain views were statistically different (see Table 4.3). This could be because different statistical methods with different power and sensitivity were used to compare the means in both cases. Nevertheless, the Kruskal-Wallis test is the One-way ANOVA alternative for non-parametric tests [91].

Performing a Kruskal-Wallis test on the Baseline measurements however also showed statistical significance in all the three strain views (see Table 4.18) as in Table 4.3. This rules out the statistical method as a reason for the difference in the trend of statistical difference. The difference could be due to the observer doing the analysis in that she demarcated the borders differently in both cases. The difference could also be due to the uncertainty in the MRI machine thus introducing some changes in the images when the volunteers were imaged.

With regards to TomTec 2D CPA MR, the radial strain is the highest reproducible strain. It should be noted that it is unusual for radial strain to be highly reproducible due to its measurement difficulties and the fact that there is only one combined value obtained in the case of TomTec 2D CPA MR which make it the least reproducible strain as was explained earlier in Section 5.3.

A study done by Morton, Schuster [94] on the interstudy reproducibility of FT method using TomTec 2D CPA MR obtained a high reproducibility for circumferential strain (CV=20.30%), and a poor reproducibility for the radial strain (CV=27.20%), while the longitudinal strain had the second lowest reproducibility (CV=26.40%). These values are much higher than the ones obtained during the current project, implying reproducibility is better in the current project than in the past study. This could be due to the observers who took the analyses having different experience in the usage of the software-based method. In addition to the observers' different experience, the software versions of TomTec FT software used were also different. The version used in the current project is Image Arena, and the one used in this paper was Diogenes MRI prototype, which is older than the former. Improvements could have been made on the software algorithm, thus producing better results in the current work.

With regards to CMR^{42} TT, the longitudinal strain is the most reproducible strain followed closely by the circumferential strain, and then the radial strain. This result is also not in agreement with the above past study with the use of TomTec 2D CPA MR.

The trend in interstudy reproducibility differs in both FT software because in each software, different strain views are highly reproducible. This confirms yet again that the FT software methods, TomTec 2D CPA MR and CMR^{42} TT may not be interchangeable.

However, the measurements are not the only factors responsible for the variance. The volunteers also contribute to the variance. This is because the time between the measurements (6 months) was adequate for the volunteers to experience significant changes in their physical state. In addition, the variance also occurs due to the inherent variability of the software algorithms, and the uncertainty of the MRI machine used.

Overall, the small values of the CV indicate a high interstudy reproducibility of TomTec 2D CPA MR and CMR^{42} TT.

5.6 Comparison of modality

In the comparison of modality that is, Ultrasound and MRI, the author sought to determine the bias between the strain values from both imaging modalities which was shown graphically in Figure 4.12. The circumferential and longitudinal strains were combined to give one value of strain. There is a bias between the two modalities but is not systematic, and it varies from individual to individual. The variation from individual to individual is because of the varying physical characteristics of the volunteers like age, and gender and the cardiac factors like the size of the Left Ventricle and the wall thickness.

This bias however is very small and thus there is a high agreement between the two modalities. The high agreement implies that strain measurements can be taken on either modality and have satisfactory results that would not need supplementary information from the other modality.

5.7 Additional comparison

5.7.1 Comparison of TomTec 2D CPA MR and STE

The high reproducibility of circumferential strain as shown in Table 4.15 is mainly attributed to the structure of the heart wall with the fibers in the midmyocardium being aligned circumferentially as was explained in Sections 2.3 and 5.1.

In a study done by Orwat, Kempny [87] that also assessed the agreement between TomTec 2D CPA MR and STE, the longitudinal strain was more reproducible than the circumferential strain (CV=14.40% versus CV=19.40%). The CV values of the current project in Table 4.15 are lower than those obtained in the above study. This could be due to the difference in the tracing of the borders by the different observers during the strain measurement. More to that, the above reproducibility trend does not agree with that of the current study.

However, the biases are small and the LOA are narrow as seen in Table 4.15 thereby suggesting a high agreement between the two software-based methods. On the whole, the small values of CV imply that the interstudy reproducibility of TomTec 2D CPA MR and STE is high.

5.7.2 Comparison of CMR^{42} TT and STE

The longitudinal strain is the more reproducible strain, according to CV values (see Table 4.16). This trend of reproducibility differs from that obtained in the comparison of TomTec 2D CPA MR and STE above. This can be attributed to the different inherent variability in each of the

FT software methods. This is also an indicator that the two FT software methods may not be interchangeable. Conversely, the trend of interstudy reproducibility of CMR[42] TT and STE is in agreement with that of the study done by Orwat, Kempny [87].

According to the author's knowledge, this is the first study done to compare CMR[42] TT with any other strain measurement method. The low CV values in the different strain views suggest that the interstudy reproducibility of CMR[42] TT and STE is high.

5.7.3 Comparison of TomTec 2D CPA MR and CMR[42] TT

The results of this comparison as shown in Table 4.17 indicate that the longitudinal strain is the most reproducible strain while the radial strain is the least reproducible strain.

In the first ever study done to compare the two FT software methods that was done by Schuster, Stahnke [95]. CV for circumferential strain was 13.8% and CV for radial strain was 31.53%. In comparison with the current project, the results are similar in that though the past study only looked at radial and circumferential strain, while the current project looked at all the three strains, the circumferential strain in the current project is more reproducible than the radial strain.

The bias and CV values in this comparison of the FT software methods are larger than those obtained from other comparisons made in previous sections, the most outstanding being the radial strain. One of the reasons for such a big difference is due to the inherent variability of the FT software methods. CMR[42] TT for example was found to have a relatively low tracking ability in the apical slices compared to TomTec 2D CPA MR as will be explained in Section 5.10. This was also seen in a study done by Schuster, Stahnke [95] where they did not use all the MRI images due to insufficient tracking. The algorithms of each software method may have been developed in such a way that it tracks a particular view of strain better than the other views. From the above analyses, TomTec 2D CPA MR seems to track circumferential strain best, while CMR[42] TT tracks longitudinal strain best.

The trend of statistical significance in this comparison is the same as that obtained during the ANOVA analysis (see Table 4.4) for the comparison of the two FT software algorithms and also for the comparison of TomTec 2D CPA MR and STE. However, this trend is different for the comparison of CMR[42] TT with STE due to a statistical significance obtained in the

circumferential strain values for the interstudy reproducibility test as shown in Table 4.17 whereas for the ANOVA analysis as seen in Table 4.4, both longitudinal and circumferential strain values are statistically similar. This is because statistical significance level obtained with ANOVA for circumferential strain for is 0.064. This p-value is close to being statistically significant. The difference in the statistical significance trends could therefore be a case of the two tests having different statistical power and as such gave a different value in that instance.

Other possible sources of the variance of strain values include the observers, and the inherent variability of the software-based methods.

5.8 General discussion

The low reproducibility of radial strain is because technically, it is difficult to obtain. The basis of all these strain measurement methods is velocity and displacement. Because the distance between the endocardial and the epicardial walls in the radial axis is so small, this makes obtaining the displacement difficult and therefore obtaining the velocity is difficult [104]. The high variability of the radial strain in reproducibility measures has also been attributed to the out of plane motion of the LV due to the longitudinal motion of the heart that these 2D strain measurement techniques do not account for [103]. This can also explain the difference in the radial values from the Feature Tracking methods as assessed by the One-way ANOVA test in Section 4.4 (see Tables 4.3 and 4.4).

On the other hand, the high reproducibility of circumferential and longitudinal strain values is because of the circumferentially oriented arrangement of fibers in the LV midmyocardium and fibers in the subendocardium and the subepicardium which are arranged longitudinally [40]. This has been explained in Section 2.3 and 5.1. More to that, the midmyocardium fibers make up almost half of the total cardiac muscle [105]. This can also explain the results obtained with the One-way ANOVA analysis presented in Section 4.4 (see Tables 4.3 and 4.4).

In conclusion, the structure of the heart wall determines the nature of results in a particular strain view.

5.9 Contribution of factors to the variance

In the five equations created in Section 4.10, the Var (test-retest) is used in all of the equations. This is because for each of the comparisons done, more than one measurement could be done.

Looking at Table 4.19, the Var (test-retest) in the circumferential strain view is 6.81%, and is the value of Var (intraobserver) as expressed in equation 4.1. Taking equation 4.2 into consideration, the Var (observer) is approximately the same as that from the intraobserver reproducibility. Thus, the variance due to the observer does not contribute significantly to the variance.

In the Var (MRI measurements) which is also equation 4.3, the variance of MRI re-measurements [Var (re-measurement)] for TomTec 2D CPA MR does not differ greatly from Var (test-retest). However, Var(re-measurement) for CMR^{42} TT differs from Var(test-retest) differs by 2.64%.

The variance of the methods (equation 4.4) which are the STE and FT software methods differ from the Var(test-retest) by 2.45% for TomTec 2D CPA MR versus STE, and 4.27% for CMR^{42} TT versus STE.

In the case of the FT software methods (equation 4.5), the variance due to each software method is large, and it differs from Var (test-retest) by 7.68%. This is the largest difference so far recorded. This leads to the conclusion that the variance due to each FT software method contributes the biggest variance to the results of the circumferential strain.

Treating the longitudinal strain in the same way as the circumferential strain, it can be seen that the significant contributors of variance are due to the method (TomTec 2D CPA MR versus STE), the MRI re-measurements for TomTec 2D CPA MR, each FT software, and the largest contributor being the variance due to the observer.

For radial strain however, the significant contributors to the variance are due to the MRI re-measurements for CMR^{42} TT, the observer, and the largest being the variance of each FT software.

In general, it can be concluded that the variance due to each FT software method contributed the largest variance in the study. Such a result emphasizes the need for the improvement of both FT software algorithms.

5.10 Feasibility of strain measurement method

Processing of images in both FT software methods to obtain strain values for one volunteer took approximately the same time (around 20 minutes) for both observers, thus making them

comparable in terms of post processing speed. However, the time in STE is much shorter since it took between 2-5 minutes to process the strain values for one volunteer depending on the quality of the Ultrasound images.

In the FT software methods, all the images were tracked although there were some challenges with some of the apical slices when CMR^{42} TT was being used. To solve this issue, additional measures were taken. For instance, all the images in the slice were traced even though this turned out to be time consuming. In a similar study done by Schuster, Stahnke [95], not all images were tracked in CMR^{42} TT which portrays that CMR^{42} TT has a lower tracking ability than TomTec 2D CPA MR.

In the case of STE, 4 frames in the longitudinal axis view, specifically the four chamber view were rejected and 28 frames in the short axis view were also rejected. This is supported by literature from past studies where frames were rejected due to suboptimal image quality [106, 107]. More frames were rejected in the short axis view compared to the longitudinal view because the direction of the ultrasound beam is in the longitudinal direction thus longitudinal axis view values are better than those of the short axis view [24].

5.11 Technical differences in the software-based methods

STE and FT software methods, though based on the same physical principles of velocity and displacement are different in terms of the structures used to carry out the measurement. Speckle Tracking Echocardiography (STE) involves the tracking of speckle patterns which are formed from the scattering of the ultrasound beam whereas Feature Tracking (FT) tracks anatomical differences in the features of the heart wall [87].

FT-CMR measures myocardial strain from the endocardial and epicardial borders, providing values for both. Speckle Tracking measures strain from a region of interest within the myocardium that is enclosed by the endocardial and the epicardial borders of the LV [73]. In addition to that, there are differences in which Speckle Tracking Echocardiography is done depending on the vendor whereby some measure myocardial strain from the endocardial and epicardial borders and others measure the strain from the mid-myocardium [22].

TomTec 2D CPA MR has dedicated analyses for the basal, mid-ventricular and apical short axis levels so it required running the analysis thrice for the circumferential and radial strains. CMR^{42} TT does not have an automated system for the determination of these short axis levels.

Hence, determination of the basal, mid-ventricular and apical levels is done by the observer and the radial and circumferential strain in all the three levels is obtained at once in a single analysis for a volunteer.

With CMR[42] TT, the endocardial and epicardial borders are placed on the MRI images automatically with a click, and thereafter are edited to ensure that the traces are on the borders of the LV. TomTec 2D CPA MR requires the manual delineation of the endocardial and endocardial borders. This however does not create any difference in the speed of strain analysis between the two Feature Tracking software-based methods.

In TomTec 2D CPA MR, the delineation is done in end systole, In CMR[42] TT, delineation is done in both end diastole and end systole. TomTec 2D CPA MR displays strain time plots and segmental values for endocardial and epicardial traces of the LV separately in the circumferential and longitudinal view, while in CMR[42] TT, the global strain values in all the views are given for the epicardial and endocardial traces but there is only one strain-time plot for each strain view which is an average of the endocardial and epicardial strains.

FT software-based methods do not provide feedback on tracking quality of images like it is in the case of STE. Thus tracking quality is left to the observer to quantify and therefore, tracking quality results differ depending on one's training and experience.

A weakness with the 2D software-based methods is that they make measurements from in plane displacements [94, 108]. They do not consider the out of plane displacements due to the twisting motion of the heart and thus they do not show a comprehensive deformation of the Left Ventricle and the heart. This has been solved in STE by introducing 3D STE in which tracks speckles in a volume even though this remains to be seen in FT CMR.

It has also been stated in past literature that Feature Tracking may not detect midmyocardial strain. This is because of the way the tracking is done. As mentioned earlier, the Feature Tracking software methods detect the endocardial and epicardial borders while STE tracks a region of interest which includes the mid myocardium [94]. Midmyocardial strain is detected in myocardial tagging thereby giving it the upper hand over Feature Tracking method in this regard.

5.12 Study limitations

The study involved a small number of healthy volunteers. This affected the statistical power of the study. Statistical power was low in this study and thus, the effect size was high [109]. However, the statistical methods used in the study were adequately robust enough to produce the required results.

The study didn't involve patient data. However, FT software method has been used in patients in previous studies and has proved to have a high reproducibility, for example in circumferential strain in patients with Duchenne muscular dystrophy [21].

Strain values from myocardial tagging were not available for comparison with Feature Tracking yet it is the standard for determining strain. However, previous studies comparing myocardial tagging and FT CMR indicate a high reproducibility between the two methods [21].

Some scholars recommend that when comparing methods, two measurements should be made by each method on the subject and each treated as a separate repeatability study [89]. However due to time limitations on the software methods, this could not be done.

The retests strain measurements were only done for CMR^{42} TT and not for TomTec 2D CPA MR due limited time with the software. CMR^{42} TT is permanently installed at St. Olav's hospital while TomTec 2D CPA was temporarily installed for a month. The interobserver reproducibility for CMR^{42} TT could also not be done due to time constraints. As such, doing a comprehensive study on the intraobserver and interobserver reproducibility on both Feature Tracking methods could not be realized in this study.

For longitudinal strain, only four chamber data was considered thus the entire representation of longitudinal strain is not provided.

A threshold of the acceptable Limits of Agreement in myocardial strain could not be obtained like in the case of cardiac output monitoring where a cutoff of 30% is used in the error [99]. Hence, decisions on agreement of methods were based on past literature where similar tests were carried out, and on personal judgement.

6 Conclusions and recommendations

6.1 Conclusions

The general aim of the thesis is to evaluate Feature Tracking Cardiac Magnetic Resonance (FT CMR) or Feature Tracking software method by comparing it with Speckle Tracking Echocardiography, which is an already established method of determining myocardial strain. From the different comparisons that were made in order to achieve the above aim, the following conclusions have been made;

From the comparison between strain methods, it can be concluded that the similarity between MRI based strain values and Ultrasound based strain values depends on the strain view. The more comprehensive interstudy reproducibility tests conclude that there is a high reproducibility MRI strain based values and the Ultrasound strain based values.

MRI based strain methods give more comprehensive values of LV myocardial strain as compared to the ultrasound method because all the MRI images were considered for the analysis due to their high spatial resolution. Ultrasound images on the other hand have a low spatial resolution and as such, a total of 32 frames or images that could not be sufficiently tracked had to be dropped from the analysis. MRI based strain therefore is more advantageous in this regard.

The generally low values of the Coefficient of Variation observed in all the different comparisons lead to the conclusion that the reproducibility of both TomTec 2D CPA MR and CMR^{42} TT or Feature Tracking method of strain determination is high. However, the reproducibility is highly variable depending on the strain view. This is attributed to the structure of the myocardium wall of the Left Ventricle.

CMR^{42} TT gives statistically different values from TomTec 2D CPA MR. In addition to that, the trend of reproducibility is not the same in both FT software methods because for each method, a different strain view was highly reproducible. This creates a need for improving these algorithms such that there is uniformity in strain results obtained and so that standardization of strain imaging is achieved in Cardiac Magnetic Resonance, and Cardiology as a whole.

6.2 Recommendations

First of all, another study with a larger sample size which would increase the statistical power of the tests should be done.

Secondly, Segmental strain has been compared in TomTec 2D CPA MR and myocardial tagging before and it showed a low reproducibility [81]. Another study that looked at the interstudy reproducibility of Feature Tracking Cardiac Magnetic Resonance concluded that segmental strain was less reproducible than global strain [94]. It remains to be known how well segmental strain in CMR^{42} TT agrees with TomTec 2D CPA MR and STE. Therefore, a study comparing the segmental strain in all the three strain measurement methods is necessary.

Thirdly, a comparison of Speckle Tracking Echocardiography should be done with Feature Tracking software methods in a number of patient situations to evaluate if there is an agreement between both methods in such situations.

Fourthly, considering the newness of CMR^{42} TT, an evaluation of its efficiency in a number of patient situations is encouraged.

The fifth recommendation concerns Feature Tracking software method. Despite the fact that Feature Tracking has previously been compared to myocardial tagging, the software algorithm compared was TomTec 2D CPA MR, and not CMR^{42} TT. Comparison of CMR^{42} TT therefore should be done to assess whether it agrees with myocardial tagging, the gold standard for myocardial deformation.

Finally, the differences in the reproducibility trends of TomTec 2D CPA MR, and CMR^{42} TT as well as the technical differences particularly the difference in tracking ability implies that more work needs to be done on both algorithms so that there is uniformity in strain results obtained. In doing so, standardization of strain imaging can be achieved in Cardiac Magnetic Resonance and Cardiology as a whole, thereby increasing the possibility of strain imaging being fully implemented into daily clinical practice.

7 References

1. *The top 10 causes of death*. May 2014; Available from: http://www.who.int/mediacentre/factsheets/fs310/en/.
2. *Standard measurement of cardiac function indexes.* Journal of Medical Ultrasonics. **33**(2): p. 123-127.
3. Møller, J.E., et al., *Wall motion score index and ejection fraction for risk stratification after acute myocardial infarction.* American Heart Journal, 2006. **151**(2): p. 419-425.
4. Moss , A.J., et al., *Prophylactic Implantation of a Defibrillator in Patients with Myocardial Infarction and Reduced Ejection Fraction.* New England Journal of Medicine, 2002. **346**(12): p. 877-883.
5. Zipes, D.P., et al., *ACC/AHA/ESC 2006 Guidelines for Management of Patients With Ventricular Arrhythmias and the Prevention of Sudden Cardiac Death: A Report of the American College of Cardiology/American Heart Association Task Force and the European Society of Cardiology Committee for Practice Guidelines (Writing Committee to Develop Guidelines for Management of Patients With Ventricular Arrhythmias and the Prevention of Sudden Cardiac Death).* Journal of the American College of Cardiology, 2006. **48**(5): p. e247-e346.
6. Wisneski, J.A., et al., *Left ventricular ejection fraction calculated from volumes and areas: underestimation by area method.* Circulation, 1981. **63**(1): p. 149-51.
7. Mizuguchi, Y., et al., *Concentric left ventricular hypertrophy brings deterioration of systolic longitudinal, circumferential, and radial myocardial deformation in hypertensive patients with preserved left ventricular pump function.* Journal of Cardiology, 2010. **55**(1): p. 23-33.
8. Buxton, A.E., et al., *Limitations of ejection fraction for prediction of sudden death risk in patients with coronary artery disease: lessons from the MUSTT study.* J Am Coll Cardiol, 2007. **50**(12): p. 1150-7.
9. Smiseth, O.A., et al., *Myocardial strain imaging: how useful is it in clinical decision making?* European Heart Journal, 2015.
10. Kalam, K., P. Otahal, and T.H. Marwick, *Prognostic implications of global LV dysfunction: a systematic review and meta-analysis of global longitudinal strain and ejection fraction.* Heart, 2014.

11. Cho, G.-Y., et al., *Global 2-Dimensional Strain as a New Prognosticator in Patients With Heart Failure.* Journal of the American College of Cardiology, 2009. **54**(7): p. 618-624.
12. Stanton, T., R. Leano, and T.H. Marwick, *Prediction of All-Cause Mortality From Global Longitudinal Speckle Strain: Comparison With Ejection Fraction and Wall Motion Scoring.* Circulation: Cardiovascular Imaging, 2009. **2**(5): p. 356-364.
13. MIRSKY, I. and W.W. PARMLEY, *Assessment of Passive Elastic Stiffness for Isolated Heart Muscle and the Intact Heart.* Circulation Research, 1973. **33**(2): p. 233-243.
14. Yingchoncharoen, T., et al., *Normal Ranges of Left Ventricular Strain: A Meta-Analysis.* Journal of the American Society of Echocardiography, 2013. **26**(2): p. 185-191.
15. Singh, A., et al., *Intertechnique agreement and interstudy reproducibility of strain and diastolic strain rate at 1.5 and 3 Tesla: a comparison of feature-tracking and tagging in patients with aortic stenosis.* J Magn Reson Imaging, 2015. **41**(4): p. 1129-37.
16. Ibrahim, E.-S., *Myocardial tagging by Cardiovascular Magnetic Resonance: evolution of techniques–pulse sequences, analysis algorithms, and applications.* J Cardiovasc Magn Reson, 2011. **13**.
17. Hor, K.N., et al., *Magnetic Resonance Derived Myocardial Strain Assessment Using Feature Tracking.* Journal of Visualized Experiments : JoVE, 2011(48): p. 2356.
18. Kowallick, J.T., et al., *Quantification of Left Ventricular Torsion and Diastolic Recoil Using Cardiovascular Magnetic Resonance Myocardial Feature Tracking.* PLoS ONE, 2014. **9**(10): p. e109164.
19. Taylor, R.J., et al., *Feature-tracking cardiovascular magnetic resonance as a novel technique for the assessment of mechanical dyssynchrony.* International Journal of Cardiology. **175**(1): p. 120-125.
20. Onishi, T., et al., *Feature tracking measurement of dyssynchrony from cardiovascular magnetic resonance cine acquisitions: comparison with echocardiographic speckle tracking.* Journal of Cardiovascular Magnetic Resonance, 2013. **15**(1): p. 95-95.
21. Hor, K.N., et al., *Comparison of Magnetic Resonance Feature Tracking for Strain Calculation With Harmonic Phase Imaging Analysis.* JACC: Cardiovascular Imaging, 2010. **3**(2): p. 144-151.

22. Taylor, R.J., et al., *Myocardial strain measurement with feature-tracking cardiovascular magnetic resonance: normal values.* European Heart Journal - Cardiovascular Imaging, 2015.
23. Schuster, A., et al., *Cardiovascular Magnetic Resonance Myocardial Feature Tracking: Concepts and Clinical Applications.* Circ Cardiovasc Imaging, 2016. **9**(4).
24. Opdahl, A., et al., *Strain, strain rate, torsion, and twist: echocardiographic evaluation.* Curr Cardiol Rep, 2015. **17**(3): p. 568.
25. Riffel, J.H., et al., *Assessment of global longitudinal strain using standardized myocardial deformation imaging: a modality independent software approach.* Clin Res Cardiol, 2015. **104**(7): p. 591-602.
26. Voigt, J.-U., et al., *Definitions for a common standard for 2D speckle tracking echocardiography: consensus document of the EACVI/ASE/Industry Task Force to standardize deformation imaging.* European Heart Journal - Cardiovascular Imaging, 2014.
27. Almutairi, H.M., et al., *A comparison of cardiac motion analysis software packages: application to left ventricular deformation analysis in hypertensive patients.* Journal of Cardiovascular Magnetic Resonance, 2015. **17**(Suppl 1): p. P57-P57.
28. Taylor, T. *Inner Body- Heart*. Available from: http://www.innerbody.com/image/card01.html.
29. *Human Heart Structure* Available from: http://www.tutorvista.com/content/biology/biology-ii/transportation/heart.php.
30. Jan Bogaert, S.D., Andrew M. Taylor, Vivek Muthurangu, *Clinical Cardiac MRI*. Second Edition ed. Medical Radiology, Diagnostic Imaging, ed. M.F.R. Albert L. Baert, Hedvig Hricak, Michael Knauth. 2012, Springer-Verlag Berlin Heidelberg 2012: Springer.
31. *Anatomy and Physiology-Heart Anatomy: chambers, valves and vessels*. 2013; Available from: http://anatomyandphysiologyi.com/heart-anatomy-chambers-vessels-valves/.
32. *Exploring holes in the heart-How the Heart Works*. July 1 , 2011; Available from: https://www.nhlbi.nih.gov/health/health-topics/topics/holes/heartworks#.
33. *Physiology of the heart*. Available from: http://training.seer.cancer.gov/anatomy/cardiovascular/heart/physiology.html.
34. *Anatomy and Physiology II , Cardiac Cycle*. Available from: https://courses.candelalearning.com/ap2x2master/chapter/cardiac-cycle/.

35. Buckberg, G., et al., *Cardiac Mechanics Revisited: The Relationship of Cardiac Architecture to Ventricular Function.* Circulation, 2008. **118**(24): p. 2571-2587.
36. Larsson, M., *Quantification and Visulization of Cardiovascular Function using Ultrasound*, in *Department of Medical Engineering*. 2009, Royal Institute of Technology: Stockholm.
37. Jiang, K. and X. Yu, *Quantification of regional myocardial wall motion by cardiovascular magnetic resonance.* Quantitative Imaging in Medicine and Surgery, 2014. **4**(5): p. 345-357.
38. Gilbert, S.H., et al., *Regional localisation of left ventricular sheet structure: integration with current models of cardiac fibre, sheet and band structure.* European journal of cardio-thoracic surgery, 2007. **32**(2): p. 231-249.
39. Poveda, F., et al., *Helical Structure of the Cardiac Ventricular Anatomy Assessed by Diffusion Tensor Magnetic Resonance Imaging With Multiresolution Tractography.* Revista Española de Cardiología (English Version), 2013. **66**(10): p. 782-790.
40. Holzapfel, G.A. and R.W. Ogden, *Constitutive modelling of passive myocardium: a structurally based framework for material characterization.* Philosophical Transactions of the Royal Society of London A: Mathematical, Physical and Engineering Sciences, 2009. **367**(1902): p. 3445-3475.
41. STREETER, D.D., et al., *Fiber Orientation in the Canine Left Ventricle during Diastole and Systole.* Circulation Research, 1969. **24**(3): p. 339-347.
42. Greenbaum, R.A., et al., *Left ventricular fibre architecture in man.* Br Heart J, 1981. **45**(3): p. 248-63.
43. Buckberg, G., et al., *Structure and function relationships of the helical ventricular myocardial band.* The Journal of Thoracic and Cardiovascular Surgery. **136**(3): p. 578-589.e11.
44. *Cardiac CT, PET and MR*, ed. G.M.P. Vasken Dilsizian. 2006: Blackwell Futura.
45. PhD, A.H.A., *Cardiovascular Magnetic Resonance Imaging*. Contemporary Cardiology, ed. M. Christopher P. Cannon, Annemarie M. Armani, MD. 2008, Totowa, New Jersey 07512: Humana Press Inc.
46. Hendee, W.R. and C.J. Morgan, *Magnetic Resonance Imaging Part I—Physical Principles.* Western Journal of Medicine, 1984. **141**(4): p. 491-500.
47. Dominik Weishaupt, V.D.K., Borut Marincek, *How Does MRI Work ? An Introduction to the Physics and Function of Magnetic Resonance Imaging*. Second Edition ed. 2006,2003, Verlag Berlin Heidelberg: Springer

48. Jeremy Jones, U.B.e.a., *K-Space*. 2005-2016.
49. Gallagher, T.A., A.J. Nemeth, and L. Hacein-Bey, *An Introduction to the Fourier Transform: Relationship to MRI.* American Journal of Roentgenology, 2008. **190**(5): p. 1396-1405.
50. Michael Loecher , O.W., *Basic Principles of Cardiovascular MRI Physics and Imaging Technique* 2015, Switzerland: Springer International Publishing.
51. Patrick T. Norton, M.D., Nicholas C. Nacey, M.D., Dominique B. Caovan, M.D., Spencer B. Gay, M.D., Christopher M. Kramer, M.D., Bryan S. Jeun, M.D. *Cardiac MRI: The Basics, Pulse Sequences*. 2013 [cited 2016 13th January]; Available from: https://www.med-ed.virginia.edu/courses/rad/cardiacmr/Techniques/Pulse.html.
52. Ginat, D.T., et al., *Cardiac Imaging: Part 1, MR Pulse Sequences, Imaging Planes, and Basic Anatomy.* American Journal of Roentgenology, 2011. **197**(4): p. 808-815.
53. Hoa, D. *Cardiac synchronization methods (cardiac gating)*. MRI step-by-step, interactive course on magnetic resonance imaging 2008-2016 [cited 2016 14th January]; Available from: https://www.imaios.com/en/e-Courses/e-MRI/Cardiac-MRI/ecg-gating.
54. Kiaran McGee, P., Matthew Martinez, MD, and Eric Williamson, MD, *Mayo Clinic Guide to Cardiac Magnetic Resonance Imaging*. Second Edition ed. 2008,2015: Mayo Clinic Scientific Press, Oxford University Press
55. Ridgway, J.P., *Cardiovascular Magnetic Resonance Imaging for Clinicians: Part 1.* Journal of Cardiovascular Magnetic Resonance, 2010. **12**(71).
56. Vivian S Lee, M., PhD, *Cardiovascular MRI: Physical Principles to Practical Protocols*. 2006, Philadephia, USA: Lippincott Williams and Wilkins.
57. Dr Tim Luijkx , D.Y.W., et al. *Steady State Free Precession MRI*. Available from: http://radiopaedia.org/articles/steady-state-free-precession-mri-2.
58. Kastler, B., *MRI of Cardiovascular Malformations* 2011, Verlag Berlin Heidelberg: Springer
59. Segmentation, A.H.A.W.G.o.M., et al., *Standardized Myocardial Segmentation and Nomenclature for Tomographic Imaging of the Heart: A Statement for Healthcare Professionals From the Cardiac Imaging Committee of the Council on Clinical Cardiology of the American Heart Association.* Circulation, 2002. **105**(4): p. 539-542.
60. Lang, R.M., et al., *Recommendations for Cardiac Chamber Quantification by Echocardiography in Adults: An Update from the American Society of*

Echocardiography and the European Association of Cardiovascular Imaging. Journal of the American Society of Echocardiography, 2015. **28**(1): p. 1-39.e14.

61. Dandel, M., et al., *Strain and Strain Rate Imaging by Echocardiography – Basic Concepts and Clinical Applicability.* Current Cardiology Reviews, 2009. **5**(2): p. 133-148.
62. Dohi, K., E. Sugiura, and M. Ito, *Utility of strain-echocardiography in current clinical practice.* J Echocardiogr, 2016.
63. Shah, A.M. and S.D. Solomon, *Myocardial Deformation Imaging: Current Status and Future Directions.* Circulation, 2012. **125**(2): p. e244-e248.
64. Antoni, M.L., et al., *Prognostic importance of strain and strain rate after acute myocardial infarction.* European Heart Journal, 2010. **31**(13): p. 1640-1647.
65. Thavendiranathan, P., et al., *Use of Myocardial Strain Imaging by Echocardiography for the Early Detection of Cardiotoxicity in Patients During and After Cancer Chemotherapy: A Systematic Review.* Journal of the American College of Cardiology, 2014. **63**(25, Part A): p. 2751-2768.
66. Saghir, M., M. Areces, and M. Makan, *Strain Rate Imaging Differentiates Hypertensive Cardiac Hypertrophy from Physiologic Cardiac Hypertrophy (Athlete’s Heart).* Journal of the American Society of Echocardiography. **20**(2): p. 151-157.
67. Richand, V., et al., *An Ultrasound Speckle Tracking (Two-Dimensional Strain) Analysis of Myocardial Deformation in Professional Soccer Players Compared With Healthy Subjects and Hypertrophic Cardiomyopathy.* American Journal of Cardiology. **100**(1): p. 128-132.
68. Bansal, M. and R.R. Kasliwal, *How do I do it? Speckle-tracking echocardiography.* Indian Heart Journal, 2013. **65**(1): p. 117-123.
69. Thomas M. Helle-Valle, M., *New Non-invasive Methods for Quantification of Regional and Global Myocardial Function in the Normal and Ischemic Left Ventricle*, in *Faculty of Medicine*. 2013, University of Oslo: AIT Oslo AS, Norway.
70. Cerqueira, M.D., et al., *Standardized myocardial segmentation and nomenclature for tomographic imaging of the heart. A statement for healthcare professionals from the Cardiac Imaging Committee of the Council on Clinical Cardiology of the American Heart Association.* Circulation, 2002. **105**(4): p. 539-42.

71. Tee, M., J.A. Noble, and D.A. Bluemke, *Imaging techniques for cardiac strain and deformation: comparison of echocardiography, cardiac magnetic resonance and cardiac computed tomography.* Expert Rev Cardiovasc Ther, 2013. **11**(2): p. 221-31.
72. Gorcsan, I.I.I.J. and H. Tanaka, *Echocardiographic Assessment of Myocardial Strain.* Journal of the American College of Cardiology, 2011. **58**(14): p. 1401-1413.
73. Mondillo, S., et al., *Speckle-Tracking Echocardiography: A New Technique for Assessing Myocardial Function.* Journal of Ultrasound in Medicine, 2011. **30**(1): p. 71-83.
74. Delgado, V., et al., *Relative Merits of Left Ventricular Dyssynchrony, Left Ventricular Lead Position, and Myocardial Scar to Predict Long-Term Survival of Ischemic Heart Failure Patients Undergoing Cardiac Resynchronization Therapy.* Circulation, 2011. **123**(1): p. 70-78.
75. Blessberger, H. and T. Binder, *Two dimensional speckle tracking echocardiography: basic principles.* Heart, 2010. **96**(9): p. 716-722.
76. Amundsen, B.H., et al., *Noninvasive Myocardial Strain Measurement by Speckle Tracking EchocardiographyValidation Against Sonomicrometry and Tagged Magnetic Resonance Imaging.* Journal of the American College of Cardiology, 2006. **47**(4): p. 789-793.
77. Ersboll, M., et al., *Early echocardiographic deformation analysis for the prediction of sudden cardiac death and life-threatening arrhythmias after myocardial infarction.* JACC Cardiovasc Imaging, 2013. **6**(8): p. 851-60.
78. Mor-Avi, V., et al., *Current and Evolving Echocardiographic Techniques for the Quantitative Evaluation of Cardiac Mechanics: ASE/EAE Consensus Statement on Methodology and Indications Endorsed by the Japanese Society of Echocardiography.* European Heart Journal - Cardiovascular Imaging, 2011. **12**(3): p. 167-205.
79. Massimo Lombardi, C.B., *MRI of the Heart and Vessels*. 2005, Verlag Italia: Springer.
80. Sitia, S., L. Tomasoni, and M. Turiel, *Speckle tracking echocardiography: A new approach to myocardial function.* World Journal of Cardiology, 2010. **2**(1): p. 1-5.
81. Wu, L., et al., *Feature tracking compared with tissue tagging measurements of segmental strain by cardiovascular magnetic resonance.* Journal of Cardiovascular Magnetic Resonance, 2014. **16**(1): p. 1-11.

82. Jeung, M.Y., et al., *Myocardial tagging with MR imaging: overview of normal and pathologic findings.* Radiographics, 2012. **32**(5): p. 1381-98.
83. Augustine, D., et al., *Global and regional left ventricular myocardial deformation measures by magnetic resonance feature tracking in healthy volunteers: comparison with tagging and relevance of gender.* J Cardiovasc Magn Reson, 2013. **15**: p. 8.
84. Andre, F., et al., *Age- and gender-related normal left ventricular deformation assessed by cardiovascular magnetic resonance feature tracking.* Journal of Cardiovascular Magnetic Resonance, 2015. **17**(1): p. 1-14.
85. *TomTec Imaging Systems, 2D Cardiac Performance Analysis MR*. Available from: http://www.tomtec.de/end_users/cardiac_mr/2d_cardiac_performance_analysis_mrc.html.
86. *Plugin- Tissue Tracking Plugin (for Research only)*. 2015; Available from: https://www.circlecvi.com/features/product-plugins/plugins-research/tissue-tracking.php.
87. Orwat, S., et al., *Cardiac magnetic resonance feature tracking: a novel method to assess myocardial strain. Comparison with echocardiographic speckle tracking in healthy volunteers and in patients with left ventricular hypertrophy.* Kardiol Pol, 2014. **72**(4): p. 363-71.
88. de Vet, H.C.W., et al., *When to use agreement versus reliability measures.* Journal of Clinical Epidemiology. **59**(10): p. 1033-1039.
89. Bartlett, J.W. and C. Frost, *Reliability, repeatability and reproducibility: analysis of measurement errors in continuous variables.* Ultrasound in Obstetrics and Gynecology, 2008. **31**(4): p. 466-475.
90. Onishi, T., et al., *Global Longitudinal Strain and Global Circumferential Strain by Speckle-Tracking Echocardiography and Feature-Tracking Cardiac Magnetic Resonance Imaging: Comparison with Left Ventricular Ejection Fraction.* Journal of the American Society of Echocardiography. **28**(5): p. 587-596.
91. Pallant, J., *A SPSS Survival Manual- A step by step guide to data analysis using SPSS for Windows (Version 12)*. 2nd ed. 2005, Crows Nest NSW 2065, Australia: Allen & Unwin.
92. Bland, J.M. and D.G. Altman, *Statistical methods for assessing agreement between two methods of clinical measurement.* Lancet, 1986. **1**(8476): p. 307-10.
93. Giavarina, D., *Understanding Bland Altman analysis.* Biochemia Medica, 2015. **25**(2): p. 141-151.

94. Morton, G., et al., *Inter-study reproducibility of cardiovascular magnetic resonance myocardial feature tracking.* Journal of Cardiovascular Magnetic Resonance, 2012. **14**(1): p. 1-8.
95. Schuster, A., et al., *Cardiovascular magnetic resonance feature-tracking assessment of myocardial mechanics: Intervendor agreement and considerations regarding reproducibility.* Clinical Radiology, 2015. **70**(9): p. 989-998.
96. Altman, D.G. and J.M. Bland, *Measurement in Medicine: The Analysis of Method Comparison Studies.* The Statistician, 1983. **32**(3): p. 307-317.
97. Marwick, T.H., et al., *Myocardial Strain Measurement With 2-Dimensional Speckle-Tracking Echocardiography: Definition of Normal Range.* JACC: Cardiovascular Imaging, 2009. **2**(1): p. 80-84.
98. Cohen, J., *Statistical power analysis for the Behavioral Sciences*. 2nd ed. 1988, Hillsdale, New Jersey, United States of America: Lawrence Erlbaum Associates.
99. Cecconi, M., et al., *Bench-to-bedside review: the importance of the precision of the reference technique in method comparison studies--with specific reference to the measurement of cardiac output.* Crit Care, 2009. **13**(1): p. 201.
100. Cheng, S., et al., *Reproducibility of Speckle-Tracking Based Strain Measures of Left Ventricular Function in a Community-Based Study.* Journal of the American Society of Echocardiography : official publication of the American Society of Echocardiography, 2013. **26**(11): p. 10.1016/j.echo.2013.07.002.
101. Schuster, A., et al., *Cardiovascular magnetic resonance myocardial feature tracking for quantitative viability assessment in ischemic cardiomyopathy.* International Journal of Cardiology, 2013. **166**(2): p. 413-420.
102. Schuster, A., et al., *Cardiovascular magnetic resonance myocardial feature tracking detects quantitative wall motion during dobutamine stress.* Journal of Cardiovascular Magnetic Resonance, 2011. **13**(1): p. 1-8.
103. Oxborough, D., K. George, and K.M. Birch, *Intraobserver Reliability of Two-Dimensional Ultrasound Derived Strain Imaging in the Assessment of the Left Ventricle, Right Ventricle, and Left Atrium of Healthy Human Hearts.* Echocardiography, 2012. **29**(7): p. 793-802.
104. *ASE's Comprehensive Echocardiography*. Second ed. 2016.
105. Biswas, M., et al., *Two- and Three-Dimensional Speckle Tracking Echocardiography: Clinical Applications and Future Directions.* Echocardiography, 2013. **30**(1): p. 88-105.

106. Aggeli, C., et al., *Two-dimensional speckle tracking for the assessment of coronary artery disease during dobutamine stress echo: clinical tool or merely research method.* Cardiovascular Ultrasound, 2015. **13**(1): p. 1-9.
107. Petersen, J.W., et al., *Speckle tracking echocardiography-determined measures of global and regional left ventricular function correlate with functional capacity in patients with and without preserved ejection fraction.* Cardiovascular Ultrasound, 2013. **11**: p. 20-20.
108. Tarr, A., et al., *Early detection of cardiotoxicity by 2D and 3D deformation imaging in patients receiving chemotherapy.* Echo Research and Practice, 2015. **2**(3): p. 81-88.
109. Sullivan, G.M. and R. Feinn, *Using Effect Size—or Why the P Value Is Not Enough.* Journal of Graduate Medical Education, 2012. **4**(3): p. 279-282.

Appendix

SCATTER DIAGRAMS OF THE DIFFERENT COMPARISONS

A1. Comparison of strain measurement method

a. TomTec 2D CPA MR and CMR[42] TT in radial (a), circumferential (b), and longitudinal (c) strain views

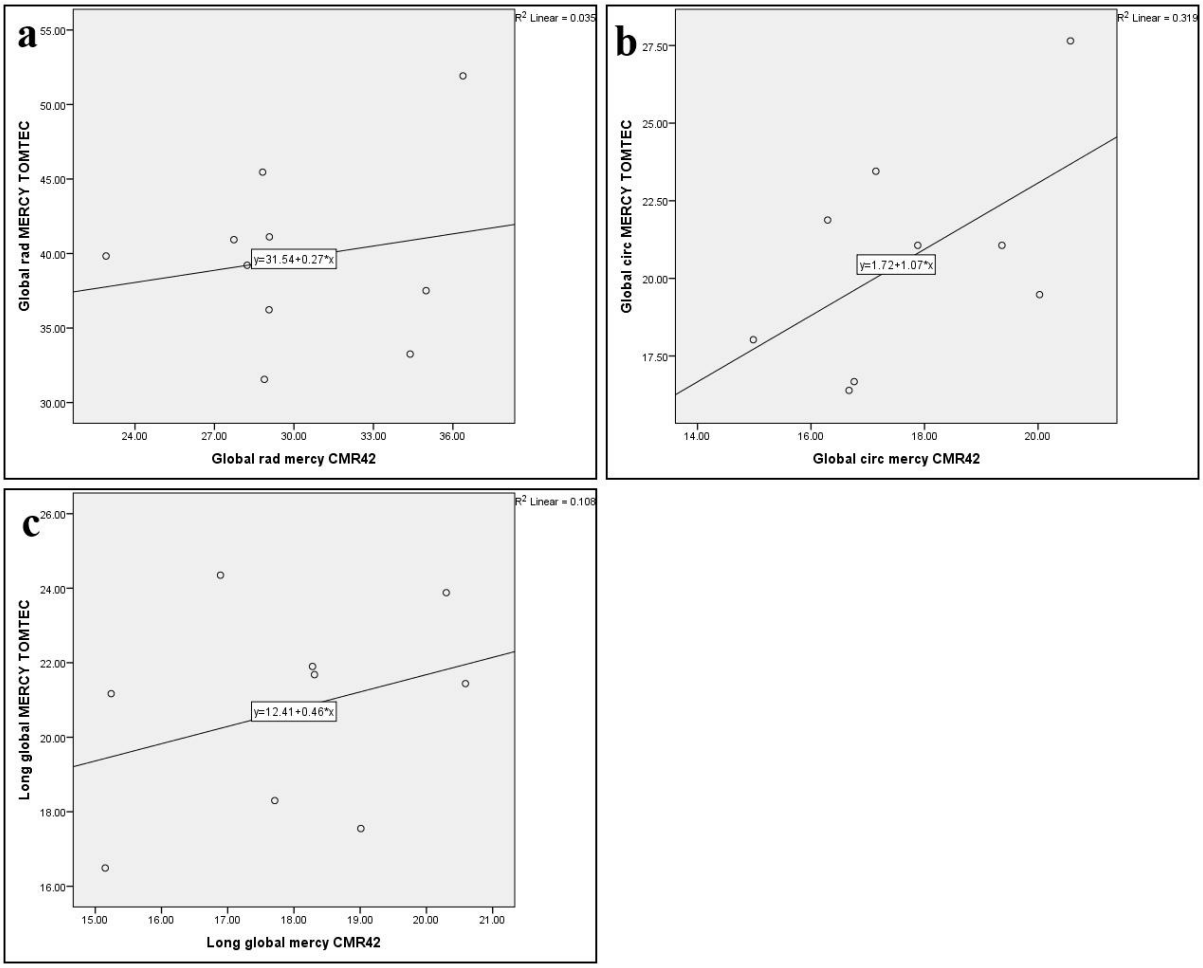

b. TomTec 2D CPA MR and CMR[42] TT in circumferential (a) and longitudinal (b) strain views

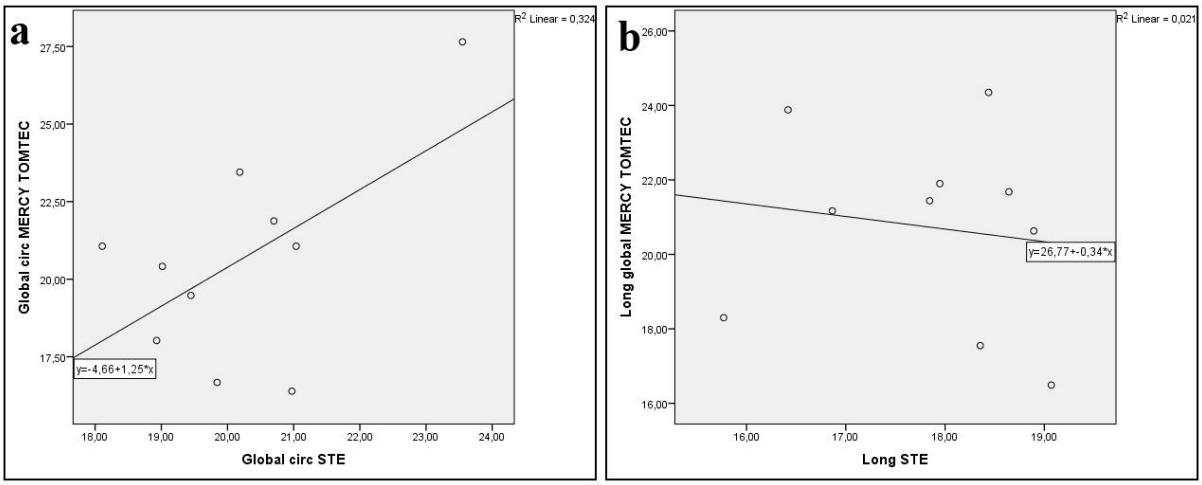

c. CMR[42] TT and STE in circumferential (a) and longitudinal (b) strain views

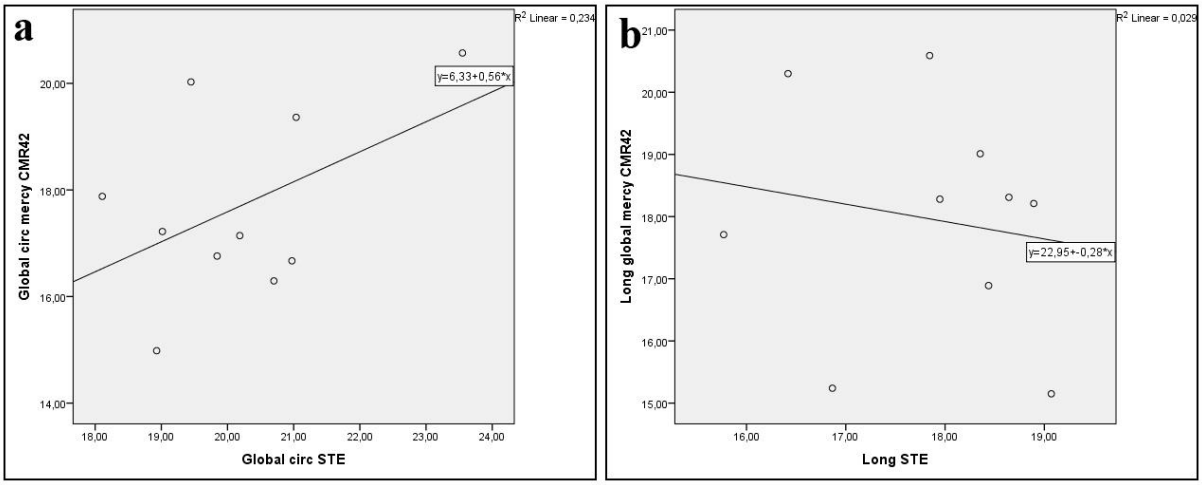

A2. Comparison of strain values from different observers in radial (a), circumferential (b), and longitudinal (c) strain views

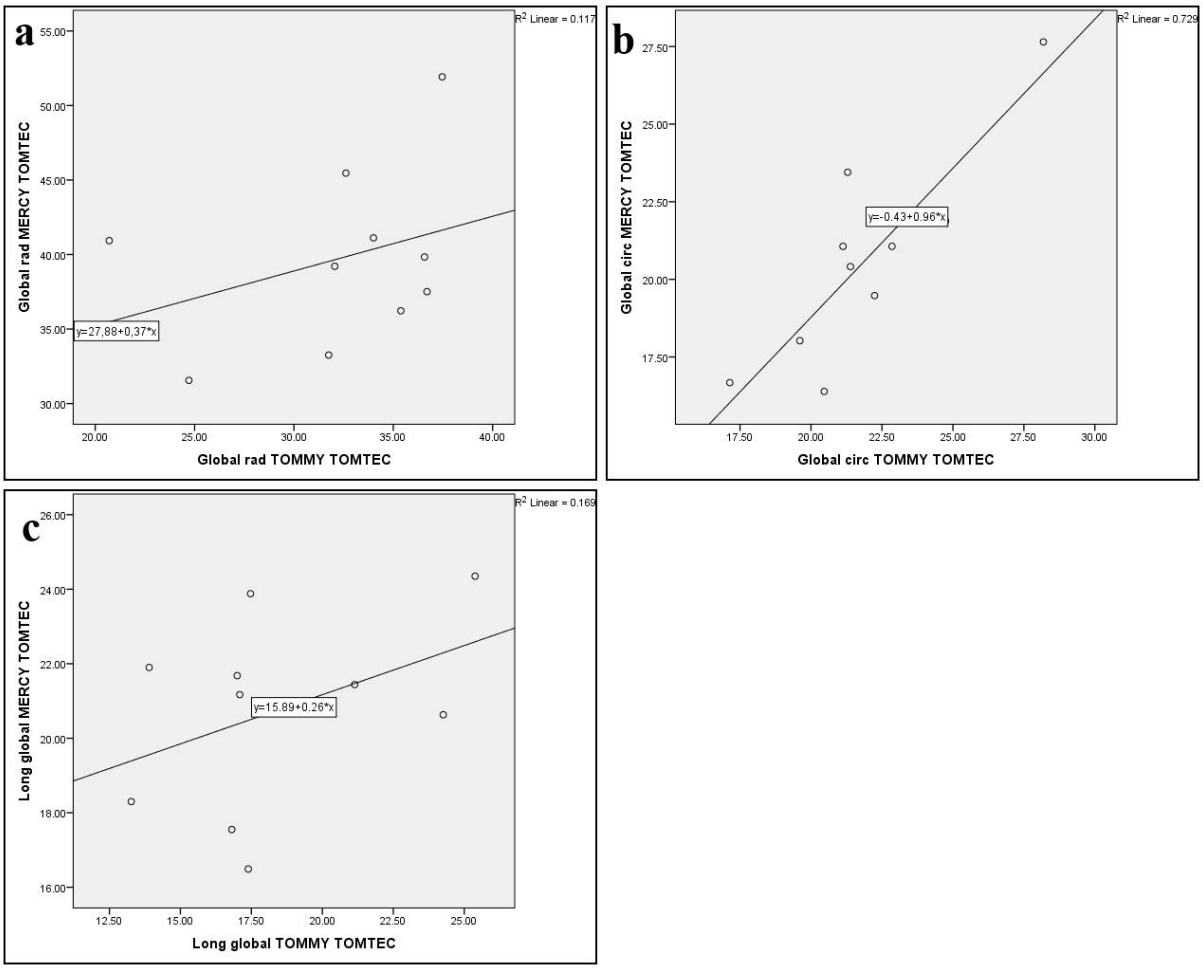

A3. Comparison of two measurements using the same method by the same observer (test-re-tests) in radial (a), circumferential (b), and longitudinal (c) strain views

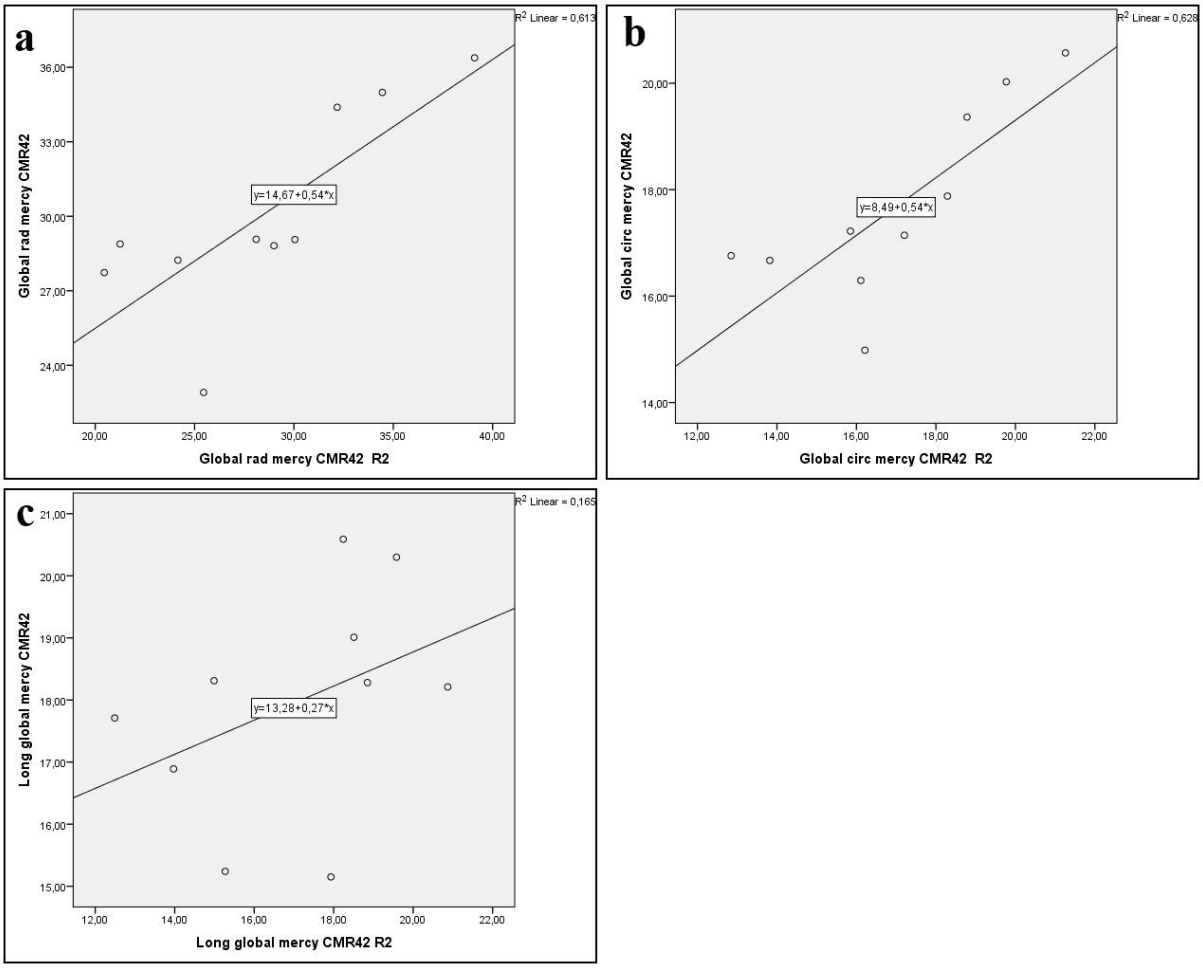

A4. Comparison of the two MRI measurements

a. Comparison of TomTec 2D CPA MR and CMR[42] TT in control measurements in radial (a), circumferential (b), and longitudinal (c) strain views

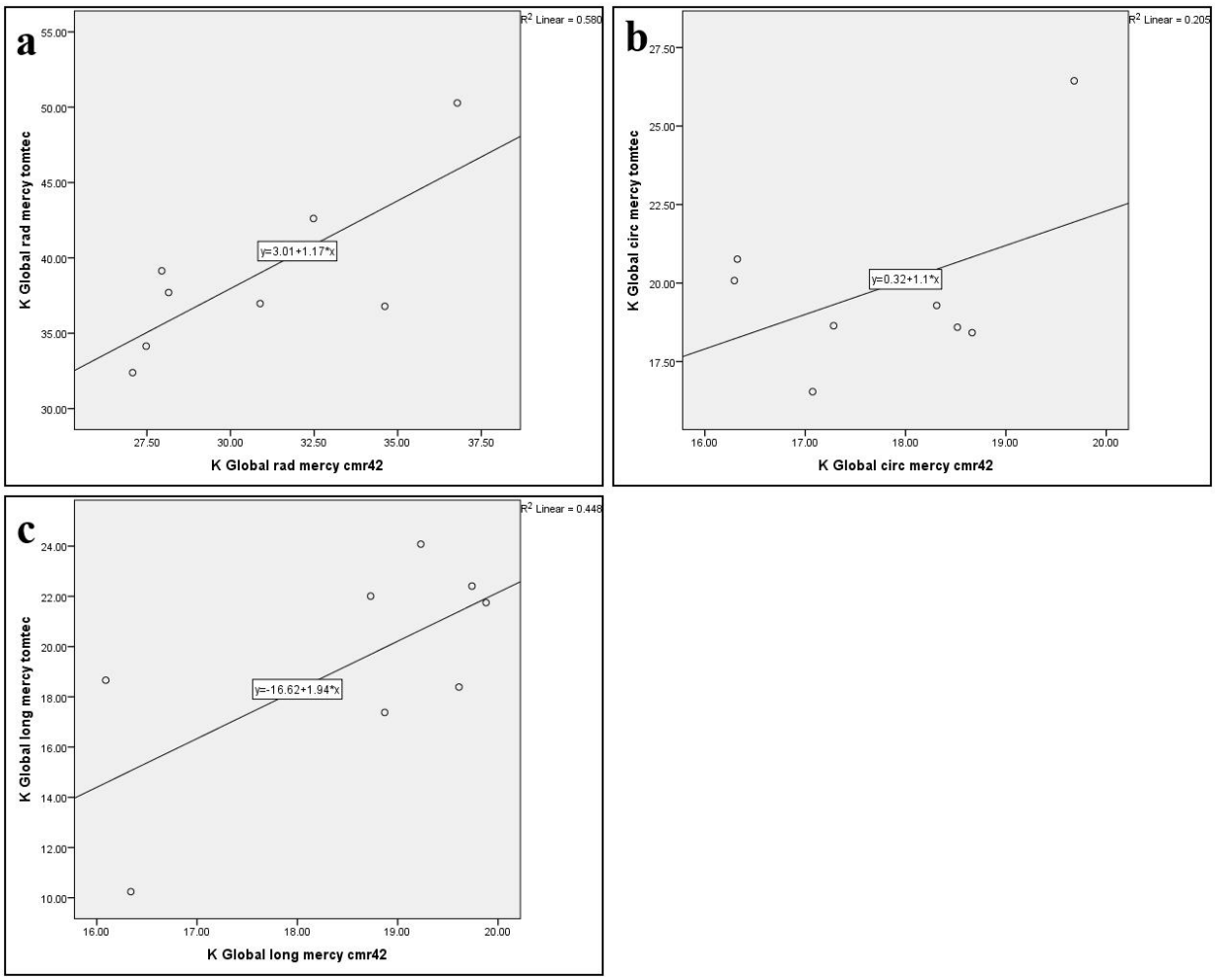

b. Comparison of baseline and control measurements of TomTec 2D CPA MR in radial (a), circumferential (b), and longitudinal (c) strain views

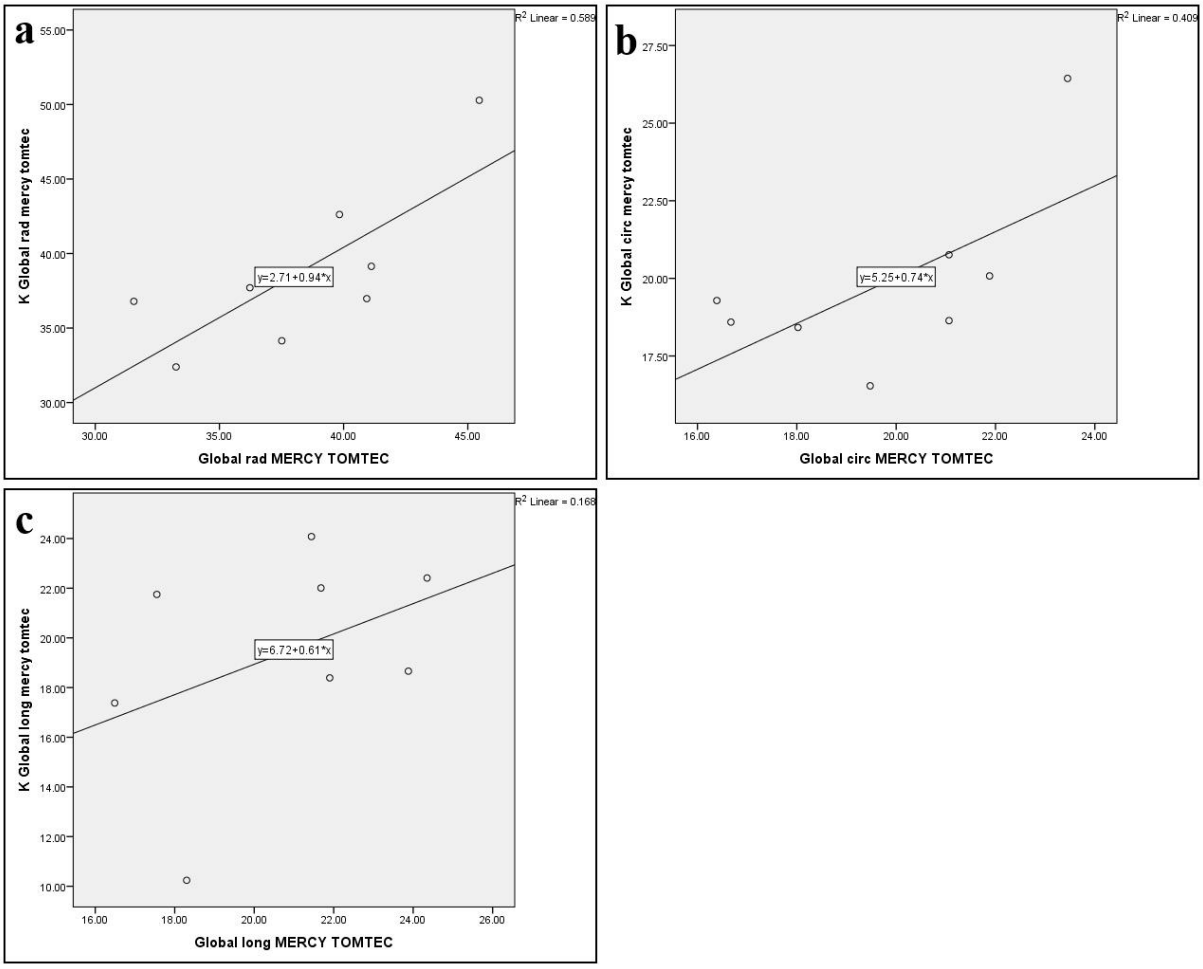

c. Comparison of baseline and control measurements of CMR^{42} TT in radial (a), circumferential (b) and longitudinal (c) strain views

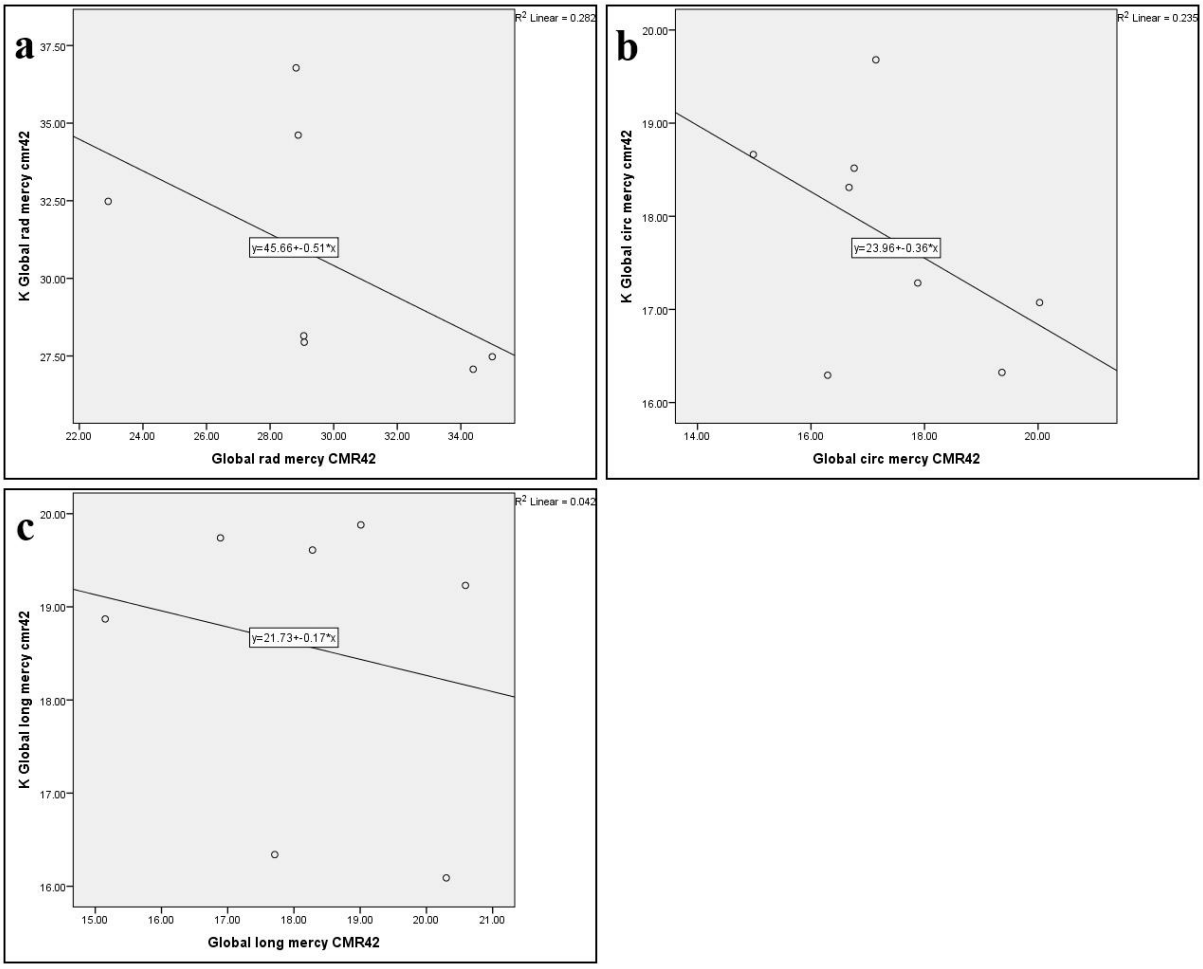

A5. Comparison of modality